THE UNIVERSITY OF CALGARY

HYDROTHERMAL METAMORPHISM OF TELKWA FORMATION VOLCANICS NEAR TERRACE, BRITISH COLUMBIA

by

KIMBERLEY JUNE FREEMAN

A THESIS

SUBMITTED TO THE FACULTY OF GRADUATE STUDIES

IN PARTIAL FULFILLMENT OF THE REQUIREMENTS FOR THE

DEGREE MASTER OF SCIENCE

DEPARTMENT OF GEOLOGY AND GEOPHYSICS

CALGARY, ALBERTA

APRIL, 1986

ISBN Ø-315-32653-Ø

THE UNIVERSITY OF CALGARY

FACULTY OF GRADUATE STUDIES

The undersigned certify that they have read, and recommend to the Faculty of Graduate Studies for acceptance, a thesis entitled, "Hydrothermal metamorphism of Telkwa Formation volcanics near Terrace, British Columbia" submitted by Kimberley June Freeman in partial fulfillment of the requirements for the degree of Master of Science.

Edward D. Ghent
Supervisor, E.D. Ghent, Geology and Geophysics

Peter Bayliss
P. Bayliss, Geology and Geophysics

D. A. Spratt
D.A. Spratt, Geology and Geophysics

April 17, 1986
Dated

K.A. Kerr, Chemistry and Physics

ABSTRACT

The Telkwa volcanics and associated rocks of the Coast Plutonic Complex in the Kleanza Creek - Kipulta Creek area near Terrace, British Columbia were subjected to a period of hydrothermal metamorphism after an earlier greenschist facies metamorphic event. The greenschist metamorphism may have been related to the intrusion of a quartz monzonite apophysis belonging to the Coast Plutonic Complex. The hydrothermal minerals include: albite, analcime, epidote, pumpellyite, prehnite, laumontite, orthoclase, chlorite and muscovite.

Detailed electron microprobe and x-ray diffraction studies were made on samples of epidote, pumpellyite, prehnite and laumontite. Increased Fe-content enlarges the unit cells of the former three minerals, but no systematic relationships could be deduced. Published determinative curves for epidote and prehnite compositions based on unit cell parameters are not valid. Laumontite samples from the study area are relatively pure (< 5 mole% substitution of alkalis for Ca^{2+}). The unit cells of these samples are smaller than those of some other natural zeolites which indicates a small amount of dehydration.

The nature of the authigenic suite of minerals was controlled by P, T, f_{CO2}, f_{H2O}, f_{O2}, and the activities of ionic species in the fluid such as Fe^{3+}, Ca^{2+}, Mg^{2+}, Na^{+}, K^{+}

and $SiO_{2(aq)}$. Maximum load pressure of approximately 1.5kb can be estimated from the presence of low-pressure assemblages such as laumontite-quartz, and from an estimated depth of burial of 6km. Hydrostatic pressure in veins and amygdales is estimated as $P_f=(1/2.6)P_s$. Comparison of the observed authigenic assemblages and published experimental stability studies of these minerals suggests a temperature range of 190°C to 255°C for the hydrothermal alteration.

Activities of ionic species were primarily controlled by the bulk composition of the host rocks. Basaltic hosts contain a wider range of authigenic calc-silicates than do the more felsic rocks. Potassium micas and feldspars are the major alteration products of the quartz monzonite.

Albitization was also controlled by bulk composition and permeability. The more permeable, more calcic basalts contain little fresh feldspar. Partial albitization of plagioclase was observed in the andesites and volcaniclastics. The albitization reaction was a probable source of Ca^{2+} ions during the hydrothermal metamorphism.

ACKNOWLEDGEMENTS

I am indebted to E.D. Ghent for suggesting this research project, his encouragement and his patience in seeing it to completion.

Thanks are extended to the following individuals for their time, advice and words of encouragement: P. Bayliss (x-ray diffraction techniques; editing; enjoyable bridge lessons); M.Z. Stout and J. Nicholls (moral support among other essentials); J. Machacek (revelation of the mysteries of the electron microprobe, and its protection); S. Resultay (high quality thin sections, probe sections and never forgetting cold-setting epoxy); K. Kerr (critical review of the manuscript and my diet); and D. Spratt (review of manuscript and sound advice). Thanks also to M. Mihalynuk for his "holistic" view of the Telkwa Formation, and to G.J. Woodsworth for his guidance in the field.

Other individuals not associated with the academics but equally important: R. Berg (typing and wine-soaked comfort); A. Flury (patience and wine); L. Melnychuk (providing a couch to sleep on); and most important to L.L. and R.A. Freeman - it's finally over, I couldn't have done it without you both.

Financial assistance for part of this research was provided by University of Calgary Graduate Teaching and Research Assistantships.

TABLE OF CONTENTS

ABSTRACT	iii
ACKNOWLEDGEMENTS	v
LIST OF TABLES	ix
LIST OF FIGURES	xi
LIST OF PLATES	xiii
LIST OF SYMBOLS AND ABBREVIATIONS	xv
INTRODUCTION AND GENERAL GEOLOGY	1
Introduction	1
Aim of Study	8
Geologic Setting	9
PETROGRAPHY OF ROCKS FROM THE KLEANZA CREEK - KIPULTA CREEK AREA	12
Introduction	12
Keap Creek Amygdaloidal Basalt	13
Kipulta Porphyritic Basalts	27
Volcaniclastics	29
Andesite	34
Kleanza Creek Pluton	35
Dikes and Large-scale Hydrothermal Veins	39
Paragenesis of Secondary Minerals	41
Actinolite	41
Albite	42
Analcime	42
Calcite	42

Chlorite 43
Clinopyroxene 44
Epidote 44
Hematite and Goethite 45
Laumontite 45
Muscovite 46
Potassium Feldspar 47
Prehnite 47
Pumpellyite 48
Quartz 49
Serpentine 49
AUTHIGENIC MINERALOGY 50
Electron Microprobe Techniques 50
X-ray Diffraction Analysis 52
Epidote - Crystallography 55
Epidote - Composition 61
Prehnite - Crystallography 68
Prehnite - Composition 69
Pumpellyite - Crystallography 73
Pumpellyite - Composition 78
Laumontite - Crystallography and Composition 79
PHYSICAL AND CHEMICAL CONDITIONS OF METAMORPHISM 89
Introduction 89
Estimate of Metamorphic Pressure 96
Estimate of Metamorphic Temperature 99
Effect of Bulk Composition on the Mineral 104

Assemblages

Fluid Composition - Activity of Ionic Species 106

Fluid Composition - Fugacities of Gaseous Components 122

Albitization and Permeability 128

CONCLUSIONS 134

Conclusions 134

PLATES 136

LIST OF REFERENCES 145

LIST OF TABLES

Table		Page
2.1	Sample Lithologies	14
2.2	Secondary Mineralogy	21
2.3	Classification of Volcaniclastics	31
3.1	Standards used in microprobe analyses	51
3.2	Precision and detection limits of microprobe analyses.	53
3.3	Unit cell - composition data for epidote	58
3.4 (A)	Electron microprobe analyses of epidote: Meta-basalts	63
3.4 (B)	Electron microprobe analyses of epidote: Volcaniclastics and andesites	65
3.5	Unit cell - composition data for prehnite	70
3.6	Electron microprobe analyses of prehnite	71
3.7	Distribution coefficients of co-existing prehnite and epidote from low-grade metamorphic rocks and experimental studies	74
3.8	Unit cell - composition data for pumpellyite	77
3.9	Electron microprobe analyses of pumpellytie	80
3.10	Representative electron microprobe analyses of authigenic minerals from Kleanza Creek-Kipulta Creek area	84
3.11	Unit cell - composition data for laumontite	87
3.12	Electron microprobe analyses of laumontite	88
4.1	Entropy values for prehnite used in Figure 4.1	93
4.2	Ordering parameter for epidote as a function of temperature	95
4.3	List of reactions in the system Na_2O-K_2O-Al_2O_3-SiO_2-H_2O used to produce curves in Figures 4.4 and 4.5	107

4.4	Thermodynamic data used in calculations	110
4.5	Electron microprobe analyses of partially albitized plagioclase grains.	131

LIST OF FIGURES

Figure		Page
1.1	Location and geological setting of study area.	2
1.2	Detailed geology of the Terrace Map Area around Kipulta Creek.	4
2.1	Map of sample locations in the Kleanza Creek-Kipulta Creek study area.	16
2.2	Sketch of the crystallization sequence of amygdaloidal phases in the meta-basalts.	25
3.1	X-ray determinative curve for epidote compositions.	59
3.2	AFM plot of epidote and prehnite compositions from the Kleanza Creek - Kipulta Creek area.	62
3.3	Electron microprobe traverse of an amygdaloidal epidote grain	67
3.4	AFM plot of pumpellyite compositions from the Kleanza Creek - Kipulta Creek area.	83
4.1	P-T curves for the reaction pr=zo+gr+q.	92
4.2	Experimental P-T stability curves for lawsonite, laumontite, wairakite and heulandite.	97
4.3	P-T diagram adapted from Liou et al. (1985) showing the distribution of phases in the system $CaO-MgO-Al_2O_3-SiO_2-H_2O$ at low pressures and temperatures.	102
4.4 (A)	Reaction curves for the system $K_2O-Al_2O_3-SiO_2-H_2O$.	108
4.4 (B)	Reaction curves for the system $Na_2O-Al_2O_3-SiO_2-H_2O$.	108
4.4 (C)	Experimental log m_{KCl}/m_{HCl} versus log m_{NaCl}/m_{HCl} relations for the system $Na_2O-K_2O-Al_2O_3-SiO_2-H_2O$, at P=1 kb, T=500°C.	109

4.5	Calculated log (a_{K+}/a_{H+}) versus log (a_{Na+}/a_{H+}) relations for the system Na_2O-K_2O- Al_2O_3-SiO_2-H_2O.	111
4.6	Activity - temperature diagram for an aqueous phase coexisting with albite, K-feldspar, muscovite, quartz and epidote solid solutions.	114
4.7	Phase relations of the system CaO-Al_2O_3-SiO_2-H_2O at P_f=P_s=1 kb in the presence of quartz and an aqueous solution.	115
4.8	Phase relations in the system CaO-Fe_2O_3-Al_2O_3-SiO_2-HCl-H_2O in the presence of quartz and an aqueous solution at P_f=1 kb, T=400 C.	116
4.9	Phase relations in the system CaO-Al_2O_3-SiO_2--H_2O as a function of log (a_{Ca} /a_{H+}) and log $a_{SiO(aq)}$ for temperatures of (A) 200°C and (B) 300°C and pressures corresponding to P_{H2O} along the liquid-vapour boundary of H_2O as calculated by Bird et al. (1984).	119
4.10	Isopleths of quartz solubility expressed as log $m_{SiO2\ (aq)}$ and temperature.	121
4.11	Log fo_2 - T diagram for the garnet-in and prehnite-out reactions of Liou et al. (1983).	123
4.12	Schematic isobaric isothermal μ_{CO2}-μ_{H2O} diagram, after Coombs et al. (1970).	127

LIST OF PLATES

Plate			Page
1	A	Photomicrograph of sample 1FL2 showing pyroxene pseudomorphed by hematite	137
	B	Photomicrograph of sample GT19A2 showing pumpellyite replacement of plagioclase	137
	C	Photomicrograph of sample 1FL1 showing olivine pseudomorphed by hematite and epidote	137
	D	Thick margin of iron oxides surrounding amygdale containing pumpellyite, prehnite and laumontite in sample GT19E	137
	E	Photomicrograph of sample GT19B under plane-polarized light	137
	F	Photomicrograph of sample GT19B under cross-polars	137
2	A	Fiamme texture in sample 13FL1	139
	B	Photomicrograph of fibrous actinolite and hematite in sample 16FL1	139
	C	Photomicrograph of allotriomorphic granular texture in sample 18FL2	139
	D	Photomicrograph of graphic granite texture in sample 10FL2	139
	E	Photomicrograph of fresh hornblende and altered biotite in sample 18FL2	139
	F	Photomicrograph of altered hornblende in sample 18FL2	139
3	A	Vein of analcite + quartz in sample 16FL2	141
	B	Photomicrograph of amygdale of epidote, diopside and calcite in sample 5FL4	141
	C	Photomicrograph of epidote grains pseudomorphing a plagioclase phenocryst in sample 3FL2	141
	D	Amygdale of epidote in GT19F	141
	E	Photomicrograph of amygdale of laumontite and prehnite in sample 2FL1 showing broadened cleavage in laumontite	141

Plate		Page
3 F	Prehnite "sunflowers" in amygdale in sample GT19B	141
4 A	Photomicrograph of epidote mantled by pumpellyite needles in amygdale in sample GT19F	143

LIST OF SYMBOLS AND ABBREVIATIONS

The symbols and abbreviations listed here for rock-forming minerals are used throughout this volume. Readers are referred to Kretz (1983) for the symbols currently preferred by the editors of American Mineralogist.

	Mineral Name	Ideal Formula
ab	albite	$NaAlSi_3O_8$
act	actinolite	$Ca_2(Mg,Fe)_5Si_8O_{22}(OH)_2$
an	anorthite	$CaAl_2Si_2O_8$
anal	analcime	$NaAlSi_2O_6 \cdot H_2O$
andal	andalusite	Al_2SiO_5
cc	calcite	$CaCO_3$
chl	chlorite	$(Mg,Al,Fe)_6(Si,Al)_4O_{10}(OH)_8$
cz	clinozoisite	$Ca_2Al_3Si_3O_{12}(OH)$
ep	epidote	$Ca_2(Al_2Fe^{3+})AlSi_3O_{12}(OH)$
gar	garnet group	$Ca_3(Fe,Al)_2Si_3O_{12}$
goe	goethite	α-$FeO(OH)$
gr	grossular	$Ca_3Al_2Si_3O_{12}$
hem	hematite	Fe_2O_3
heul	heulandite	$CaAl_2Si_7O_{18} \cdot 6H_2O$
kaol	kaolinite	$Al_2Si_2O_5(OH)_4$
Kspar	K-feldspar group	$KAlSi_3O_8$
lm	laumontite	$CaAl_2Si_4O_{12} \cdot 4H_2O$
lws	lawsonite	$CaAl_2Si_2O_7(OH)_2 \cdot H_2O$
marg	margarite	$CaAl_2(Al_2Si_2)O_{10}(OH)_2$
mont	montmorillonite	$Na_{0.3}(Al,Mg)_2Si_4O_{10}(OH)_2 \cdot nH_2O$
mt	magnetite	Fe_3O_4
musc	muscovite	$KAl_2(Si_3Al)O_{10}(OH)_2$

or	orthoclase	$KAlSi_3O_8$
parag	paragonite	$NaAl_2(Si_3Al)O_{10}(OH)_2$
ps	pistacite	variety of epidote; commonly used to denote mole% $Ca_2Fe_3Si_3O_{12}(OH)$ in epidote solid-solutions
plag	plagioclase	$NaAlSi_3O_8$-$CaAl_2Si_2O_8$
pr	prehnite	$Ca_2Al_2Si_3O_{10}(OH)_2$
pu	pumpellyite	$Ca_4Al_4(Al_{2-x-z}Fe_xMg_z)Si_6O_{21}(OH)_7$
pyroph	pyrophyllite	$Al_2Si_4O_{10}(OH)_2$
q	quartz	SiO_2
ser	sericite	generic term for fine-grained mica of unkown composition, usually muscovite, but may be paragonite or illite
serp	serpentine	group of minerals of the general formula $A_3Si_2O_5(OH)_4$, A=Mg,Fe^{2+},Ni
st	stilbite	$CaAl_2Si_7O_{18}\cdot 7H_2O$
tr	tremolite	$Ca_2Mg_5Si_8O_{22}(OH)_2$
ural	uralite	descriptive term for fibrous blue-green amphibole
wr	wairakite	$CaAl_2Si_4O_{12}\cdot 2H_2O$
zo	zoisite	$Ca_2Al_3Si_3O_{12}(OH)$

AFM	Aluminum - Iron - Magnesium, Al_2O_3 - Fe_2O_3 - MgO
CASH	Calcium - Aluminum - Silica - H_2O, Ca^{2+}-Al^{3+}-SiO_2-H_2O

HM	Hematite-Magnetite buffer, Fe_2O_3-Fe_3O_4
NNO	Nickel-Nickel Oxide buffer, Ni-NiO
QFM	Quartz-Fayalite-Magnetite buffer, SiO_2-Fe_2SiO_4-Fe_3O_4
IM	Iron-Magnetite buffer, Fe-Fe_3O_4
IW	Iron-Wustite buffer, Fe-FeO
MW	Magnetite-Wustite buffer, Fe_3O_4-FeO

Glossary of Symbols and Abbreviations

a_i	activity of species i
(aq)	aqueous phase
f	fluid
f_i	fugacity of gaseous component i
K	equilibrium constant
m_i	molality of i
sat´n	saturation
ΔG^o_r	standard molal Gibb´s free energy of reaction
ΔH^o_f	standard molal enthalpy of formation from the elements at 298.15K, 1bar
ΔH^o_r	standard molal enthalpy of reaction
ΔS^o_f	standard molal entropy of formation from the elements at 298.15K, 1bar
ΔS^o_r	standard molal entropy of reaction
S^o	third law entropy
$\bar{V}$	standard molal volume
$\Delta \bar{V}^o_r$	standard molal volume of reaction

Γ_i	fugacity coefficient of species i
	ordering parameter for epidote
μ_i	chemical potential of species i
P_f	fluid pressure
P_{load}	load (geostatic pressure)
X_{Fe}	mole fraction of Fe in mineral; X_{Fe}=Fe/Fe+Al
keV	10^3 electron volts
μA	10^{-6} amperes
b.d.	below detection - detection limits given in Table 3.2
n.a.	not analyzed
XRD	x-ray diffraction
I-BG	intensity minus background
gm (g)	groundmass; (Table 2.1)
pheno (p)	phenocryst; (Table 2.1)
amyg (a)	amygdale; (Table 2.1)
fr (f)	fracture; (Table 2.1)
83-15F	sample location
15FL2	sample identification
82-GT-19	location sampled by Dr. E.D. Ghent in July, 1982; corresponds to author's 83-1F locality
GT19A	sample identification

CHAPTER 1 INTRODUCTION and GENERAL GEOLOGY

Introduction

The Kleanza Creek - Kipulta Creek study area is located approximately 35km northeast of Terrace, British Columbia (Figures 1.1, 1.2). It is situated between the Bornite and O.K. Ranges, close to the western margin of the Intermontane Belt. The study area can be accessed by logging roads leading in from Highway 16.

Prospecting and mining have been important in the development of the Terrace Map area and in the surveying of the area around Kleanza Creek (Duffell and Souther, 1964). Placer gold deposits along Kleanza Creek were worked as early as 1884. By 1914, copper lode deposits had been discovered at the head of Kleanza Creek. Most of the properties have been idle since World War II. Gold, silver and copper deposits in this region were generally associated with large pyrite-bearing quartz veins.

Duffell and Souther (1964) completed the first detailed mapping of the Terrace Map area in 1955. They assigned the volcanic rocks of the Kleanza Creek - Kipulta Creek area to the lower division of the Jurassic Hazelton Group. This division consisted of massive breccias, minor andesitic flows and intercalated fine clastic material. They noted the alteration of the andesites to chlorite, epidote, uralite and saussuritized plagioclase and the presence of amygdales

Figure 1.1 Location and geologic setting of the study area. Adapted from Carter (1982) and Tipper and Richards (1976).

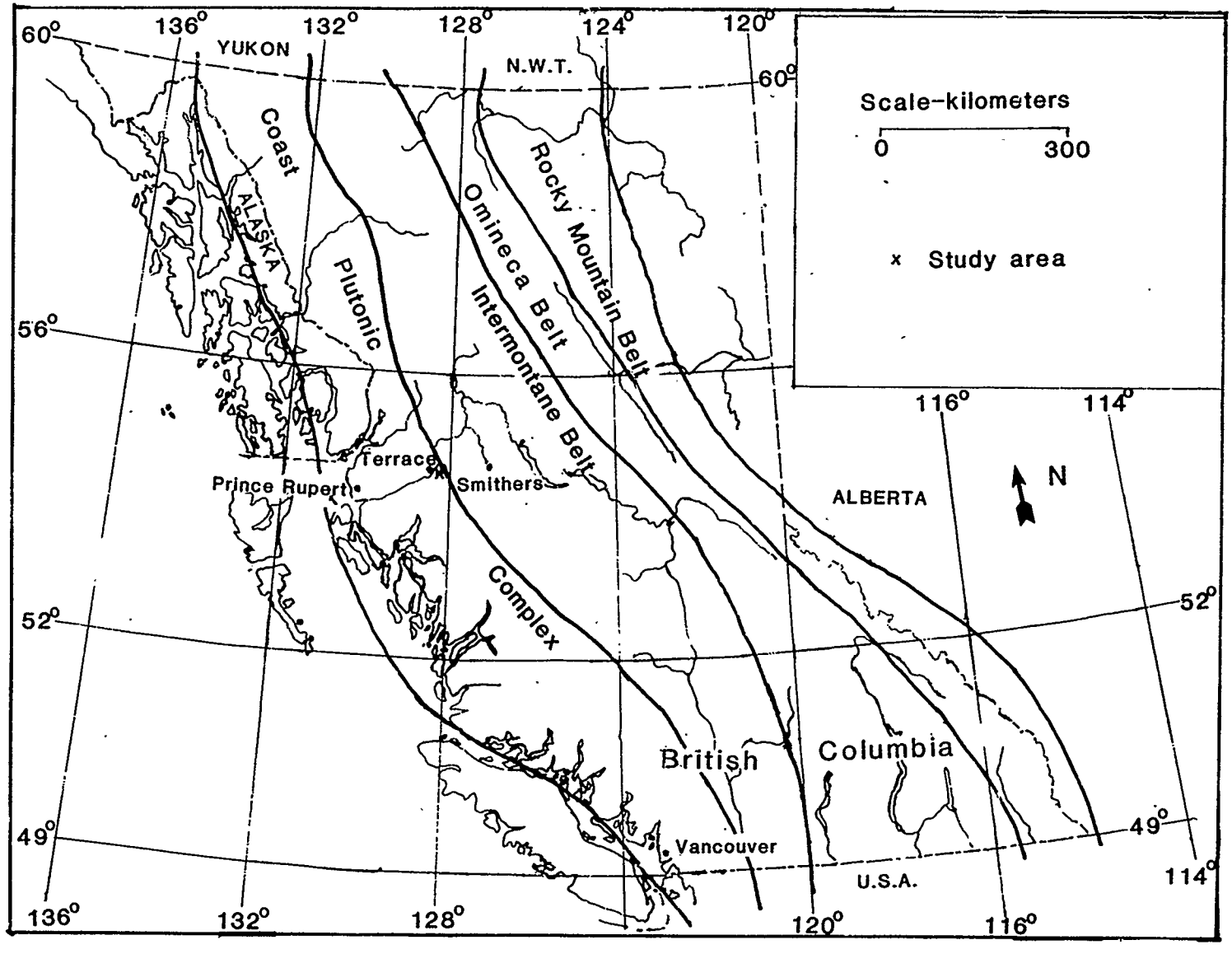
60°
136°
132°
128°
124°
120°
YUKON
N.W.T.
Coast
ALASKA
Plutonic
Omineca Belt
Intermontane Belt
Rocky Mountain Belt
Scale-kilometers
0
300
x Study area
56°
116°
114°
Terrace
Prince Rupert
Smithers
ALBERTA
N
52°
Complex
British
Columbia
49°
Vancouver
U.S.A.

Figure 1.2 Detailed geology of the Terrace Map Area around Kleanza Creek. Adapted from Woodsworth et al. (1985).

Legend

- ○ Lower Permian cherty volcanics, tuff, breccia
- ● Lower Permian limestones
- Triassic argillite, chert
- ▲ Early to Middle Jurassic granodiorite to granite
- ■ Lower Sinemurian Telkwa Formation calc-alkaline volcanics
- □ Lower Sinemurian rhyolitic breccia, tuff
- △ Late Cretaceous, pre- to synkinematic granodiorite, tonalite
- ▽ Late Cretaceous, post-tectonic quartz diorite, diorite, granodiorite
- ◆ Late Cretaceous to Early Tertiary pre- to post-kinematic granodiorite, tonalite ,granite
- ▼ Tertiary post-tectonic granite, granodiorite; commonly leucocratic and miarolitic
- ◇ Tertiary post-tectonic granite, granodiorite; generally fresh
- ✪ City
- ▨ Kleanza Creek-Kipulta Creek study area
- Limit of overburden mapping
- Contact (mapped; approximate)

Thrust fault

Fault or shear; nature unknown

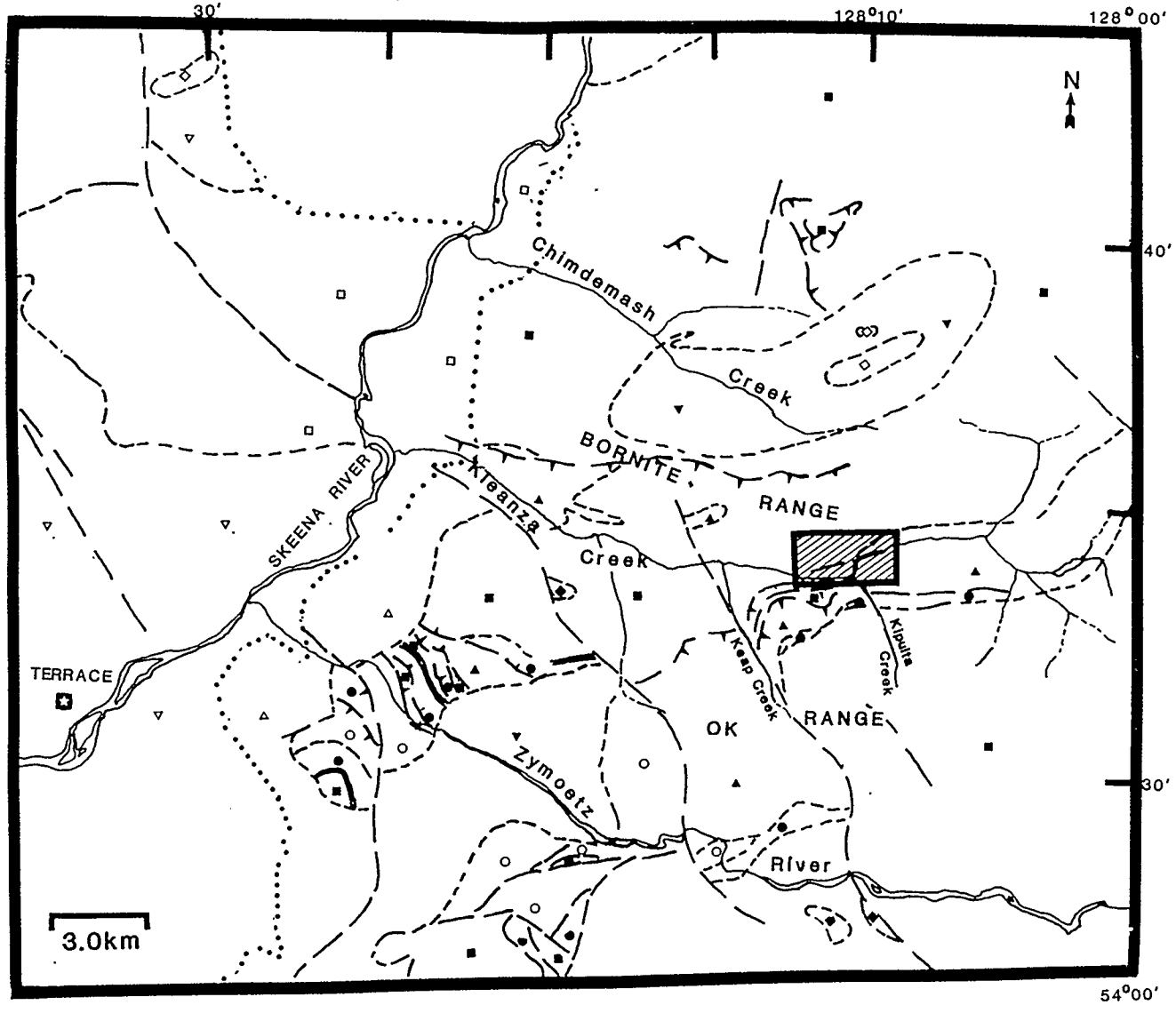
30'
128°10'
128°00'
N
40'
Chimdemash
Creek
BORNITE
RANGE
SKEENA RIVER
Kleanza
Creek
TERRACE
Keep Creek
Kipulis
Creek
OK
RANGE
Zymoetz
River
30'
3.0km
54°00'

consisting of calcite, epidote or quartz and rare pink zeolite. The plutonic rocks along Kleanza Creek were assigned to the pink granodiorite facies of the Coast Plutonic Complex. These rocks also contained secondary chlorite, epidote and muscovite. The authigenic minerals were assumed to be the result of deuteric alteration.

Tipper and Richards (1976) produced a more detailed stratigraphy of the Hazelton Group in north-central British Columbia and discussed the Jurassic history of the area. On the basis of their stratigraphy and the petrography of samples collected in the study area during July 1983, the volcanics and volcaniclastics of the Kleanza Creek - Kipulta Creek area represent the Telkwa Formation of the Hazelton Group. Assignment to a particular facies within the Formation is difficult due to the lack of observed contacts in the field and the lithologic similarity of the two subaerial facies, the Howson and Bear Lake facies. Tipper and Richards (1976) noted the presence of zeolite-facies mineral assemblages in the Howson facies and proposed a paleo-hot spring origin for the metamorphism contemporaneous with the volcanism.

Dudley (1983) also examined the zeolitization of the Howson subaerial facies in the Smithers Map area. He described the stratigraphy of the facies, lack of metamorphic fabric in the volcanics, and the distribution of the zeolites within each stratigraphic section and within individual

samples. He concluded that the metamorphism was the result of a convecting hydrothermal cell, and that temperature, f_{CO2}, permeability and bulk rock composition were among the controls on the zeolite assemblages.

Duffell and Souther's (1964) observations of the ubiquitous presence of large quartz veins, the hydrous authigenic minerals, and lack of metamorphic fabric in most rocks in the Kleanza Creek - Kipulta Creek area lead to the hypothesis that the metamorphism in this area was related to hydrothermal metamorphism rather than burial metamorphism.

Aim of Study

The purpose of this study was to determine if the alteration was due to hydrothermal metamorphism and to investigate the relationship between the alteration and the intrusion of the Kleanza Creek apophysis and the regional sub-greenschist to greenschist facies metamorphism.

The petrography of the volcanic and plutonic rocks and parageneses of the authigenic minerals were studied to determine metamorphic grade and the number and timing of metamorphic events. Compositions of epidote, laumontite, analcime, pumpellyite, chlorite and prehnite were obtained using an electron microprobe to determine the physical and chemical conditions of metamorphism, specifically: P, T, f_{O2}, f_{CO2}, a_{SiO2} and the activities of ionic species in solution. The effects of bulk rock composition and permeability on

low-grade metamorphic assemblages were also examined. Finally the significance of albitization in the volcanics and plutonic rocks is discussed.

Samples of prehnite, epidote, pumpellyite and laumontite were selected to determine the relationship between mineral composition and unit cell size. These data are compared to published results from similar areas (e.g., the Karmutsen Volcanics) to see whether they were typical of sub-greenschist facies or greenschist facies metamorphism. Partition coefficients of Fe^{+3} between these phases are also compared to data from other areas of low grade metamorphism.

Geologic Setting

During the Late Triassic of north-central British Columbia the alkaline basalt and andesite island-arc volcanics of the primarily submarine Takla Group were deposited (Tipper and Richards, 1976). Uplift of the Pinchi belt during Late Triassic to Early Jurassic produced two distinctive basins: the Whitehorse - Quesnel troughs to the north and east; and the Hazelton trough to the south. In Early to mid-Jurassic time, the calc-alkaline island arc basalt to rhyolite volcanics and eugeosynclinal sediments of the Hazelton Group were deposited in the Hazelton trough. The Hazelton trough was succeded by the Bowser Basin, which was produced by the uplift of the Skeena Arch. The development of the Skeena Arch and the deposition of the deltaic clastic

sediments of the Bowser Lake Group in Middle to Late Jurassic marked the end of island-arc volcanism in north-central British Columbia.

The subaerial Telkwa Formation is the oldest part of the Hazelton Group. It is of Sinemurian to Pliensbachian in age. Tipper and Richards (1976) divided it into five facies. Of these, the Bear Lake subaerial facies is the oldest and outcrops primarily to the northeast of central British Columbia, around Bait Range. The Howson subaerial facies is the youngest and outcrops predominantly in the southwest around the Howson and Telkwa Ranges. The Telkwa Formation is intruded by the coeval Lower Jurassic Topley Intrusions throughout north-central British Columbia.

In the Terrace Map area, the Telkwa Formation is in contact with the Coast Plutonic Complex (abbreviated the CPC). The CPC consists of three zones, which are younger and more potassic eastward (Carter, 1982). The Kleanza Creek apophysis is an eastward extension of the main mass of the eastern zone. The dominant rock type of the eastern zone of the CPC is quartz monzonite, as observed in the study area. K-Ar dates indicate a Middle Eocene (43 to 51 m.y.) age of emplacement of the granitic rocks of the eastern zone (Carter, 1982). Carter (1982) observed that contacts between granitic rocks and Mesozoic layered rocks are generally sharp and that evidence of forceful emplacement is common. Slickensides and sheared rock near volcanic - plutonic

contacts in the Kleanza Creek - Kipulta Creek area are typical evidence of forceful emplacement.

The Intermontane Belt near Terrace is dominated by brittle deformation and block faults (Woodsworth et al., 1983). Most fault movement appears to be Eocene. The presence of a cooling pluton, and fault movement would provide a heat source and fluid conduits necessary to produce the typically hydrothermal assemblages in the plutonic and volcanic rocks of the Kleanza Creek - Kipulta Creek area. This would indicate a Mid- to Late Eocene or younger age for the hydrothermal alteration.

CHAPTER 2 PETROGRAPHY OF ROCKS FROM THE KLEANZA CREEK - KIPULTA CREEK AREA

Introduction

Dudley (1983) and Tipper and Richards (1976) describe the Telkwa Formation as a calc-alkaline volcanic suite. Dudley (1983) used the classification scheme of Carmichael, Turner and Verhoogen (1974) to subdivide the facies into three lithologic units: 1)olivine basalt; 2)andesite; and 3)rhyolite. Dudley (1983) also described a fourth, volcaniclastic, unit.

Due to the high degree of alteration in most samples in the study area, it is difficult to use a classification scheme such as Carmichael, Turner and Verhoogen (1974), which is based on volume percent and identity of mafic silicates and composition of feldspars. Samples from this area contain little (<<20%) unaltered feldspar; generally plagioclase has been altered to albite and/or muscovite and other secondary minerals. Olivine is generally pseudomorphed by thick rims of hematite, with epidote, chlorite or serpentine comprising the rest of the grain. Clinopyroxene is generally altered similarly to olivine, but fresh clinopyroxene is present at 83-4F, 83-5F and 83-19F.

Dudley (1983) was able to obtain relatively fresh samples of each lithology, and noted that the colour indices of the andesites were similar to and slightly lower than those of

the basalts. He also noted that olivine pseudomorphs were not present in the andesites. These criteria were used to subdivide the flow units into olivine basalts and andesites. The basalts are porphyritic and have been subdivided into amygdaloidal and porphyritic units based on the presence or absence respectively of amygdales (Table 2.1).

Other lithologies observed in the Kleanza Creek - Kipulta Creek area are volcaniclastics, basaltic dikes, and quartz monzonite. These units were described in considerable detail by Duffell and Souther (1964). Outcrop localities of all units are given in Table 2.1 and Figure 2.1.

Each sample was examined using optical microscopy, powder x-ray diffraction, and reflecting microscopy when necessary. Detailed descriptions of the form, size and contact relationships of the secondary minerals are provided in a later section of this chapter.

Keap Creek Amygdaloidal Basalt

Amygdaloidal basalt flows outcrop sporadically 1km east of Keap Creek for approximately 350m along Kleanza Creek (Figure 2.1). This olivine basalt weathers reddish-grey and has numerous amygdales and filled fractures. The lack of observed contact relationships and poor quality of outcrop impedes recognition in the field of the number of flows present. Due to the high degree of alteration and rough similarity in bulk composition and nature of alteration

Table 2.1 Sample Lithologies

Sample	Amygdaloidal Basalt	Porphyritic Basalt	Andesite	Volcaniclastic	Quartz Monzonite	Dike
82-GT-19A	X					
-19B	X					
-19C	X					
-19D	X					
-19E	X					
-19F	X					
-19G	X					
-19H	X					
-19HZ	X					
83-1F-L1	X					
-L2	X					
83-2F-L1	X					
83-3F-L1	X					
-L2				X		
-L3				X		
-L4				X		
83-4F-L1						X
-L2		X				
-L3	X					
-L4		X				
83-5F-L1		X				
-L2						X
-L3						X
-L4	X					
83-6F-L1					X	
83-7F-L1						X
-L2	X					
-L3			X			
-L4			X			
83-8F-L1			X			
-L2				X		
-L3			X			
83-9F-L1			X			
83-10F-L1				X		
-L2					X	
83-11F-L1					X	
-L2					X	

Table 2.1 Sample Lithologies (cont'd)

Sample	Amygdaloidal Basalt	Porphyritic Basalt	Andesite	Volcaniclastic	Quartz Monzonite	Dike
83-12F-L1				X		
-L2				X		
-L3			X			
83-13F-L1				X		
-L2				X		
83-14F-L1				X		
83-15F-L1				X		
-L2				X		
-L3				X		
83-16F-L1			X			
-L2			X			
83-17F-L1			X			
-L2			X			
83-18F-L1					X	
-L2					X	
83-19F-L1					X	
-L2						X
83-20F-L1			X			
-L2			X			

Figure 2.1 Map of the sample locations in the Kleanza Creek - Kipulta Creek study area.

---- Inferred contact between quartz monzonite and volcanics

X Sample location

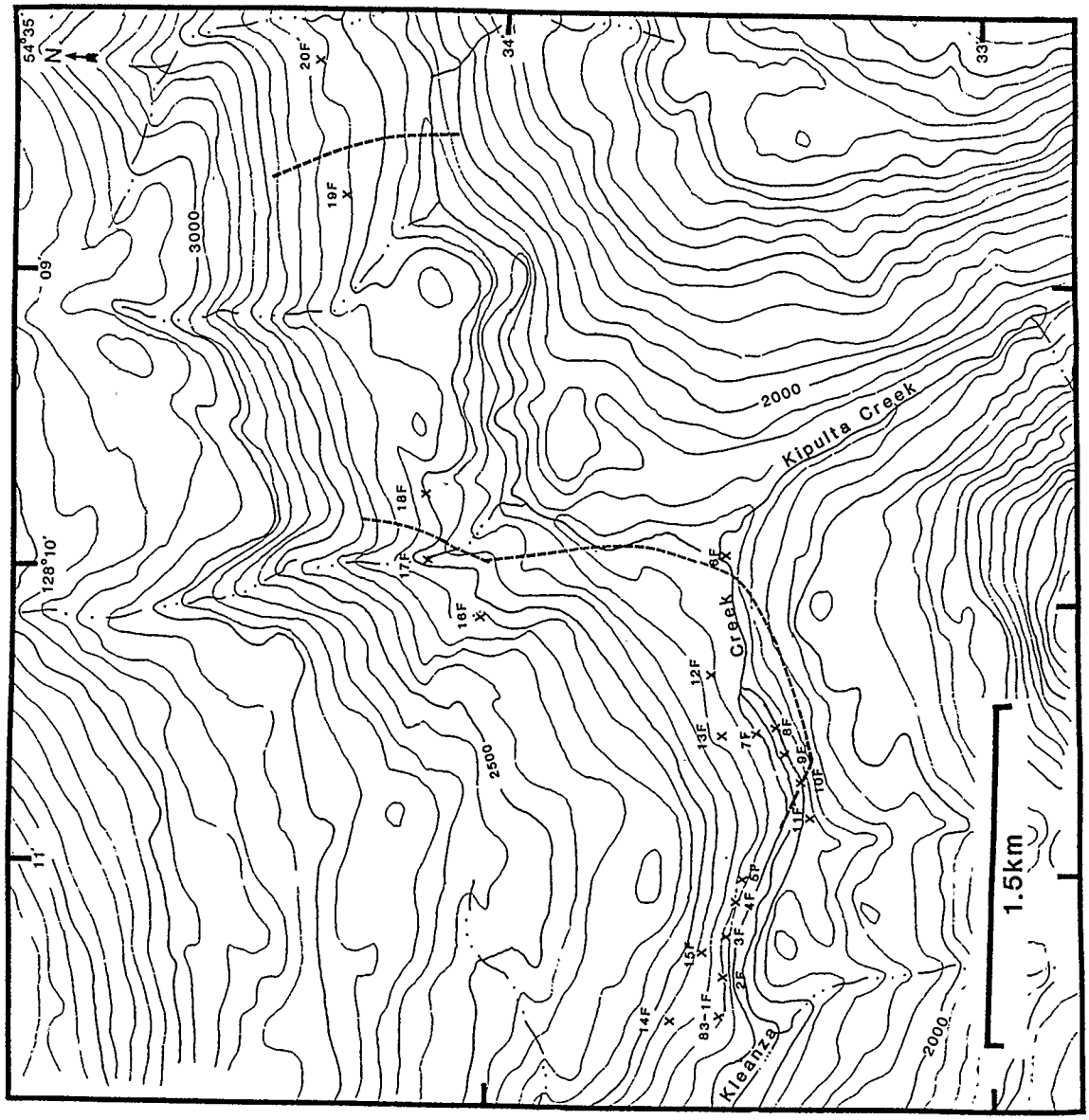
54°35'
N
09'
128°10'
11'
34'
33'
3000
2500
2000
2000
20F
19F
18F
17F
16F
15F
14F
13F
12F
11F
10F
9F
8F
7F
6F
5F
4F
3F
2F
1F
83-1F
Kipulta Creek
Creek
Kleanza
1.5km

distinguishing between flows in thin section is not possible with any degree of certainty.

Olivine and pyroxene pseudomorphs and glomeroporphyritic plagioclase phenocrysts are set in an aphanitic groundmass of euhedral trachytic plagioclase laths and anhedral opaques, or intersertal devitrified glass (Plate 1A). Plagioclase has poikiolitic inclusions of opaques. Reflecting microscopy was used to identify the opaques as magnetite, generally partly altered to hematite. Typical primary modal mineralogy is: 15-20% magnetite, 5% olivine and pyroxene, 30-40% groundmass plagioclase, and 5-10% plagioclase phenocrysts.

As noted above, the most striking feature of the rocks in the project area is the high degree of alteration. Individual plagioclase phenocrysts have a cloudy surface appearance produced by pseudomorphic replacement by albite + epidote $\pm$ chlorite, albite + pumpellyite $\pm$ epidote, or albite + chlorite. The alteration tends to be spotty and comprises 1% to 90% of individual grains in each sample (Plate 1B). Relic albite twinning, oscillatory zoning on an overall normal trend and normal zoning are generally well-preserved. Alteration of normally zoned plagioclase crystals is generally concentrated in the more anorthitic cores of these grains (Plate 1B).

Olivine and pyroxene phenocrysts in these samples are completely pseudomorphed by hematite + chlorite $\pm$ epidote $\pm$ quartz $\pm$ pumpellyite. Serpentine alteration was identified

in only one sample (GT19F), by the strong 7.10 Å x-ray diffraction peak, lack of a 14Å peak, and its strong green colour. It occurs with hematite. Hematite primarily occurs as a rim (~0.02mm wide) outlining these phenocrysts and along partings within the grains. The preserved characteristic subhedral {111} form and rectangular outlines are used to identify olivine and pyroxene respectively (Plate 1A,C). The high degree of alteration of these phases makes their positive identification in the groundmass impossible.

Pseudomorphic replacement of groundmass plagioclase is similar to the alteration of plagioclase phenocrysts in each sample, but is generally less extensive.

Groundmass magnetite is altered to hematite ± goethite, the latter recognized by strong 4.18Å, 2.45Å and 2.69Å x-ray diffraction peaks. Microprobe analyses indicate that the cores of approximately 10% of the opaque grains consist of sphene. These intergrowths are similar to those described by Kuniyoshi and Liou (1976) in the Karmutsen volcanic rocks of Vancouver Island, B.C..

Intersertal glass is devitrified and, along with other fine grained material, is replaced by chlorite and hematite. Margins of hematite and devitrified glass, approximately 0.6mm wide, are present around amygdales in 3 samples (Plate 1D).

Amygdales range from 1-80% of the volume of individual samples, but commonly account for 5-15% of volume. Amygdales

are roughly spherical, slightly elongate and range in size from less than 1.0mm to 15mm in diameter. Amygdale mineralogy consists of quartz - chlorite - pumpellyite - epidote - laumontite - prehnite and calcite (Table 2.2).

Individual amygdales may have any or all of these phases in any combination, but some general observations are made below:

1) chlorite is generally limited to the rims of amygdales where phases other than quartz are present;

2) quartz also occurs as a `rim phase´ but can occur throughout the amygdale;

3) pumpellyite tends to be concentrated near the rim of the amygdale in the presence of other phases such as epidote;

4) epidote occurs throughout the amygdale, while prehnite and laumontite tend to be concentrated toward the center.

These observations lead to a rough crystallization sequence of chlorite + quartz, pumpellyite, epidote, laumontite and prehnite. Figure 2.2 is a diagram which shows this general crystallization sequence. When present, calcite occurs throughout the amygdale, possibly indicating continuous to late stage crystallization.

Fractures in this unit are generally filled with quartz, calcite $\pm$ epidote, or chlorite (Table 2.2). Laumontite, prehnite, pumpellyite and minor albite are also present.

Three samples of Keap Creek amygdalolidal basalt show very unusual alteration: GT19B, GT19D and 3FL1. In sample

Table 2.2 Secondary Mineralogy

Sample	Cc	Q	Chl	Musc	Or	Ab	Lm	Pr	Pu	Ep	Act	Serp	Hem	Goe
GT-19A	a	a	pf			p	a	a	apg	apg			p	g
B	af							fp ga		ap			pg	
C		af				gpf	af	af	paf	gaf			g	
D		a				pg	a	apg		apg			g	g
E		a	pga			pg	a	a	a	pga			p	
F	a	a	ga			pg	a		pga	pga		p	p	g
G		af	paf			p	f	f	pgf	paf			pg	g
H			a			p			a	p			pg	g
HZ	a	a	ap			pg	a		pga	pga			p	
1F-L1	af		apg			pg				afpg			p	g
-L2	a	a	pa			pg	a	a	pag	ga			pg	g
2F-L1	a		pa	p		pg	a	af		apg			p	
3F-L1	f		pg	f	f	pg							g	g
-L2	pfa	pf a	pa	a	a	pfg				pfg			pg	
-L3	pf	pf g		p		p				pg			p	
-L4		gp	gp	p		p				pg			p	g

Table 2.2 Secondary Mineralogy (cont'd)

Sample	Cc	Q	Chl	Musc	Or	Ab	Lm	Pr	Pu	Ep	Act	Serp	Hem	Goe
4F-L1	fp		apg				f		pg	pg		p	p	p
-L2	fg		gp			gp	f		p			g		
-L3	af		apg			pg		ap g	pg			g		
-L4	fpg	f	pg							pg			p	g
5F-L1		gf	p	p		p	f			pgf	p		p	
-L2			a				gp a	gp a	pa			g	g	
-L3			a				pg a	pf ga	pa			g	g	
-L4	fa	f	g				f	f		pga	a		g	g
6F-L1	f	f	p	p									g	g
7F-L1		f												
-L2			apg	pg		pg				pga				g
-L3			pg			p	a			pa	ga	p	p	g
-L4	gf	f	g	pg		pg				pgf			p	
8F-L1		af	pg af		f	pg				pgf				
-L2		pg	gp	p		p				p			p	g
-L3		fg	pg	pg		pg				pgf			g	

Table 2.2 Secondary Mineralogy (cont'd)

Sample	Cc	Q	Chl	Musc	Or	Ab	Lm	Pr	Pu	Ep	Act	Serp	Hem	Goe
9F-L1	f	gp	gp	p									p	g
10F-L1	f		p	p		p							g	
-L2	p		p	p		p				p	ural p		p	
11F-L1	f	f		p		p							p	
-L2	f	f		p		p							p	
12F-L1			p							p				
-L2			p							p				
-L3	f	f	p							p			p	
13F-L1	fg	fg		pf									p	
-L2	fg	fg		pf									p	
14F-L1	pg					p							p	
15F-L1	pf		pg	pg		pg				pfg			g	g
-L2	f	f	pg	p		p				pf			p	g
16F-L1	f	p	pg	pg		pf	anal f				g		g	g
-L2	f	p	pg			p					g		g	g

Table 2.2 Secondary Mineralogy (cont'd)

Sample	Cc	Q	Chl	Musc	Or	Ab	Lm	Pr	Pu	Ep	Act	Serp	Hem	Goe
17F-L1	f	gp f	gpf	pg		p				pg			g	g
-L2	f	f	fg	gp		p	anal f						g	g
18F-L1	pf	f	p	p		p					ural		p	
-L2	p			p		p					ural			
19F-L1			p	p		p				p	ural		p	
-L2	a	a	gap	p		p		a	p	p				
20F-L1	f	pg	g	pg		g					g		g	g
-L2	gf p	gf	g	gp		pg				g			g	g

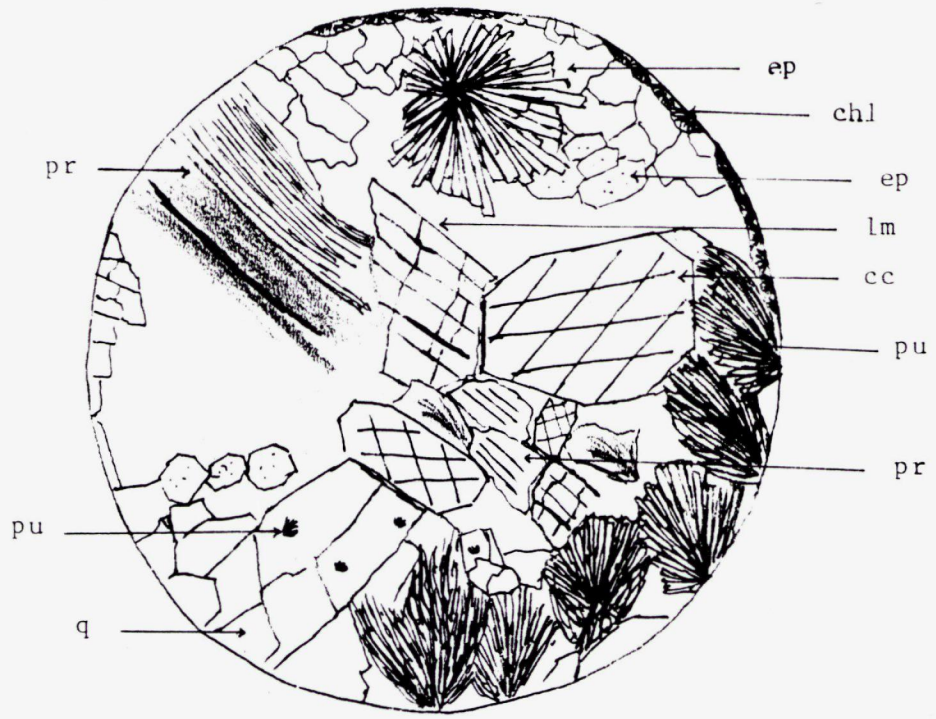

Figure 2.2 Sketch of the crystallization sequence of amygdaloidal phases in the meta-basalts. Detailed description is given in the text.

GT19B the mafic phenocrysts have been pseudomorphically replaced by hematite + chlorite + quartz as described above. All of the plagioclase in the sample has been pseudomorphed by prehnite and epidote (Plate 1E, 1F). The outlines of the groundmass laths are severely disrupted. The prehnite grains are xenoblastic, range in size from 50μm to 300μm and comprise ~80% of the total volume of the sample. The epidote grains are xenoblastic; their average grain size is approximately 50μm, and they account for less than 5% of the total alteration. Amygdale mineralogy in this sample consists of prehnite + epidote (Table 2.2). Detailed descriptions are given in the Paragenesis section of this chapter. Fractures in this sample range in diameter from 0.04mm to 0.25mm. The largest fractures contain prehnite ± calcite and are cut by later calcite-filled fractures.

Sample GT19D is extensively replaced by epidote. The basalt host consists of plagioclase phenocrysts pseudomorphed by epidote + albite in an intersertal groundmass of devitrified glass, hematite and pseudomorphed plagioclase laths. Approximately 60% of the fine-grained groundmass material has been altered to epidote + quartz + prehnite.

Amygdales comprise approximately 80% of the volume of this sample and range in diameter from 0.3mm to ~5.0mm. The amygdales contain quartz, epidote, prehnite and laumontite in decreasing order of abundance (Table 2.2). Detailed descriptions of the amygdale phases are provided in the

Paragenesis section of this chapter.

In sample 3FL1, muscovite pseudomorphs unidentifiable subhedral phenocrysts and also occurs with a pink K-feldspar (identified by strong 3.23Å, 3.33Å and 3.29Å x-ray peaks) in large amygdales where it appears to replace calcite. The groundmass material surrounding these amygdales is also strongly altered to muscovite.

Kipulta Porphyritic Basalts

Basalt flows sampled near Kipulta Creek at 83-4F and 83-5F are separated from those at 83-3F by 153m of intervening volcaniclastics and lack of outcrop (Figure 2.1). These rocks are less amygdaloidal than the Keap basalts and are generally more highly fractured. The outcrop at 83-4F is approximately 10m thick and occurs approximately 80m west of 83-5F. Contact between the units was not observed. Basalts from 83-4F have a strong green colour; 5FL1 is also green. Sample 5FL4 is similar in colouring to the red-grey Keap basalts. A light green basaltic dike ~2m thick intrudes into the red basalts at 83-5F.

The Kipulta basalts at 83-4F differ from the Keap Basalts in that primary clinopyroxene is preserved. Modal mineralogy of the green basalts at 83-4F is approximately 5-10% magnetite and/or hematite, 15-30% clinopyroxene (augite), 50-60% plagioclase, and ~1% olivine pseudomorphs. The

mineralogy of sample 5FL4 is similar, however, primary clinopyroxene is not preserved, and hematite is more abundant (~30%).

The alteration of the Kipulta basalts differs markedly at each outcrop. At 83-4F plagioclase is generally pseudomorphed by albite ± pumpellyite + epidote ± chlorite ± calcite. Plagioclase alteration at 83-5F generally consists of albite + muscovite ± epidote or chlorite ± sphene ± albite. Sample 4FL3 contains plagioclase pseudomorphically replaced by pumpellyite ± prehnite + albite ± chlorite. In this sample the dominant opaque phase is magnetite rather than hematite, possibly indicating a lower f_{O2} in the metamorphic fluid.

Olivine is pseudomorphed by serpentine at 83-4F, and by hematite + chlorite ± epidote at 83-5F. Clinopyroxene at 83-5F tends to have a more corroded appearance than in the samples from 83-4F. Fibrous green actinolite comprises as much as 15% of samples from 83-5F and is closely associated with large hematite grains, which have diffuse stringers extending into the amphibole. Epidote also appears with actinolite rimming hematite. These epidote grains are subidioblastic, have diffuse contacts with hematite, and sharp concave contacts with plagioclase.

Amygdales in 4FL1 consist of fibrous chlorite. Amygdales in sample 5FL4 are filled with diopside + calcite + epidote ± actinolite. All phases in the clinopyroxene-bearing amygdales are in sharp contact with each other.

Fractures in both units are filled with laumontite + quartz ± epidote, or prehnite + calcite ± epidote (Table 2.2). These filled fractures range in size from 50μm to 1cm in width.

Volcaniclastics

Volcaniclastics outcrop on two stratigraphic levels along Kleanza Creek. On the lower level (~1150 feet) (Figure 2.1) they are in sharp contact with the Keap basalts (83-3F), and andesites (83-8F) and are also in sharp contact with the Kleanza Creek pluton. Approximately 50m above this, volcaniclastics outcrop irregularly and are not observed in contact with any other lithology (Figure 2.1; 83-13F, 83-14F, 83-15F). The degree of fracturing in these latter rocks increases noticeably from west to east, towards the pluton.

The extent of volcaniclastic outcrop at the 1300 ft level may indicate the presence of either a pyroclastic flow or a lahar. Unfortunately, the outcrop's volcanic composition, presence of fiamme, subangular poorly sorted clasts, and lack of bedding are not especially characteristic of either type of deposit (Fisher and Schmincke, 1984. p.309 Table 11-3). These characteristics are however, sufficient to distinguish this layer from fluvial deposits of volcanic material (Fisher and Schmincke, 1984). Further detailed mapping would be required to adequately differentiate between a lahar and a pyroclastic flow.

The volcaniclastics in the Kleanza Creek area have been subdivided into breccias and tuffs (Table 2.3) based on the classification scheme of Schmid (1981), which refers to clast size. Breccias are easily recognized in the field because of the different colours of the clasts: generally grey or dark red. Tuffs are more difficult to identify in outcrop as they resemble porphyritic basalts.

The coarse tuffs consist of plagioclase and orthoclase (identified by length fast Carlsbad twinning and K-feldspar composition) crystals (~0.25 - ~1.5mm) in a fine matrix of quartz, feldspar and hematite. Average grain size of the matrix is approximately 50um. Altered mafic crystals are also present in 13FL1, 13FL2.

The alteration of the feldspars in the coarse tuffs is similar to that of the amygdaloidal basalts. Plagioclase has sharp relic albite twinning, and is pseudomorphically replaced by albite + muscovite $\pm$ chlorite. Orthoclase shows relic Carlsbad twinning and is replaced by muscovite.

Because the matrix material is extremely fine-grained, it was difficult to determine the exact nature of the matrix feldspar alteration. The feldspars have a cloudy surface, but appear less altered than the larger crystals.

Elongate lenses of quartz bound by hematite in 13FL1, and 13FL2 (Plate 2A), may represent the fiamme texture described by Dudley (1983). These lenses consist of up to 50% hematite and run subparallel to each other throughout the sample. The

Table 2.3 Classification of Volcaniclastics[1].

Sample	Clast Size	Classification
83-3F-L2	0.1mm - 3.5mm	Lapilli Tuff
-L3	20mm - 67mm	Pyroclastic Breccia
-L4	40mm - 70mm	Pyroclastic Breccia
83-8F-L2	10mm - 25mm	Lapilli Tuff
83-10F-L1	0.25-1.5mm	Coarse Tuff
83-12F-L1	0.1mm-3.2mm	Lapilli Tuff
-L2	0.3mm- 3.0mm	Lapilli Tuff
83-13F-L1	0.25mm-1.8mm	Coarse Tuff
-L2	0.2mm- 1.8mm	Coarse Tuff
83-14-L1	8mm-65mm	Pyroclastic Breccia
83-15-L1	10mm-21mm	Lapilli Tuff
-L2	10mm-32mm	Lapilli Tuff
-L3	10mm-20mm	Lapilli Tuff

1. After Schmid (1981).

matrix grains appear to be elongated approximately parallel to these lenses. This elongation may indicate flow and compression and/or welding (Fisher and Schmincke, 1984).

Calcite is present as tiny (~0.035mm wide) lenses of replacement of fine grained matrix material and also in calcite-filled fractures ~0.04mm wide cutting through the samples.

Subidioblastic tabular grains of epidote, approximately 0.02mm across replace fine-grained matrix material in sample 10FL1.

Most of the lapilli tuffs are composed of lithic clasts ranging in composition from intermediate to mafic in individual samples. In sample 15FL1, the clasts are felsic. Clast sizes are given for each sample in Table 2.3, and generally range from 1mm to 2mm.

Of the lapilli tuffs, sample 3FL2 is the only one which consists of discrete feldspar crystals (0.1mm-3.5mm) and relic olivine pseudomorphs set in a fine-grained matrix of magnetite and plagioclase (average grain size ~0.02mm).

In general, the alteration of lapilli tuffs is very similar to that of the nearby flow units (Table 2.2). Plagioclase is replaced by albite + epidote + quartz, albite + muscovite + quartz, or albite + muscovite + calcite + epidote $\pm$ chlorite. Chlorite is a pervasive alteration product of the fine-grained matrix material. Magnetite is generally partly altered to hematite $\pm$ goethite. Olivine is

typically pseudomorphed by hematite + chlorite ± epidote.

Fractures in the lapilli tuffs generally occur between adjacent lithic clasts as well as throughout the rock. Fractures range in size from 0.1mm to 1.0mm across and are filled with quartz, epidote + calcite ± quartz, or calcite.

The pyroclastic breccias are composed of lithic clasts ranging in size from 8mm to 70mm (Table 2.3). The clasts are mafic in composition, but mineralogy varies slightly in each clast. Common phenocryst phases are plagioclase, relic olivine and pyroxene pseudomorphs, relic igneous amphibole and phlogopite.

At locality 83-3F, plagioclase phenocrysts are pseudomorphed by albite + muscovite ± epidote ± chlorite. Pyroxene and olivine are pseudomorphed by hematite + chlorite. Groundmass feldspar is pseudomorphed by albite + chlorite + quartz ± epidote. Patches of groundmass material in the clasts have been replaced by chlorite, epidote + quartz, and calcite.

The secondary mineralogy of sample 14FL1 is very similar to that described above, except that chlorite is minor and calcite comprises approximately 20% of the sample. Calcite occurs with albite pseudomorphing plagioclase, and also occurs replacing fine-grained groundmass material.

Andesite

Andesites and the adjacent Kleanza Creek pluton make up the bulk of the eastern part of the study area (Figure 2.1). The contact between the andesites and the Kipulta Creek basalts is not readily distinguishable in the field as both are aphanitic and weather reddish-grey. Individual outcrop height is approximately 3m. Slickensides are present at localities 83-16F, and 83-20F. The outcrop at 83-17F has well-developed striations and is highly fractured. This may indicate that a shear zone, roughly paralleling the unobserved contact with the pluton, is present over an area of approximately 6 - 10m from 83-16F to 83-17F on the west, and another shear zone parallels the contact on the east.

Modal mineralogy of the samples is generally 70% - 80% plagioclase and 10% - 20% opaques, with approximately 10% of fine grained groundmass material altered to chlorite, calcite or quartz. Sample 20FL2 contains 5% corroded clinopyroxene grains. Sample 8FL1 consists of approximately 30% plagioclase laths in a matrix of devitrified glass.

The alteration of the andesites is very similar to that of the basalts. Plagioclase phenocrysts are altered to albite + chlorite $\pm$ epidote, albite + muscovite $\pm$ epidote, or, albite + chlorite + muscovite + quartz. Groundmass plagioclase is generally altered to albite + muscovite $\pm$ epidote or albite + chlorite $\pm$ epidote. Magnetite is typically altered to hematite + goethite.

Fine-grained groundmass material is typically altered to chlorite + quartz or calcite + quartz. Due to the very fine nature of the groundmass in some samples (e.g. ~50μm - 100μm in 17FL1), it is difficult to determine if quartz is primary or secondary. Fibrous actinolite in the andesites is generally closely associated with corroded hematite grains (Plate 2B).

Kleanza Creek Pluton

The contact between the Kleanza Creek pluton and the surrounding volcanics is marked by extensive fracturing in both units. Where direct contact is not observed, striations and slickensides in the volcanics may indicate the presence of shear zones paralleling the inferred contact. This evidence and the high degree of faulting in the region (Figure 1.2) probably indicates that the faulting occurred along the contacts after intrusion.

Except in one location, discussed below, cross-cutting relationships within the pluton were not observed, possibly due to sparse outcrop.

The plutonic rocks have a strong pink colour and consist of approximately 30% quartz, 30-40% plagioclase and 30-40% potassium feldspar. Biotite and hornblende comprise ~1-5% of the rock. Biotite is more predominant than hornblende. Chalcopyrite and hematite are present in trace amounts. The allotriomorphic-granular and graphic textures characterisitic

of these rocks are shown in Plates 2C and 2D. Grain size ranges from 0.3mm to 3.7mm; average grain size is approximately 0.6mm. The lack of observed contact relationships in the field and the relatively uniform modal mineralogy may indicate that only one pluton is present.

Carmichael et al. (1974) classify plutonic rocks with subequal amounts of K-feldspar and oligoclase-andesine and minor biotite and/or hornblende as quartz monzonites (adamellites). Due to the extent of alteration, original plagioclase composition could not be determined. The pluton is classed as an adamellite based on the estimates of bulk composition given above.

Streckeisen (1974) published a classification and nomenclature scheme for plutonic rocks based on the recommendations of the IUGS Subcommission on the Systematics of Igneous Rocks (Streckeisen, 1974). Using this system, the Kleanza Creek pluton, which has >20% quartz, plagioclase as 10-65% total feldspar, and <10% mafic minerals, is classed as a leuco-granite (Streckeisen, 1974).

Duffell and Souther (1964) describe most of the Kleanza Creek apophysis as the pink granodiorite subfacies of the Inner Facies of the Coast Intrusions. The subfacies consists of granodiorite and adamellite, both of which have a strong pink colour (Duffell and Souther, 1964). It is likely that the Kleanza Creek pluton corresponds to the pink granodiorite subfacies.

Plagioclase in the plutonic rocks has been pseudomorphically replaced by albite + muscovite ± epidote ± calcite. Epidote generally accounts for ~1% of the total alteration. In 19FL1, epidote comprises ~15% of the volume of the plagioclase grains and may be related to the later intrusion of a basalt dike. This alteration, and the poikiolitic inclusions of hematite produce a cloudy pink surface appearance to the plagioclase. Relic normal zoning, oscillatory zoning on a normal trend, and albite twinning are poorly preserved. As noted in the volcanic units, the alteration tends to be concentrated in the cores of zoned crystals.

The alkali feldspar is far more altered than the plagioclase, having a very dark brown colour and clayey appearance. The clay alteration was identified in the powder x-ray diffraction patterns as muscovite. In sample 18FL2, the alteration is concentrated along the margins and cleavage planes of individual grains. This alteration is more pervasive in the other samples.

Approximately 40% of the biotite in 18FL2 is dark red-brown and unaltered. Biotite in the remainder of the adamellite samples has been completely replaced by chlorite + hematite + sphene with a trace of epidote. The biotites are fibrous and have pleochroic haloes preserved around zircon inclusions (Plate 2E). Kink bands were observed in less than one percent of the grains.

Approximately 50% of the hornblende in 18FL2 is unaltered. The rest shows partial to complete replacement by a fibrous blue-green mineral, uralite (Plate 2F). The hornblende in the remaining samples has been pseudomorphically replaced by uralite and hematite and is principally recognized by the characteristic basal section outline of amphiboles (Plate 2F). The pseudomorphic replacement matches the description of uralitization of amphibole given by Duffell and Souther (1964) and by Deer et al. (1978).

The quartz monzonite at 83-6F and 83-19F is more highly fractured and altered than at the other localities. Quartz-filled fractures (~0.02mm wide) are cut by wider fractures filled with calcite (~0.2mm wide). A large silicic vein, consisting of fine-grained quartz + plagioclase + alkali feldspar + biotite, cuts through the adamellite in 18FL1 as do several smaller subparallel fractures filled with quartz and calcite.

The contact relationships between the silicic vein in 18FL1 and the host adamellite are more clearly observed around a 0.3mm wide subsidiary vein. Here, grains cut by the vein remain optically continuous, have not been rotated, and show no evidence of intrusion-related reaction. This evidence may indicate the presence of dilation fractures, possibly formed during cooling, which were later filled by a melt of approximately the same composition as the adamellite host.

Dikes and Large-scale Hydrothermal Veins

Three different dikes and veins were sampled in the Kleanza Creek - Kipulta Creek area: a 2.5m thick light green basalt dike at 83-5F, a 0.3m thick quartz vein at 83-7F, and a 0.6m thick basalt dike at 83-19F.

Dikes in the Terrace Map Area were briefly described by Duffell and Souther (1964). They concluded that the majority of these intrusives are of the dilation type, fracturing having occurred either contemporaneous with or subsequent to their emplacement. They discovered that deposition of hydrothermal quartz veins, generally ore-bearing, often occurred along contacts of dikes with the country rocks. This was not readily apparent in the Kleanza Creek area. From their field observations, Duffell and Souther (1964) proposed an order of emplacement of the various types of dikes: porphyritic, lamprophyric, aplitic, basaltic, all of which are related to the late stages of emplacement of the Coast Intrusions. Thus, the basalt dikes in the study area may represent the latest stage of igneous intrusion.

The basalt dike at 83-5F is intruded into a basalt flow. Contact between the units is easily recognized because of the very light green colour of the dike. No chill margins were observed. Primary mineralogy of the dike is: ~20% unaltered clinopyroxene, <5% serpentine pseudomorphs of olivine, ~1% subhedral hematite grains, and ~50% plagioclase. Amygdales

comprise approximately 1-5% of the volume of the dike.

Plagioclase in this dike is pseudomorphed by laumontite ± prehnite and by prehnite ± pumpellyite. Prehnite accounts for less than 10% of total feldspar alteration, and tends to be concentrated near a 0.2mm thick fracture filled with xenoblastic prehnite grains. Pumpellyite occurs in ~1% of the replaced plagioclase grains. It occurs as small (~0.02mm) patches of xenoblastic grains. Laumontite in plagioclase forms fibrous tabular grains with poorly developed cleavages.

Amygdales consist of laumontite ± prehnite ± chlorite ± pumpellyite in decreasing order of abundance. The forms of these minerals are the same as in amygdales from 83-1F.

The host basalt contains the greenschist facies assemblage, epidote + actinolite, which is not present in the dike rocks. This probably indicates that the greenschist facies metamorphism pre-dated the intrusion of the dike. The fresher appearance of clinopyroxene and the predominance of laumontite in the dike seem to support this interpretation.

The dark grey-green basaltic dike at 83-19F is intruded into the leuco-granite pluton. Chill margins were not observed, possibly indicating that intrusion occurred while the pluton was still fairly warm. In that case, the pluton may have acted as an insulator and allowed the dike to cool slowly. This is supported by the relatively uniform grain size of the dike (average grain size is ~0.4mm).

The basalt is comprised of approximately 50% plagioclase,

30% clinopyroxene, 20% intergranular material replaced by chlorite, 1% chalcopyrite and pyrite, and 1% amygdales. Plagioclase is pseudomorphed by albite + chlorite ± pumpellyite ± epidote. Relic albite twinning is well-preserved. Clinopyroxene grains adjacent to pumpellyite- or epidote- bearing plagioclase are corroded and have sharp concave contacts with these secondary minerals.

Amygdales in this dike consist of prehnite ± calcite ± chlorite + quartz. Prehnite occurs as typical sheaths of fine prisms and is intergrown with xenoblastic calcite. Chlorite has sharp convex contacts into prehnite and appears to be replacing it. Quartz is generally limited to the rims of amygdales.

The third feature is a milky white quartz vein, sample 7FL1. The quartz vein is barren of sulphides and fluid inclusions, and has an average grain size of approximately 1cm. Well-developed crystals of smoky quartz are present in cavities within the vein.

Paragenesis of Secondary Minerals

Actinolite

Actinolite occurs as fibrous, green-brown pleochroic crystals in several samples (Table 2.2). The average size of the prismatic subidioblastic grains is approximately 0.2mm. Actinolite generally has diffuse convex boundaries with

adjacent opaques and plagioclase.

Actinolite occurs as narrow prisms (0.05mm - 0.8mm long) in amygdales associated with quartz and epidote in sample 7FL3, and associated with diopside, epidote and calcite in sample 5FL4. It has sharp contacts with all phases.

Uralite is present as blue-green alteration of primary hornblende in the quartz monzonite.

Albite

Albite is present in fractures, and most commonly as an alteration product of plagioclase. In fractures, the grains are idioblastic, 0.10mm long and have straight sharp contacts with quartz. In plagioclase, albite forms optically continuous rims around the altered cores of zoned crystals. It also occurs as patches approximately 50um to 0.01mm wide scattered throughout the plagioclase grain.

Analcime

Analcime is only present in two samples (Table 2.2) and occurs as a fracture-filling phase (Plate 3A). The grains are isotropic to weakly anisotropic, and are approximately 0.16mm long. Analcime has sharp contacts with calcite. Analcime is readily identified in a powder x-ray diffraction pattern by strong 3.43Å, 5.60Å and 2.93Å peaks.

Calcite

Calcite generally occurs filling fractures or in amygdales. It can occur as small idioblastic prisms (~0.12mm long) or as large xenoblastic grains that comprise most of an

amygdale. Calcite has sharp contacts with epidote, chlorite, quartz, diopside, and actinolite. Its contacts with laumontite and prehnite are generally serrated and concave.

Calcite also occurs as xenoblastic grains replacing plagioclase phenocrysts and fine-grained groundmass material. In plagioclase the grains are approximately 0.12mm across and have sharp convex contacts with the feldspar. Calcite patches in the groundmass are typically 0.04mm across.

Chlorite

Chlorite is present in fractures, amygdales, altered phenocrysts and groundmass. Chlorite in fractures and amygdales tends to be confined to the rim when phases other than quartz are present. The two main void-filling habits of chlorite are:

1) vermicular chlorite forming clusters approximately 0.1mm long; and

2) fibrous needles ranging in size from 0.025mm to 0.8mm in one amygdale.

In general, both forms do not appear in the same amygdale. Amygdular chlorite has sharp straight contacts with pumpellyite, quartz, epidote and calcite. It has diffuse contacts with prehnite.

Chlorite is a common alteration product of olivine, pyroxene and plagioclase. In the mafic minerals it is associated with hematite and forms areas of tiny fibrous grains up to 0.08mm across. In plagioclase, chlorite occurs

as isolated patches 50μm to 0.02mm in diameter, except in 5FL4, where whole phenocrysts of plagioclase have been pseudomorphed by chlorite. As replacement of fine-grained groundmass material, chlorite occurs as elongate xenoblastic patches 0.04mm to 0.5mm across.

Clinopyroxene

The only occurrence of secondary clinopyroxene is in amygdales in sample 5FL4, where it is associated with epidote + actinolite + calcite. It forms subidioblasitic tabular grains and has sharp contacts with these associated phases.

Epidote

Epidote occurs in amygdales, fractures, and as replacement of plagioclase. In plagioclase, epidote has sharp convex boundaries with the feldspar and any coexisting pumpellyite. The grains are xenoblastic and range in size from ~0.01mm in groundmass plagioclase, to ~0.05mm in plagioclase phenocrysts. If the epidote alteration of a phenocryst is extensive, clusters of xenoblastic grains up to 0.6mm wide can occur along with scattered smaller grains. Plate 3C of 3FL1 shows beautiful idioblastic prisms of epidote 0.02mm-0.4mm in length radiating outward from one side of a single plagioclase crystal.

In amygdales, epidote has three main habits (Plate 3D): 1) fan-shaped aggregates (1.0 - 2.0mm wide) of idioblastic prisms (0.3 - 0.8mm long) radiating outward from a cluster of tabular, xenoblastic grains approximately 0.04mm in size;

2) clusters of xenoblastic grains (0.06mm -0.9mm) having cloudy brown cores, possibly indicating a high nucleation rate; and

3) as idioblastic tabular crystals ranging in size from 0.03mm to 0.3mm in one amygdale. In fractures, epidote occurs as subidioblastic tabular and acicular grains.

Hematite and Goethite

Magnetite has been at least partly altered to hematite and goethite in most samples. The grain size of the opaques range from 0.01mm to 0.1mm. The rims of the opaques are corroded and have diffuse orange-brown goethite surrounding them.

Hematite also forms rims 0.02mm to 0.06mm wide around pyroxene and olivine pseudomorphs. These grains are xenoblastic and have diffuse contacts with the other pseudomorphic replacement phases. Hematite has diffuse corroded contacts with actinolite.

Laumontite

Laumontite occurs primarily in amygdales and fractures. It generally forms large (up to ~1.0mm) optically continuous grains having a very coarse appearance with warped, broad (~50μm) (Plate 3E). Laumontite has sharp serrated contacts with quartz with which it is generally in contact. Epidote inclusions in laumontite tend to be elongated approximately parallel to the long direction of the laumontite. The epidote grains have diffuse convex contacts with it, possibly

indicating replacement of the laumontite by epidote.

Laumontite and prehnite generally do not occur in direct contact with each other. For example, in sample 2FL1, a 0.01mm rim of calcite + epidote having diffuse contacts with laumontite and prehnite, separates the two phases. In sample 1FL2, prehnite does have diffuse serrated contacts with laumontite, however tiny (~0.015mm) elongate quartz grains occur between the two phases above the contact. About 50% of the laumontite/prehnite contacts in this sample are marked by tiny (0.04mm) grains of epidote growing over the contact into both phases. These epidote crystals have diffuse convex contacts with both prehnite and laumontite.

Muscovite

Muscovite is used here to describe fine-grained, 10A-mica which is present throughout the study area (Table 2.2). The clay is identified in powder x-ray diffraction patterns by strong 3.32Å, 10.0Å and 4.48Å peaks.

Muscovite generally occurs as the alteration product of feldspar and can account for 1% to 70% of the alteration of individual grains. It occurs as fibrous grains in xenoblastic patches 50μm to 200μm across. In the quartz monzonite samples where the sericitization of the K-feldspar is pervasive, it is difficult to recognize a specific habit.

In sample 3FL1, muscovite replaces calcite + quartz in an amygdale and also strongly replaces the groundmass material surrounding this amygdale. The muscovite alteration forms a

rim extending 0.10mm to 0.74mm away from the amygdale. Pervasive muscovite alteration such as this may indicate the presence of a very alkali-rich fluid (Deer et al. 1978).

Potassium Feldspar

As a secondary mineral, K-feldspar occurs lining amygdales in samples from 83-1F, 83-2F, 83-3F and 83-8F. It forms elongate xenomorphic grains approximately 0.5mm long, and has sharp serrated contacts with muscovite when present. X-ray patterns indicate that the feldspar is orthoclase, however the fine-grained nature of the feldspar made optical identification extremely difficult.

Prehnite

Prehnite occurs in amygdales, fractures and as pseudomorphic replacement of plagioclase. In amygdales and fractures, prehnite generally occurs as optically continuous grains 0.3mm to 0.7mm across, and has sharp convex contacts with quartz. However, prehnite comprises 95% of the amygdale mineralogy in sample GT19B and exhibits two different habits:
1) the `sunflower´ texture shown in Plate 3F, in which single grains of calcite, epidote or prehnite form the suns and prehnite blades form the petals; and
2) subidioblastic to xenoblastic blades, approximately 0.18mm long filling the rest of the amygdale.

Prehnite pseudomorphing plagioclase forms clusters of thin sheaths of crystals ranging in size from 50μm to 300μm. Prehnite replacement can comprise 100% to 1% (with

pumpellyite ± chlorite ± albite as the remainder) of the alteration of individual plagioclase grains.

In sample GT19D, prehnite occurs as a replacement of fine-grained groundmass material in large (1.5mm x 2.5mm) patches of tiny (~0.035mm) grains intergrown with quartz and opaques. Small aggregates of radiating prehnite prisms are also present.

Prehnite was observed as matrix feldspar alteration in samples in which primary magnetite was relatively unoxidized. This indicates that f_{O2} was low relative to the more hematite-rich samples, most of which contained epidote. This observation is consistent with the findings of Liou (1973) that high f_{O2} favours the development of epidote over prehnite.

Pumpellyite

Pumpellyite is present as thin randomly oriented needles, 0.025mm long pseudomorphing plagioclase. These needles also occur in clusters approximately 0.08mm wide in the plagioclase grains.

Pumpellyite also occurs in amygdales as clusters of blades 0.01mm to 0.09mm long having sharp straight contacts with epidote and quartz (Plate 4A). Towards the cores of amygdales in four samples, the epidote/pumpellyite contacts are more diffuse and epidote appears to be forming blocky crystals at the expense of pumpellyite. In sample GT19E acicular pumpellyite blades appear to be pseudomorphing an

earlier idioblastic phase.

Quartz

Quartz occurs as elongate xenoblastic crystals in amygdales. Grain size varies considerably, for example ranging from 0.18mm to 1.0mm in one amygdale. Quartz has sharp contacts with all phases.

Amygdaloidal and vein quartz generally have a very spotty surface appearance due to a large number of fluid inclusions. A noticeable exception to this, is the milky-white quartz vein 7FL1, which is barren of fluid inclusions.

Quartz also occurs as replacement of fine-grained groundmass material, generally in xenoblastic patches ranging in size from 50μm to 100μm.

Serpentine

Serpentine occurs as a fibrous, low birefringent alteration product of olivine. It was identified by the strong 7.10Å peak and lack of a 14Å peak, and its characteristic green colour.

CHAPTER 3 AUTHIGENIC MINERALOGY

Electron Microprobe Techniques

Sample mounts for electron microprobe analysis were prepared using cold-setting epoxy to minimize dehydration of the zeolites and prehnite. Mineral analyses were obtained using an eight-channel ARL SEMQ Microprobe. Routine operating conditions were: accelerating voltage of 15keV; emission current of 300μA; beam current of 0.15μA; counting time of 20 seconds; and beam diameter of 1μm for epidote, pumpellyite, prehnite and feldspars, and 3μm for laumontite and analcime. Calculated structural formulae for laumontite and analcime indicate that volatilization was minimal.

The relationship between the composition of each mineral and its paragenesis was determined by analyzing at least five spots per grain when possible. The tabulated data are representative of analyses of several grains in each of the assemblages or locations of interest within the probe section.

Standards used during this study are on file at the Department of Geology and Geophysics, University of Calgary, and are given in Table 3.1. All elements were analyzed as oxides and the data were corrected following the procedures of Bence and Albee (1968) after corrections for background and drift. These corrections were made using a package of computer programs designed by Nicholls *et al*. (1977), which

Table 3.1 Standards used in microprobe analyses.

Oxide	Epidote/Pumpellyite	Prehnite/Laumontite/Analcite	Feldspar	Chlorite
SiO_2	Tanzanite	Albite	Albite	Garnet
TiO_2	Aenigmatite	Aenigmatite		Aenigmatite
Al_2O_3	Tanzanite	Tanzanite	Albite	Biotite
FeO	Kak. garnet	Biotite	Pyroxene	Biotite
MnO	Mn-Cummingtonite	Mn-Cummingtonite		Mn-Cummingtonite
MgO	Garnet	Biotite	Pyroxene	Garnet
CaO	Tanzanite	Tanzanite,Pyroxene	An_{50}glass	Garnet
Na_2O	Albite	Albite	Albite	Albite
K_2O	Orthoclase	Orthoclase	Orthoclase	Biotite
BaO	Hyalophane	Hyalophane	Hyalophane	Hyalophane

includes STDS, SLAVE, and BUNK. Precision and detection limit statistics for each oxide are generated by SLAVE. Representative statistics for precision and detection limits for individual oxides within each type of mineral are given in Table 3.2.

Water content of epidote, pumpellyite, prehnite, analcime, laumontite and chlorite was estimated as the difference from 100% of the total weight percent of the analyzed oxides. This approach was used because the water contents of these minerals are variable. These results generally agree with published mineral composition data for which water was directly analyzed.

Structural formulae of the minerals excluding pumpellyite were calculated using FORM, a computer program designed by Nicholls and Stout (unpublished). Structural formulae of pumpellyite were calculated using the computer program PUFORM written by the author.

X-ray Diffraction Analysis

As discussed in Chapter 2, powder x-ray diffraction data were used to identify bulk, amygdaloidal and vein mineral phases. The samples were ground and prepared as acetone smears on glass slides, and were analyzed using FeK^{α} radiation.

XRD data were also collected on individual minerals to determine unit cell size and its relationship to composition.

Table 3.2 Precision and detection limits of microprobe analyses. Values represent detection for oxides of each type of mineral analyzed (at 3σ or 99% confidence). Second column values represent counting precision in wt.% oxides (Nicholls et al., 1977).

Oxide	Epidote/Pumpellyite	Prehnite/Laumontite/Analcite	Feldspar	Chlorite
SiO_2	0.05/0.33	0.04/0.35	0.06/0.37	0.05/0.28
TiO_2	0.02/0.01	0.02/0.01	n.a.	0.02/0.01
Al_2O_3	0.03/0.28	0.04/0.28	0.03/0.22	0.03/0.20
FeO	0.04/0.10	0.04/0.04	0.03/0.02	0.03/0.11
MnO	0.06/0.04	0.06/0.02	n.a.	0.06/0.05
MgO	0.03/0.02	0.03/0.01	0.02/0.01	0.03/0.14
CaO	0.01/0.07	0.01/0.06	0.01/0.01	0.01/0.01
Na_2O	0.02/0.01	0.02/0.01	0.02/0.07	0.02/0.01
K_2O	0.01/0.01	0.01/0.01	0.01/0.01	0.01/0.01
BaO	0.13/0.04	0.11/0.04	0.08/0.03	0.12/0.04

The minerals were hand picked from veins and amygdales on the basis of colour, cleavage and habit. These specimens were then mounted in glass capillaries 0.1mm in diameter and exposed to CuKα_1 radiation for six hours and twelve hours. A capillary filled with NBS Silicon Standard was exposed on each film for 35 minutes to provide a reference for 2θ correction. An internal standard was not used because of the small amount of each sample, and the possible masking of peaks by the standard material.

The exposed films were digitized using a film-reading densitometer and the program DENSIT provided by the Nicolet Corporation. Step widths of 0.1° 2θ , and step times of 1 second were used to measure the film. Peaks were visually picked from the diffractograms displayed on the terminal screen. Peak positions were determined as half-width of half peak height. Notes on peak shape and intensity (I-BG) were made to aid in indexing of the powder patterns.

Indexing of the powder films was carried out in two steps:

(1) comparison with theoretical powder patterns calculated from published structural crystallographic data and/or reliable published powder patterns; and

(2) refinement of the preliminary indexing and approximate unit cell parameters using the least squares program of Appleman et al. (1972).

The theoretical powder patterns were calculated using the

computer program PHKLI also provided by Nicolet.

Selected published unit cell - composition data have been included in the following tables for comparison.

Epidote - Crystallography

The structure of epidote was refined by Ito et al. (1954) using Patterson-Harker functions and three-dimensional Fourier synthesis. They described the structure as a mixed-silicate type containing both single and double tetrahedral groups (SiO_4 and Si_2O_7) bound by AlO_4 and $AlO_3(OH)$ chains. They placed the Al(Fe) [M(3)] and Ca atoms between the chains. Ito et al. (1954) also noted that the Fe atoms do not replace Al atoms in chains.

Dollase (1971) further refined the epidote structure with isotropic temperature factors for all atoms except the three heaviest [A(1), A(2), and M(3)], which were refined with anisotropic temperature factors. The structure contains chains of edge-sharing octahedra of two types: a single chain of M(2) octahedra and a multiple chain of central M(1) and peripheral M(3) octahedra. These chains are cross-linked by SiO_4 and Si_2O_7 groups, as described by Ito et al. (1954). The location of the A(1) and A(2) cations in the large cavities between the chains and cross-links also reflects the structure proposed by Ito et al. (1954).

Occupancy of the sites is as follows:

A(1) Ca;

A(2) Ca, Sr, Mg, Na, etc.;

M(1) Al, Fe, Mn;

M(2) Al;

M(3) Fe, Al, Mn;

The distribution of Fe^{3+} between the octahedral M sites [M(2) < M(1) < M(3)] was studied by Dollase (1973) using Moessbauer spectra. The M(2) site was found to contain only Al; therefore he concluded that the Al atoms preferred the OH-coordinated, M(2) sites to the exclusion of the transition metals (Fe and Mn). In addition, the transition metals preferred the larger and more distorted M(3) site over the M(1) site. Substitution for Al in M(1) occurs only at high Mn+Fe concentrations.

The distribution of the cations between the A-sites is also related to site size. The larger A(2) site has a higher co-ordination number than the A(1) site and can accomodate atoms larger than Ca^{2+} (Dollase, 1971).

The ideal structural formula for an epidote based on Dollase (1971) is therefore:
$Ca_{1.00}Ca_{1.00}(Al,Fe)Al_{1.00}(Fe,Al)(Si_2O_7)(SiO_4)O(OH)$. This distribution of atoms in the M-sites of the structure has been adopted by many subsequent authors (e.g. Liou, 1973; Bird and Helgeson, 1980, 1981). The cell dimensions of the epidote analyzed by Dollase (1971) are a=8.914(9)Å,

b=5.640(3)Å, c=10.162(9)Å, and B=115.4(2)°, in the space group $P2_1/m$. These data, atomic positions, and temperature factors were used in PHKLI as described above to index powder patterns of epidote samples of known composition from Kleanza Creek. These results and published unit cell - composition data are presented in Table 3.3, and plotted on the epidote composition determinative curves of Myer (1965) (Figure 3.1).

It is evident that the unit cell size of epidote does increase with increasing Fe-content, however, the simple relationships proposed by Myer (1965) do not seem to hold. His unit cell determinations were based on diffractograms from acetone slurries of epidote and NBS Si standard scanned at unspecified "slow" speeds. The diffractograms were produced by a chart recorder at a relatively small scale of one inch per degree 2θ. Charts of diffractometer scans are accurate to approximately 0.1° 2θ at best under these conditions. Myer (1965) also based his calculations on the indexing of only eight strong peaks. A minimum of twenty peaks were indexed for the determination of unit cell parameters in the present study. The conclusion that can be safely drawn from Myer (1965) and Seki (1959) is that unit cell parameters can be used to distinguish between zoisite, clinozoisite and pistacite (Table 3.3). More exact determinations of composition are not possible.

The indexed patterns for epidote produced in this study (available on request) differ from that given in the Powder

Table 3.3 Unit cell - composition data for epidote

Sample	a(Å)	b(Å)	c(Å)	β	V(Å^3)	X_{Fe}
1.GT19C1	8.911 ±.005	5.638 ±.003	10.190 ±.006	115°33′ ±3′	461.90 ±0.40	0.30
2.GT19D2	8.946 ±.010	5.625 ±.008	10.195 ±.011	115°17′ ±5′	463.90 ±0.80	0.23
3.15FL1	8.908 ±.006	5.635 ±.003	10.164 ±.008	115°24′ ±24′	460.87 ±0.48	0.32
4. cz	8.87	5.59	10.15	115°27′	454.5	0.08
5. ps	8.88	5.61	10.17	115°25′	457.6	0.20
6. ps	8.89	5.63	10.19	115°24′	460.7	0.30
7. ep	8.907 ±.009	5.642 ±.004	10.189 ±0.012	115°29′ ±3′	462.19 ±0.65	0.33
8. ep	8.897 ±.009	5.659 ±.004	10.168 ±0.012	115°19′ ±3′	462.76 ±0.65	0.27
9. ep	8.891 ±.009	5.667 ±.004	10.178 ±0.012	115°19′ ±3′	463.57 ±0.65	0.35
10. ep	8.894 ±.009	5.630 ±.004	10.169 ±0.012	115°22′ ±3′	460.10 ±0.65	0.25

1-3 Epidote from Kleanza Creek-Kipulta Creek area

4-6 Seki (1959)- natural epidotes

7-10 Liou *et al.* (1983) synthetic epidotes
7. HM buffer P_f=8000b, T=513°C
8. HNO buffer P_f=8000b, T=522°C
9. HM buffer P_f=2000b, T=499°C
10. QMF buffer P_f=2000b, T=376°C

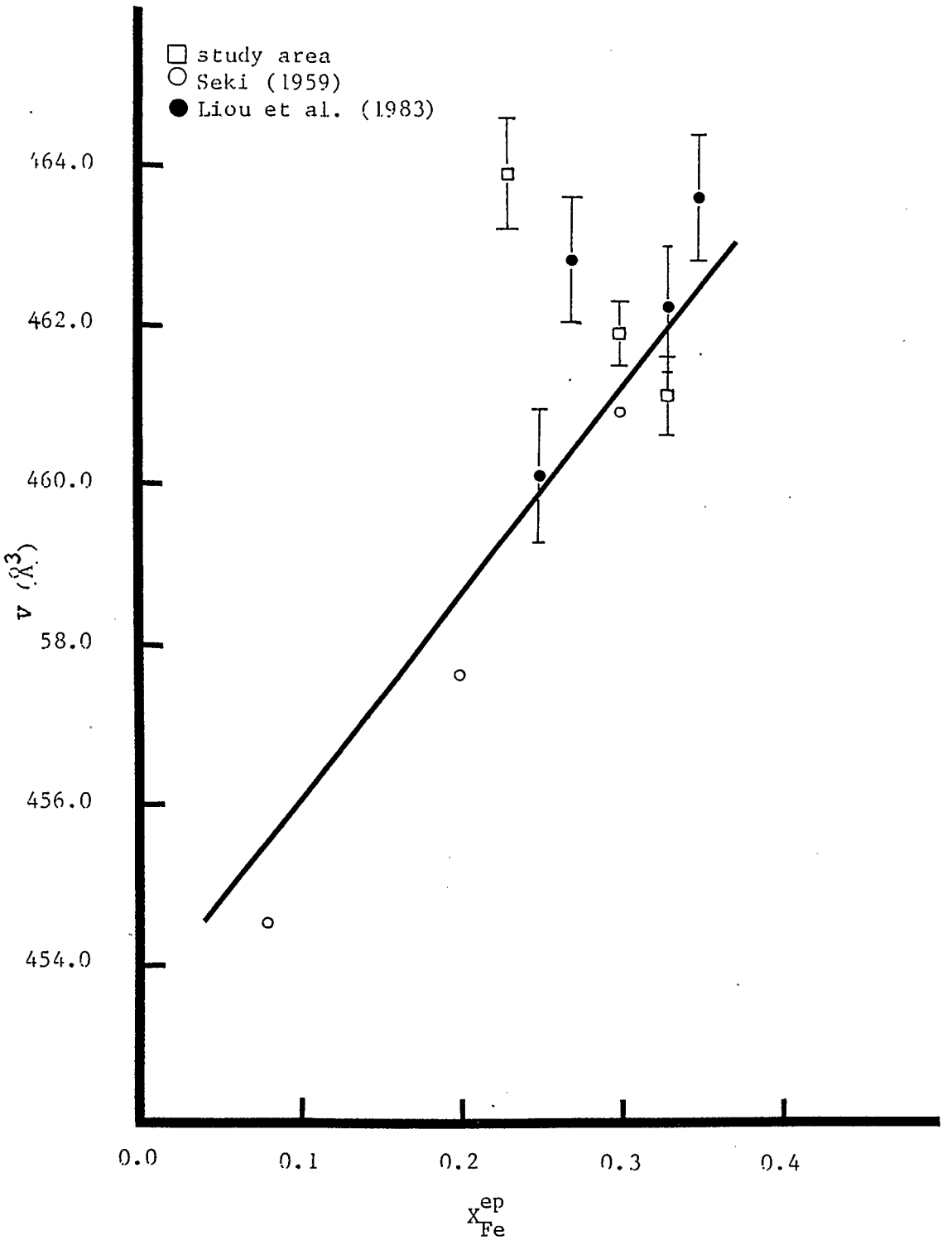

Figure 3.1 (A) X-ray determinative curve for epidote compositions: unit cell volume versus composition. Curve from Myer (1965). Note the wide scatter of data points above the line at high X_{Fe} values.

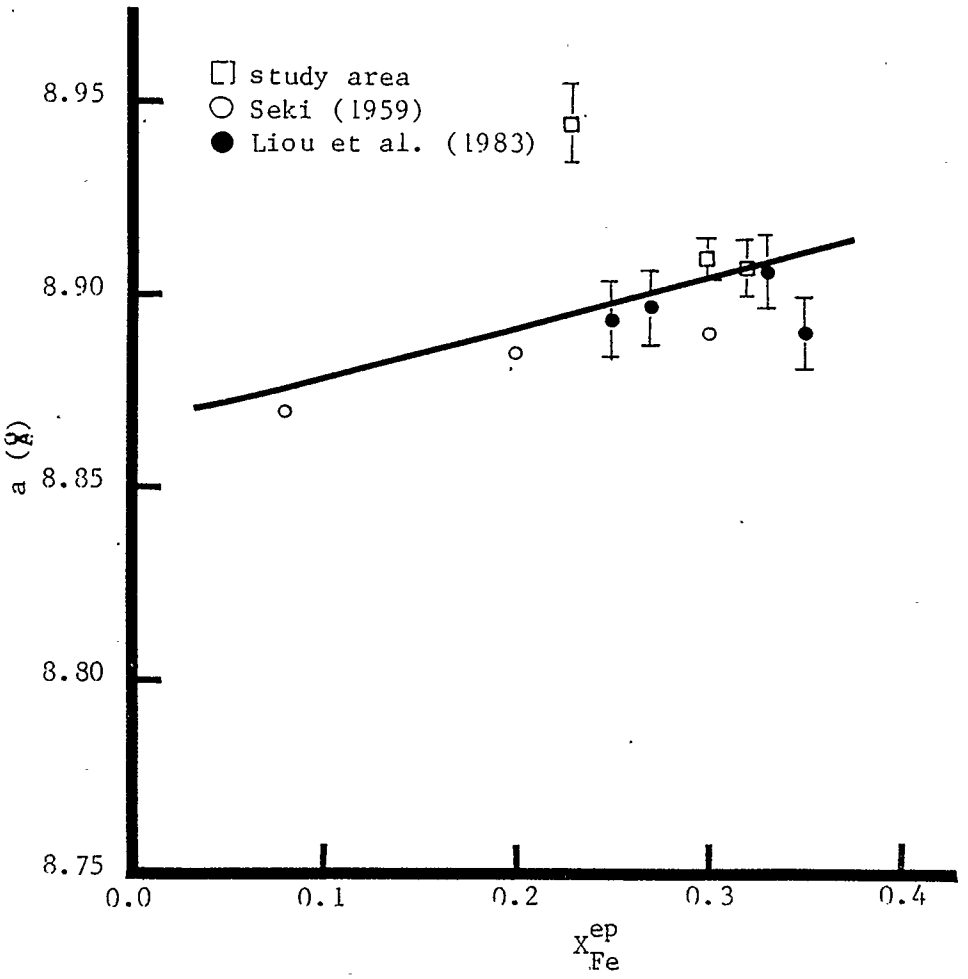

Figure 3.1 (B) X-ray determinative curve for epidote compositions : a-axis length versus composition. Note that the linear relationship seems to fit most of the data points. Curve from Myer (1965).

Diffraction File (1984) in that more peaks are indexed, and relative intensities are more comparable with the calculated powder pattern. Indexing of these `extra´ peaks was made with reference to high intensity peaks in the calculated pattern. Some difficulty was encountered during the indexing of the pattern of the GT19D epidote, evident in the unusually large value for a (a=8.946Å, Table 3.3). High background values impeded recognition of some peaks and may account for this difference. However, at three standard deviations (95% confidence limit) this unit cell is comparable to the results of Myer (1965) and Seki (1959) for epidotes of similar composition.

Epidote - Composition

Epidote compositions are uniformly Fe-rich (X_{Fe}=0.22 to 0.33) in samples from the Kleanza Creek - Kipulta Creek area (Table 3.4; Figure 3.2). Epidotes in the andesites and volcaniclastics tend to be more Fe-rich compared to epidotes in the basalts (compare Tables 3.4 (A) and 3.4 (B)). As shown in Figure 3.2, epidote compositions from the study area are very similar to those reported by Viereck et al. (1982) from the Reydarfjordur drill hole, Iceland, and by Evarts and Schiffman (1983) from the Del Puerto Ophiolite, California.

Traverses across amygdales of epidote revealed that most epidote grains are not homogeneous in composition over their full length. Figure 3.3 is a typical traverse showing the

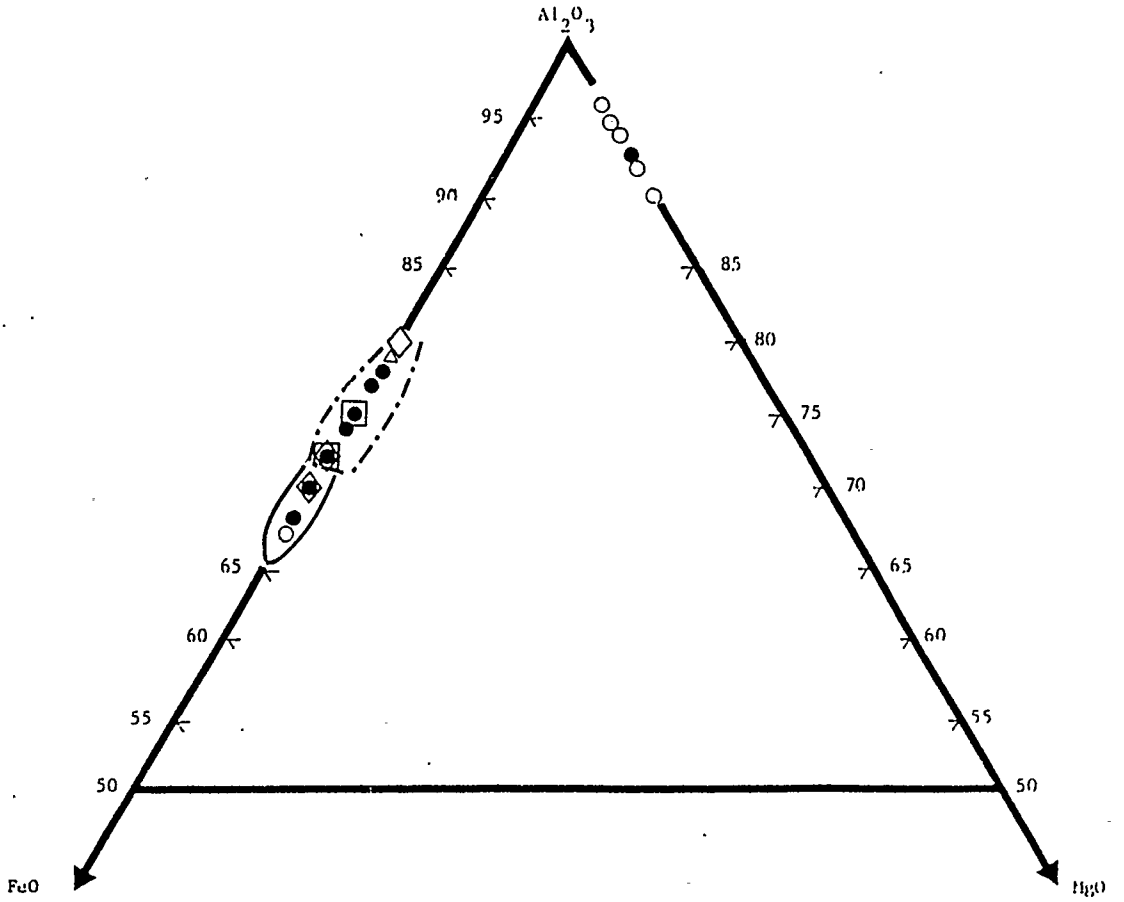

Figure 3.2 AFM plot of epidote and prehnite compositions from the Kleanza Creek - Kipulta Creek area.

△ amygdaloidal epidote or prehnite from the study area

○ groundmass epidote or prehnite from the study area

● overlap of groundmass and amygdale compositions

-·-·- epidotes in meta-basalts from study area

——— epidotes in andesites and volcaniclastics from study area

□ from Viereck et al. (1982)

◇ from Evarts and Schiffman (1983)

Table 3.4 Electron microprobe analyses of epidote.
(A) Meta-basalts

Sample	(1)GT19C2	(2)GT19D2	(3)GT19D2	(4)GT19HZ
SiO_2	37.60	37.08	37.35	37.71
TiO_2	0.03	0.14	0.08	0.02
Al_2O_3*	22.28	25.26	25.21	24.24
Fe_2O_3	14.73	10.98	11.77	12.50
MnO	0.09	0.54	0.31	0.20
MgO	b.d.	0.63	0.14	0.24
CaO	23.19	23.04	23.10	23.11
BaO	n.a.	b.d.	0.34	n.a.
Na_2O	b.d.	b.d.	b.d.	b.d.
Anhydrous Totals	97.93	97.67	98.31	98.02
Number of cations on the basis of 25 positive charges, 13(O,OH) groups.				
Si	3.008	2.943	2.954	2.989
Ti	0.002	0.009	0.005	0.001
Aliv	-	0.048	0.041	0.010
Al*	2.101	2.314	2.309	2.254
Fe*	0.887	0.656	0.700	0.746
Mn	0.006	0.036	0.021	0.013
Mg	-	(a)0.075	0.017	0.028
Ca	1.988	1.959	1.958	1.963
Ba	-	-	0.011	-
Na	-	-	-	-
$X_{Fe}=Fe^*/Fe^*+Al$	0.297	0.217	0.229	0.248

(1)pseudomorph of plag phenocryst; (2)pseudomorph of plag phenocryst; (3)ep pseudomorph of groundmass plag; (4)ep in amygdale with lm, pr, pu, q, chl.

* Total Fe as Fe_2O_3
(a) Note unusually high Mg-content.

Table 3.4 (A) continued

Sample	(5)GT19HZ	(6)GH19HZ	(7)19FL2
SiO_2	37.64	37.98	37.59
TiO_2	0.08	0.05	0.02
Al_2O_3*	24.10	23.97	23.91
Fe_2O_3	11.14	12.58	13.18
MnO	0.18	0.12	0.08
MgO	1.21	0.18	0.04
CaO	22.78	23.53	23.52
BaO	n.a.	n.a.	n.a.
Na_2O	b.d.	b.d.	0.02
Anhydrous totals	97.13	98.41	98.43
Number of cations on the basis of 25 positive charges, 13(O,OH) groups.			
Si	2.998	3.001	2.978
Ti	0.005	0.003	0.001
Aliv	-	-	0.021
Al_*	2.262	2.232	2.212
Fe^*	0.668	0.748	0.786
Mn	0.012	0.008	0.006
Mg	(a)0.144	0.021	0.004
Ca	1.944	1.992	2.002
Ba	-	-	-
Na	-	-	0.003
$X_{Fe}=Fe^*/Fe^*+Al$	0.228	0.251	0.260

(5)pseudomorph of plag phenocryst; (6)pseudomorph of plag phenocryst; (7)pseudomorph of plag phenocryst with ab+pu.

* Total Fe as Fe_2O_3

Table 3.4 Electron microprobe analyses of epidote.
(B) Volcaniclastics and andesites

Sample	(1)7FL3	(2)7FL3	(3)7FL3
SiO_2	38.15	38.21	38.34
TiO_2	b.d.	0.09	0.15
Al_2O_3	22.66	22.14	23.05
Fe_2O_{3*}	14.79	14.88	14.05
MnO	0.20	0.24	0.39
MgO	b.d.	0.52	b.d.
CaO	23.46	22.97	23.20
BaO	n.a.	n.a.	n.a.
Na_2O	b.d.	b.d.	b.d.
Anhydrous totals	99.26	99.05	99.18
Number of cations on the basis of 25 positive charges, 13(O,OH) groups.			
Si	3.011	3.021	3.020
Ti	-	0.005	0.009
Aliv	-	-	-
Al	2.108	2.063	2.140
Fe_*	0.879	0.885	0.833
Mn	0.013	0.016	0.026
Mg	-	0.061	-
Ca	1.984	1.946	1.958
Ba	-	-	-
Na	-	-	-
$X_{Fe}=Fe^*/Fe^*+Al$	0.294	0.300	0.280

(1)in amygdale with diopside; (2)pseudomorph of groundmass plag; (3)pseudomorph of plag phenocryst.

* Total Fe as Fe_2O_3

Table 3.4 (B) continued

Sample	(4)15FL1	(5)15FL1
SiO_2	38.01	37.69
TiO_2	0.03	b.d.
Al_2O_3*	22.25	21.43
Fe_2O_3*	15.29	16.56
MnO	0.31	0.11
MgO	b.d.	b.d.
CaO	23.60	23.54
BaO	n.a.	n.a.
Na_2O	b.d.	b.d.
Anhydrous totals	99.49	99.33
Number of cations on the basis of 25 positive charges, 13(O,OH) groups.		
Si	3.003	2.996
Ti	0.002	-
Aliv	-	0.004
Al*	2.072	2.003
Fe*	0.909	0.990
Mn	0.021	0.007
Mg	-	-
Ca	1.998	2.005
Ba	-	-
Na	-	-
$X_{Fe}=Fe^*/Fe^*+Al$	0.302	0.330

(4)pseudomorph of groundmass plag; (5)pseudomorph of plag phenocryst.

* Total Fe as Fe_2O_3

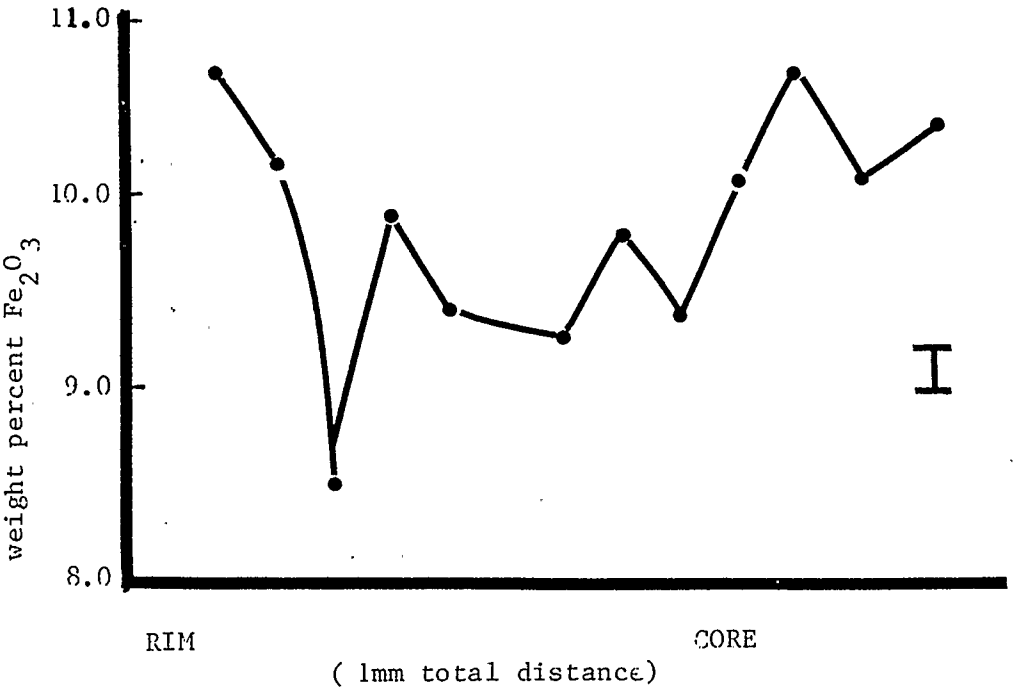

Figure 3.3 Electron microprobe traverse of an amygdaloidal epidote grain.
Vertical bar represents one standard deviation on either side of the mean.

change in weight % Fe_2O_3 from the rim to the core of a large epidote crystal in an amygdale in sample GT19HZ. The amygdales used in the unit cell - composition study were selected for their relative homogeneity ($^{\Delta}X_{Fe} < 0.01$) to minimize this problem. As shown in Plate 3D, epidote frequently appears in its three main habits within one amygdale. Microprobe traverses across such amygdales also show no systematic variation; however, the brown, tightly clustered epidote grains tend to be slightly Fe-poor compared to the other forms (generally $^{\Delta}$wt% $Fe_2O_3 < 0.5\%$).

Prehnite - Crystallography

Nuffield (1943) determined the space group and unit cell parameters of prehnite using an optically homogeneous prehnite fragment from Ashcroft, British Columbia. Initial interpretation of systematic extinctions in the Weissenberg films indicated that the space group was either P*ncm* or P*nc*2. However, these space groups contradicted the pyroelectric data of Traube (1894). He then suggested that since prehnite belongs to the crystal class 2*mm*, supplementary twinning about any of the missing elements of symmetry would occur. He assumed that the x-ray crystal was twinned and determined that the only space group which, when twinned, would give the symmetry P*ncm*, was the space group P2*cm*. Aumento (1968) confirmed that the space group of prehnite is P2*cm* using transmission electron microscopy and x-ray diffraction. He

was also able to observe interpenetrational twins which produced the systematic extinctions of space group Pncm.

Prehnite patterns were indexed using the hkl values suggested by Nuffield (1943), which have also been adopted in the Powder Diffraction File (1984). The resulting unit cells and compositions are given in Table 3.5 along with values from the literature. The unit cell parameters of the Kleanza Creek prehnites agree very well with those of similar prehnites from the Karmutsen Group (Surdam, 1969). However, as noted by Surdam (1969) relatively large differences in weight percent Fe_2O_3 produce negligible changes in the unit cell volume (Table 3.5). Thus, though unit cell size does increase with Fe^{3+} content, a determinative curve for prehnite composition based on unit cell parameters would not be valid.

Rudashevskiy et al. (1974) attributed the increase in unit cell volume with increasing Fe content to the Fe^{3+} ions replacing tetrahedrally co-ordinated Al. The iron cations enter the lattice between the $AlSi_2O_{10}$ layers in the structure. The size difference between the cations tends to limit the amount of Fe-Al substitution.

Prehnite - Composition

Prehnite compositions in samples from the Kleanza Creek - Kipulta Creek area occur in a very narrow range of X_{Fe}=0.03 to X_{Fe}=0.07 (Table 3.6; Figure 3.2). Surdam (1969) observed

Table 3.5 Unit cell - composition data for prehnite

Sample	a(Å)	b(Å)	c(Å)	V(Å^3)	X_{Fe}
1.GT19B	4.607 ±0.003	5.478 ±0.002	18.564 ±0.007	468.30 ±0.24	0.03
2.GT19D2	4.611 ±0.005	5.486 ±0.003	18.465 ±0.009	467.07 ±0.29	0.05
3. pr	4.63	5.48	18.5	470	0.09
4. pr	4.62	5.47	18.5	467	0.03
5. pr	4.62	5.49	18.5	469	0.02
6. pr	4.644 ±0.003	5.490 ±0.03	18.452 ±0.03	470.44 ±0.30	0.10
7. pr	4.642 ±0.003	5.473 ±0.03	18.421 ±0.03	470.00 ±0.30	0.02

3-5 Surdam (1969) Karmutsen Volcanics, British Columbia

6. Liou *et al*. (1983) synthetic prehnite; P_f=2kb, T=376°

7. Liou *et al*. (1983) Prospect, New South Wales.

Table 3.6 Electron microprobe analyses of prehnite.

Sample	(1)GT19B	(2)GT19B	(3)GT19B	(4)GT19C1
SiO_2	41.32	41.46	42.80	43.16
TiO_2	0.55	0.04	b.d.	n.a.
Al_2O_3*	23.74	23.98	25.64	23.04
Fe_2O_3	3.08	3.25	1.81	4.20
MnO	0.07	0.10	0.04	0.05
MgO	0.06	b.d.	0.05	0.02
CaO	26.19	26.31	27.17	26.86
BaO	b.d.	b.d.	b.d.	n.a.
Na_2O	0.06	0.04	b.d.	b.d.
K_2O	0.02	b.d.	b.d.	b.d.
Anhydrous Totals	95.09	95.20	97.52	97.33
Number of cations on basis of 44 positive charges and 24(O,OH) groups.				
Si	5.783	5.795	5.805	5.911
Ti	0.058	0.004	-	-
Aliv	0.159	0.201	0.195	0.089
Al*	3.757	3.750	3.904	3.629
Fe*	0.324	0.342	0.184	0.433
Mn	0.008	0.012	0.005	0.006
Mg	0.013	-	0.011	0.005
Ca	3.927	3.941	3.949	3.942
Ba	-	-	-	-
Na	0.016	0.011	-	-
K	0.004	-	-	-
$X_{Fe}=Fe^*/Fe^*+Al$	0.076	0.079	0.043	0.104

(1)pseudomorph of groundmass plag (Plate 1E,F); (2)prehnite in pseudomorph of olivine; (3)blade of pr in amygdale (Plate 3F); (4)in amygdale with ep.

* Total Fe as Fe_2O_3

Table 3.6 continued

Sample	(5)GT19D	(6)2FL1	(7)5FL4	(8)19FL2
SiO_2	43.15	42.77	43.65	43.08
TiO_2	b.d.	b.d.	b.d.	0.06
Al_2O_3*	22.65	21.62	22.43	22.60
Fe_2O_3	2.28	3.03	1.92	2.96
MnO	0.08	0.10	0.14	0.10
MgO	0.02	0.83	b.d.	0.04
CaO	27.46	26.56	26.86	26.78
BaO	n.a.	n.a.	n.a.	n.a.
Na_2O	b.d.	b.d.	0.03	0.03
K_2O	n.a.	n.a.	n.a.	n.a.
Anhydrous totals	95.64	94.92	95.01	95.65
Number of cations on basis of 44 positive charges and 24 (O,OH) groups.				
Si	5.992	5.994	6.076	5.983
Ti	-	-	-	0.006
Aliv	0.008	0.006	-	0.011
Al*	3.699	3.566	3.680	3.688
Fe*	0.238	0.319	0.201	0.309
Mn	0.010	0.012	0.016	0.012
Mg	0.003	0.173	-	0.008
Ca	4.085	3.989	4.006	3.985
Ba	-	-	-	-
Na	-	-	0.007	0.008
K	-	-	-	-
$X_{Fe}=Fe^*/Fe^*+Al$	0.060	0.040	0.052	0.077

(5)in amygdale with ep; (6)in amygdale with ep+q; (7)in vein with ep+q; (8)pseudomorph of plag with ep+pu.

* Total Fe as Fe_2O_3

a similar range of Fe^{3+} content in prehnite from the Karmutsen volcanics, with the exception of three samples of $X_{Fe} \geq 0.30$. Liou et al. (1983) found that unit cell size increased with increasing f_{O2}, probably due to increasing iron content. The low-Fe prehnites observed in the study area may therefore represent low f_{O2} conditions during the hydrothermal metamorphism. The effects of oxygen fugacity on authigenic assemblages are discussed in detail later.

Liou et al. (1983) tabulated K_D values calculated from published data and their experimental work for Fe^{3+} - Al^{3+} for epidote - prehnite assemblages. Table 3.7 contains some of this data and two K_D values from amygdaloidal epidote - prehnite assemblages, where these minerals were observed in contact. The values are quite different and appear to be most closely related to the K_D value for the low pressure, low temperature assemblage from the Cerro Prieto geothermal field.

Pumpellyite - Crystallography

The unit cell and space group of pumpellyite were first determined by Coombs (1953), using Weissenberg photographs for a sample from the Calumet type locality of Palache and Vassar (1925). From the oscillation photographs and pyroelectric and piezoelectric tests, he concluded that pumpellyite is holosymmetric in the space group A2/m. The unit cell of the Calumet pumpellyite is: $a=8.81 \pm 0.02$ Å,

Table 3.7 Distribution coefficients of co-existing prehnite and epidote from low-grade metamorphic rocks and experimental studies. Data from Liou et al. (1983) and this study.

Assemblage (locale)	X_{Fe}^{pr}	X_{Fe}^{ep}	K_D	Suggested P-T conditions
ep+pr+pu+ab+chl (Pennsylvania)	0.11	0.27	3.0	pr-pu facies
ep+pr+q (Cerro Prieto geothermal field)	0.18	0.24	3.9	0.4kb, 320°C
ep+pr+chl+Kspar+cpx (Larderello-Travale geothermal field)	0.03	0.23	9.6	0.5kb, 250-350°C
pr+ep+mt+q (Liou et al. (1983), experimental work)	0.10	0.25	3.0	2kb, 376°C
pr+ep+q (GT19D2, Kipulta basalt)	0.05	0.23	5.68	0.5kb, ~200°C
pr+ep+q (GT19C1, Kipulta basalt)	0.10	0.30	3.85	0.5kb, ~200°C

b=5.94±0.01 Å, c=19.14±0.02 Å, and β=97.6°±0.2°. Coombs (1953) also noted that the lattice parameters of pumpellyite changed slightly as Fe^{3+} replaced Al.

Galli and Alberti (1969) refined the structure of pumpellyite using a sample from Hicks Ranch, California. The unit cell data of this sample were a=8.83±0.01 Å, b=5.90±0.01Å, c=19.17±0.02 Å and β=97°7′±5′. They found that the cyrstal structure of pumpellyite is quite similar to that of epidote. There are two types of symmetrically equivalent chains of octahedral co-ordination. One type of chain contains Al, Fe and Mg atoms, while the second is composed of only Al atoms. As in the epidote structure, these chains are linked by SiO_4 and Si_2O_7 groups and there are two independent calcium sites situated between the chains.

Galli (1972) continued the study of the Hicks Ranch sample and indexed the x-ray diffraction powder pattern on the basis of the structure factors obtained previously (Galli and Alberti, 1969). The unit lattice constants were determined using a least squares treatment as: a=8.8204±0.0003 Å, b=5.9038±0.0003 Å, c=19.118±0.001 Å, β=97°24′42′′±13′′.

Yoshiasa and Matsumoto (1985) refined the crystal structure of an Al-rich pumpellyite [a=8.812(4) Å, b=5.895(2) Å, c=19.116(11) Å, β=97.41(7)°] in the space group A2/m using single-crystal counter-collected data. The resulting R value

for the structure of 2.69% indicates that it is more accurate than that of Galli and Alberti (R=12.3%). The structure contains octahedra that share edges to form linear chains parallel to the [010] direction. They confirmed the presence of two symmetrically independent chains, one composed of M(2) octahedra on a special position, while the other consists of M(1) octahedra on the general position. As in epidote, both double tetrahedra ($Si_2O_6(OH)$) and isolated tetrahedra (SiO_4) cross-link the octahedral chains to form an open three-dimensional framework that accommodates the calcium atoms.

Distribution of cations in the pumpellyite structure is also similar to that of epidote, the Al, Fe and Mg substituting between two distinct octahedral sites. The M(1) sites are almost completely occupied by Al^{3+}, and M(2) sites are occupied by Mg^{2+}, Fe^{2+}, Fe^{3+}, and Al^{3+}. The electric charge of the M(2) site is compensated by the amount of hydrogen atoms as follows: $M^{2+}_{M(2)} + H^{+}_{H(11)} + O^{2-}_{O(11)} = M^{3+}_{M(2)} + O^{2-}_{O(11)}$. There is no molecular water in the pumpellyite structure.

The crystal structure data of Yoshiasha and Matsumoto were used in PHKLI to calculate the theoretical powder pattern used to index the patterns from the Kleanza Creek - Kipulta Creek study area. The resulting unit cell parameters and relevant compositions are given in Table 3.8 along with data from the literature. The cell volumes of the

Table 3.8 Unit cell - composition data for pumpellyite

Sample	a(A)	b(A)	c(A)	B(°)	V(A^3)	X_{Fe}
1.GT19E2	8.811 ±0.004	5.923 ±0.002	19.182 ±0.006	97°48′ ±2′	991.81 ±0.44	0.16
2.1FL2	8.832 ±0.009	5.938 ±0.006	19.135 ±0.025	97°33′ ±6′	994.76 ±0.15	0.14
3.pu	8.812 ±0.004	5.895 ±0.002	19.116 ±0.011	97°25′ ±4′	984.75	0.08
4.pu	8.8204 ±0.003	5.9038 ±0.0003	19.118 ±0.001	97°24′43" ±13"	987.3 ±0.1	0.08
5.pu	8.81	5.94	19.14	97°36′	992 ±1	0.15
6.pu	8.84	5.92	19.21	97°30′	1000 ±1	0.23
7.pu	8.82	5.92	19.20	97°24′	994 ±1	0.19

3. Yoshiasha and Matsumoto (1985) Sanbagawa, Japan

4. Galli (1972) Hicks Ranch, California

5. Coombs (1953) Calumet, Michigan

6. Surdam (1969) Karmutsen Volcanics, British Columbia

7. Surdam (1969) Karmutsen Volcanics, British Columbia

pumpellyites from the study area compare favourably with cell volumes of other relatively Fe-poor pumpellyites. From Table 3.8, it is evident that unit cell volume does reflect increases in Fe-content, but that no systematic relationship exists.

Pumpellyite - Composition

Coombs (1953) determined from his analyses of pumpellyite that the chemical formula proposed by Irving et al. (1932) $Ca_4R_6Si_6O_{23}(OH)_3.2H_2O$ was valid. Later, Galli (1972) suggested that the chemical formula for pumpellyite should reflect Na and Fe^{2+} substitution in the Ca sites, and Mg^{2+}, Fe^{2+}, and Fe^{3+} substitution for Al^{3+}. Allman and Donnay (1971) rejected the presence of molecular water in the structure, and used 26 O(OH) groups to determine the structural formula.

Passaglia and Gottardi (1973) reviewed the crystal chemistry of pumpellyites and juglodite to propose a set of rules to be used in the calculation of the chemical formula. They also proposed a new nomenclature system for the mineral group based on the dominant cation in the X [M(2)] site. Coombs et al. (1976) modified these rules by calculating the chemical formula on the basis of 16 cations per formula unit. These modified rules form the basis of the computer program PUFORM, which was used in this study to calculate structural formulae of pumpellyite analyses. Coombs et al. (1976) also

modified the nomenclature system for use with microprobe analyses for which the distinction between Fe^{2+} and Fe^{3+} has not been made. This modified nomenclature was used to classify the pumpellyites given in Table 3.9. The Kleanza Creek - Kipulta Creek pumpellyites are in general pumpellyite-Fe; those analyses corresponding to pumpellyite-Mg have almost equal amounts of Fe and Mg in the M(2) site.

These pumpellyite compositions are more typical of pumpellyite-actinolite and glaucophane schist assemblages than low-grade hydrothermal pumpellyites (Figure 3.4). This may be due to the presence of very iron rich epidotes (Table 3.4) and chlorites (Table 3.10) associated with these pumpellyites. In general, the metamorphic assemblages indicate low pressure and low temperature conditions for the metamorphism. There is no evidence that the groundmass pumpellyites are relics of the earlier greenschist facies metamorphism.

Laumontite - Crystallography and Composition

Amirov et al. (1967) and Bartl and Fischer (1967) studied the crystal structure of laumontite using single crystal x-ray diffraction. Laumontite consists of an alumino-silicate framework of silica tetrahedra and larger more distorted Al tetrahedra both of which form 6-unit, 4-unit and 8-unit rings. Unlike the other zeolites such as

Table 3.9 Electron microprobe analyses of pumpellyite.

Sample	(1)19FL2	(2)GT19C2	(3)GT19C1	(4)1FL2
SiO_2	36.83	37.48	36.96	37.54
TiO_2	b.d.	0.03	0.06	b.d.
Al_2O_3*	24.79	25.33	25.68	24.81
Fe_2O_3	7.30	5.48	6.24	6.72
MnO	0.13	0.18	0.23	0.24
MgO	2.94	3.16	2.62	2.92
CaO	22.92	23.19	23.17	22.87
Na_2O	b.d.	b.d.	b.d.	b.d.
Anhydrous Total	94.91	94.85	94.96	95.01
Number of cations on basis of 16 positive charges.				
Si	5.857	5.926	5.861	5.952
Ti	-	0.004	0.007	-
Al*	4.648	4.721	4.801	4.638
Fe*	0.874	0.652	0.745	0.802
Mn	0.018	0.024	0.031	0.032
Mg	0.697	0.745	0.619	0.689
Ca	3.906	3.929	3.937	3.885
Na	-	-	-	-
W	3.92	3.95	3.97	3.92
X	2.08	2.05	2.03	2.08
Y	4.00	4.00	4.00	4.00
Z	6.00	6.00	6.00	6.00
$X_{Fe}=Fe^*/Fe^*+Al$	0.158	0.121	0.134	0.148
$X_{Fe}=Fe^*/Fe^*+Al+Mg$	0.140	0.107	0.121	0.131
X[M(2)] Fe	0.874	0.652	0.745	0.802
Mg	0.697	0.745	0.619	0.689
Al	0.506	0.651	0.669	0.592
	pu-Fe	pu-Mg	pu-Fe	pu-Fe

(1)pseudomorph of plag with ep; (2)in amygdale with epidote; (3)in amygdale with ab+ep; (4)in amygdale with ep+pr+lm+chl.

* Total Fe as Fe_2O_3

Table 3.9 continued

Sample	(5)1FL2	(6)GT19F1	(7)GT19E3	(8)GT19E3
SiO_2	37.38	36.84	37.52	36.97
TiO_2	b.d.	b.d.	b.d.	0.03
Al_2O_3*	24.61	23.27	23.44	23.09
Fe_2O_3	7.01	8.88	6.75	7.00
MnO	b.d.	0.14	0.24	0.23
MgO	2.85	2.79	3.72	3.34
CaO	23.49	23.27	22.71	22.39
Na_2O	b.d.	b.d.	b.d.	0.06
Anhydrous totals	95.34	95.19	94.38	93.11
Number of cations on basis of 16 positive charges.				
Si	5.916	5.884	5.984	5.989
Ti	-	0.002	-	0.004
Al_*	4.592	4.382	4.408	4.410
Fe*	0.835	1.068	0.810	0.853
Mn	-	0.019	0.032	0.032
Mg	0.673	0.665	0.884	0.806
Ca	3.983	3.982	3.881	3.887
Na	-	-	-	0.019
W	3.98	4.00	3.91	3.94
X	2.02	1.98	2.09	2.06
Y	4.00	4.00	4.00	4.00
Z	6.00	6.00	6.00	6.00
$X_{Fe}=Fe^*/Fe^*+Al$	0.139	0.196	0.155	0.162
$X_{Fe}=Fe^*/Fe^*+Mg+Al$	0.123	0.175	0.133	0.141
X[M(3)] Fe	0.835	1.068	0.810	0.854
Mg	0.673	0.665	0.884	0.806
Al	0.508	0.266	0.392	0.403
	pu-Fe	pu-Fe	pu-Mg	pu-Fe

(5)pseudomorph of plag; (6)only phase in amygdale; (7)in amygdale with chlorite; (8)pseudomorph groundmass plag.

* Total Fe as Fe_2O_3

Table 3.9 continued

Sample	(9)GT19HZ	(10)GT19HZ
SiO_2	37.02	37.04
TiO_2	0.03	0.07
Al_2O_3*	23.58	23.83
Fe_2O_3	6.76	6.81
MnO	0.26	0.20
MgO	3.30	3.05
CaO	22.78	22.73
Na_2O	b.d.	b.d.
Anhydrous totals	94.07	93.73
Number of cations on the basis of 16 positive charges.		
Si	5.954	5.963
Ti	0.004	0.008
Al*	4.471	4.523
Fe*	0.818	0.825
Mn	0.035	0.027
Mg	0.791	0.732
Ca	3.926	3.921
Na	-	-
W	4.06	3.95
X	2.04	2.05
Y	4.00	4.00
Z	6.00	6.00
$X_{Fe}=Fe^*/Fe^*+Al$	0.155	0.154
$X_{Fe}=Fe^*/Fe^*+Mg+Al$	0.134	0.136
X[M(2)] Fe	0.818	0.825
Mg	0.791	0.732
Al	0.429	0.495
	pu-Fe	pu-Fe

(9)pseudomorph of groundmass plag; (10)pseudomorph of plag phenocryst.

* Total Fe as Fe_2O_3

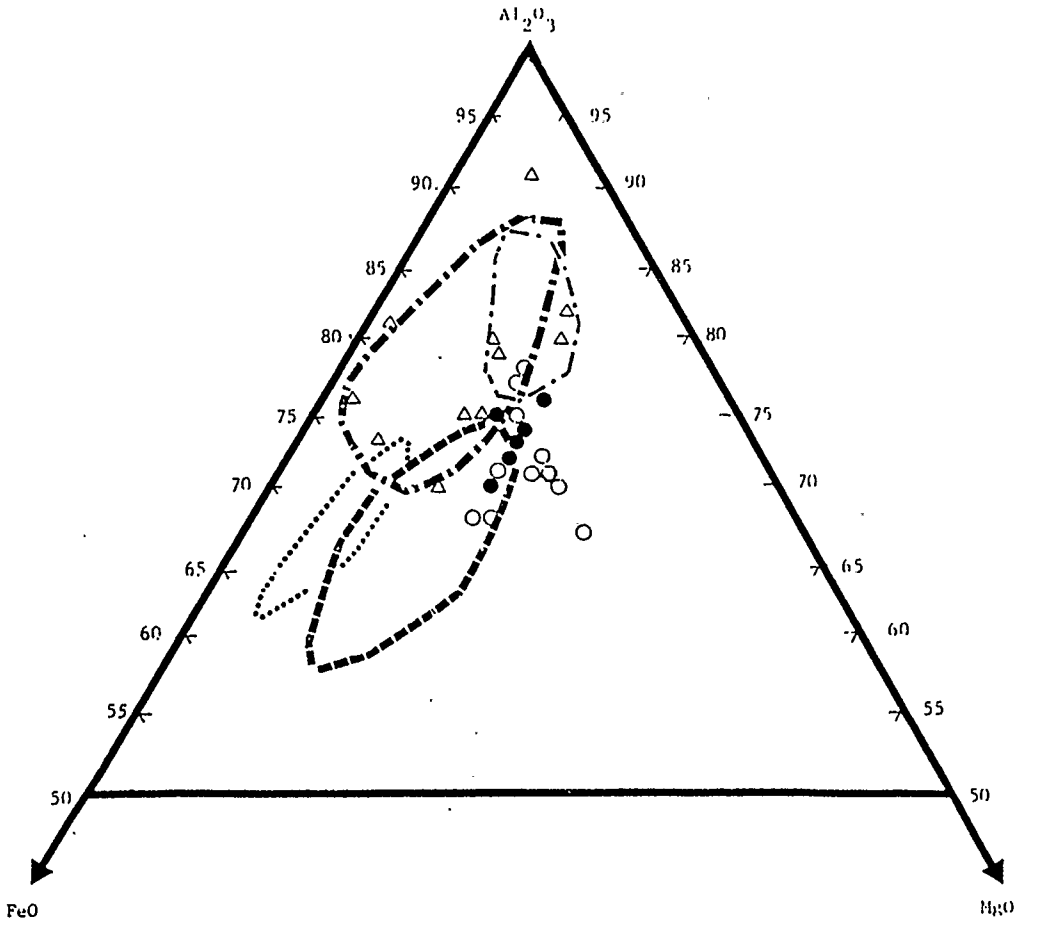

Figure 3.4 AFM plot of pumpellyite compositions from the Kleanza Creek - Kipulta Creek area.

△ amygdaloidal pumpellyite from study area

○ groundmass pumpellyite from study area

● overlap of amygdale and groundmass compositions

..... Karmutsen Volcanics

▬▬▬▬ Jamestown, Pennsylvania (pumpellyite - actinolite)

▬ ▬ ▬ Loeche, Switzerland (pumpellyite - actinolite)

— · — · — · Glaucophane schists, California

Adapted from Liou (1979).

Table 3.10 Representative electron microprobe analyses of authigenic minerals from the Kleanza Creek - Kipulta Creek area.

Sample	(1)16FL1 analcite	(2)12FL1 chlorite	(3)5FL4 chlorite	(4)17FL1 chlorite
SiO_2	55.66	29.32	29.52	25.77
TiO_2	n.a.	b.d.	b.d.	n.a.
Al_2O_3	22.00	14.56	15.32	22.23
FeO*	b.d.	17.66	13.03	17.17
MnO	0.03	0.61	0.62	b.d.
MgO	b.d.	22.67	27.32	19.19
CaO	b.d.	0.16	0.11	0.05
BaO	b.d.	n.a.	n.a.	n.a.
Na_2O	13.07	b.d.	b.d.	b.d.
Anhydrous totals	90.78	85.00	85.92	84.40
Number of cations				
Si	2.050	6.143	5.974	5.390
Ti	-	-	-	-
Aliv	-	1.857	2.026	2.610
Al	0.955	1.737	1.626	2.871
Fe*	-	3.095	2.205	3.003
Mn	0.001	0.109	0.107	-
Mg	-	7.080	8.238	5.984
Ca	-	0.036	0.024	0.011
Ba	0.000	-	-	-
Na	0.933	-	-	-
K	-	-	-	-

(1)in vein with calcite; (2)groundmass alteration; (3)groundmass alteration; (4)groundmass alteration.

* Total Fe as FeO

natrolite and heulandite, the silica and alumina tetrahedra are independent of each other. Open channels pass through the axis of the eight channel rings and control the zeolitic properties of the mineral (such as cation exchange) in the absence of the large cavities which characterize the other zeolites. Molecular water is located in these channels. Ca cations are located in the framework beneath the silica tetrahedra.

The unit cell parameters for laumontite from the study area are given in Table 3.11 along with values from the literature for laumontite and its dehydrated equivalent, leonhardite. The unit cell volume for natural laumontite reported by Bartl and Fischer (1967) is smaller than that given by Amirov et al. (1967), Liou (1971c), and the data from this study. It is closer to the values for leonhardite reported by Liou (1971c), which may indicate that their sample was dehydrated. The unit cell volumes of the samples from the Kleanza Creek - Kipulta Creek area are very similar to those of the synthetic laumontites (Liou, 1971c, $\pm 1\sigma$). This indicates that little or no dehydration of laumontite has occurred.

The laumontite samples from the Kleanza Creek - Kipulta Creek are almost pure Ca end-member laumontites (Table 3.12) with less than 5 mole% substitution of Ba+Na+K. The relative purity of these minerals permits the application of experimental results directly to laumontite-bearing

assemblages.

Table 3.11 Unit cell data for laumontite and leonhardite

Sample	a(Å)	b(Å)	c(Å)	β(°)	V(Å^3)
1.Laumontite	14.75 ±0.03	13.10 ±0.03	7.57 ±0.03	112°2′ ±12′	1346 ±4
2.Laumontite	14.90	13.7	7.55	111°30′	1367
3.Laumontite (synthetic)	14.758 ±0.009	13.072 ±0.004	7.562 ±0.004	112°1′ ±2′	1353 ±2
4.Laumontite (synthetic)	14.764	13.082	7.560	112°2′	1354
5.Leonhardite	14.75 ±0.03	13.10 ±0.02	7.55 ±0.01	112°0′ ±12′	1343 ±4
6.Leonhardite	14.75 ±0.05	13.08 ±0.02	7.57 ±0.05	112°	1344 ±5
7.Laumontite GT19F1	14.800 ±0.010	13.084 ±0.010	7.566 ±0.007	112°15′ ±5′	1356.1 ±0.2
8.Laumontite GT19A	14.766 ±0.004	13.090 ±0.008	7.573 ±0.003	111°53′ ±43′	1358.3 ±0.1

1. Bartl and Fischer (1967)

2. Amirov *et al*. (1967)

3.- 6. Liou (1971c)

4. Liou (1971c)

Table 3.12 Electron microprobe analyses of laumontite.

Sample	(1)1FL2	(2)1FL2	(3)GT19F1	(4)GT19A2	(5)GT19F1
SiO_2	51.17	51.68	51.84	50.32	51.75
TiO_2	n.a.	n.a.	n.a.	n.a.	n.a.
Al_2O_3*	21.96	22.15	21.88	22.45	22.05
Fe_2O_3	b.d.	b.d.	b.d.	0.03	b.d.
MnO	n.a.	n.a.	n.a.	n.a.	n.a.
MgO	b.d.	b.d.	b.d.	b.d.	b.d.
CaO	11.54	11.37	11.65	11.76	11.24
BaO	b.d.	b.d.	b.d.	b.d.	b.d.
Na_2O	0.04	0.06	0.06	0.07	0.10
K_2O	0.19	0.44	0.23	0.40	0.64
Anhydrous Totals	84.90	85.70	85.66	85.04	85.78
Number of cations on basis of 24 positive charges.					
Si	3.995	4.000	4.012	3.939	4.006
Ti	-	-	-	-	-
Al*	2.021	2.021	1.996	2.071	2.012
Fe	-	-	-	0.002	-
Mn	-	-	-	-	-
Mg	-	-	-	-	-
Ca	0.965	0.943	0.966	0.986	0.932
Ba	-	-	-	-	-
Na	0.006	0.009	0.009	0.011	0.015
K	0.019	0.043	0.023	0.040	0.063

(1)in amygdale surrounded by q; (2)lm alone in amygdale;
(3)in amygdale with calcite; (4)in amygdale with ep;
(5)lm alone in amygdale.

CHAPTER 4 PHYSICAL AND CHEMICAL CONDITIONS OF METAMORPHISM

Introduction

Duffell and Souther (1964) described the alteration of the Kleanza Creek Pluton and the surrounding volcanics as deuteric, and the regional metamorphism as being of lowest grade. Dudley (1983) discussed the hydrothermal nature of the zeolitization of the Howson subaerial facies in the Smithers Map Area. He concluded that the metamorphism occurred in a regime of high temperature/pressure ratio typical of geothermal fields, and that the nature of the alteration was primarily controlled by temperature, bulk composition, and fluid chemistry (Dudley, 1983). Other controls on the metamorphism were fluid and load pressures, porosity, permeability, f_{O2}, and activities of ionic species.

In the Kleanza Creek - Kipulta Creek area, the widespread occurrence of sub-greenschist facies minerals, patchy nature of the alteration, presence of fracture-filling phases and quartz veins of obvious hydrothermal origin, suggest that the most recent metamorphic process was hydrothermal. The relatively shallow depth of burial (approximately 6km, M. Mihalynuk pers. comm.) and lack of metamorphic fabric in the samples collected also support this conclusion.

Recent field studies of the Telkwa Formation in the nearby Zymoetz River area by Mihalynuk (1985) also revealed

extensive development of laumontite, prehnite and other calc-silicates of probable hydrothermal origin. The occurrence of these hydrothermal assemblages over such a large area indicates that geothermal activity was relatively widespread and likely related to the presence of apophyses of the Coast Plutonic Complex.

The authigenic assemblages described in Chapter 2 are similar to those documented in active geothermal fields such as Wairakei, New Zealand (Steiner, 1968), Cerro Prieto, Mexico (Bird et al., 1984) and several fields in Iceland (Kristmannsdottir, 1978; Viereck et al., 1982). Such assemblages have also been studied in fossil geothermal systems (Coombs et al., 1959; Dudley, 1983).

Wells in which hydrothermal minerals have been observed have generally been limited to depths of 2 - 3km. The range of depths (pressures) over which each mineral occurs varies from well to well, but the temperature range over which each occurs is fairly constant. For example, at Cerro Prieto (Bird et al., 1984), wairakite persists from 1500m to 2000m ($P_T=P_{hydrostatic}$ ~ 150b - 200b), over a temperature range of 200°C - 300°C. At Wairakei, wairakite was found between 180m and 600m of depth ($P_T=P_{hydrostatic}$ ~ 18b - 60b), but again in the temperature range of 200°C - 250°C (Coombs et al., 1959). This indicates that reactions forming low-grade minerals such as zeolites, prehnite, epidote and pumpellyite in hydrothermal areas tend to be more strongly dependent on

temperature than pressure.

Experimental stability studies of zeolites and other calc-silicate phases have been published by several investigators (e.g. Liou, 1971b, 1971c, 1973; Schiffman and Liou 1980, 1984; Johnson et al. 1980, 1983). Pressures greater than 1kb and runs in excess of 50 days were generally required to overcome the slow reaction rates involved. Pressure - temperature reversal brackets were used to derive univariant curves for the reactions and thermodynamic properties for the mineral phases (e.g. Helgeson et al. 1978; Bird and Helgeson 1980, 1981; Bird et al. 1984). Hammerstrom (1981) and Halbach and Chatterjee (1984) used linear parametric programming to derive internally consistent thermodynamic data for the CASH system from experimentally determined P - T pairs.

Thermodynamic data for the zeolites and prehnite are not well established. For example, Liou (1971b), Kerrick and Ghent (1979), Hammerstrom (1981) and Chatterjee et al. (1984) have produced quite different P - T curves for the reaction (4.1) pr = zo + gr + q + H_2O, which defines the maximum pressure and temperature limits for prehnite stability (Figure 4.1). The latter three papers were based on the experimental points from Liou (1971b). The curves presented in these papers show that the location of the univariant line in P - T space is uncertain. Entropy values for prehnite used for each curve are given in Table 4.1.

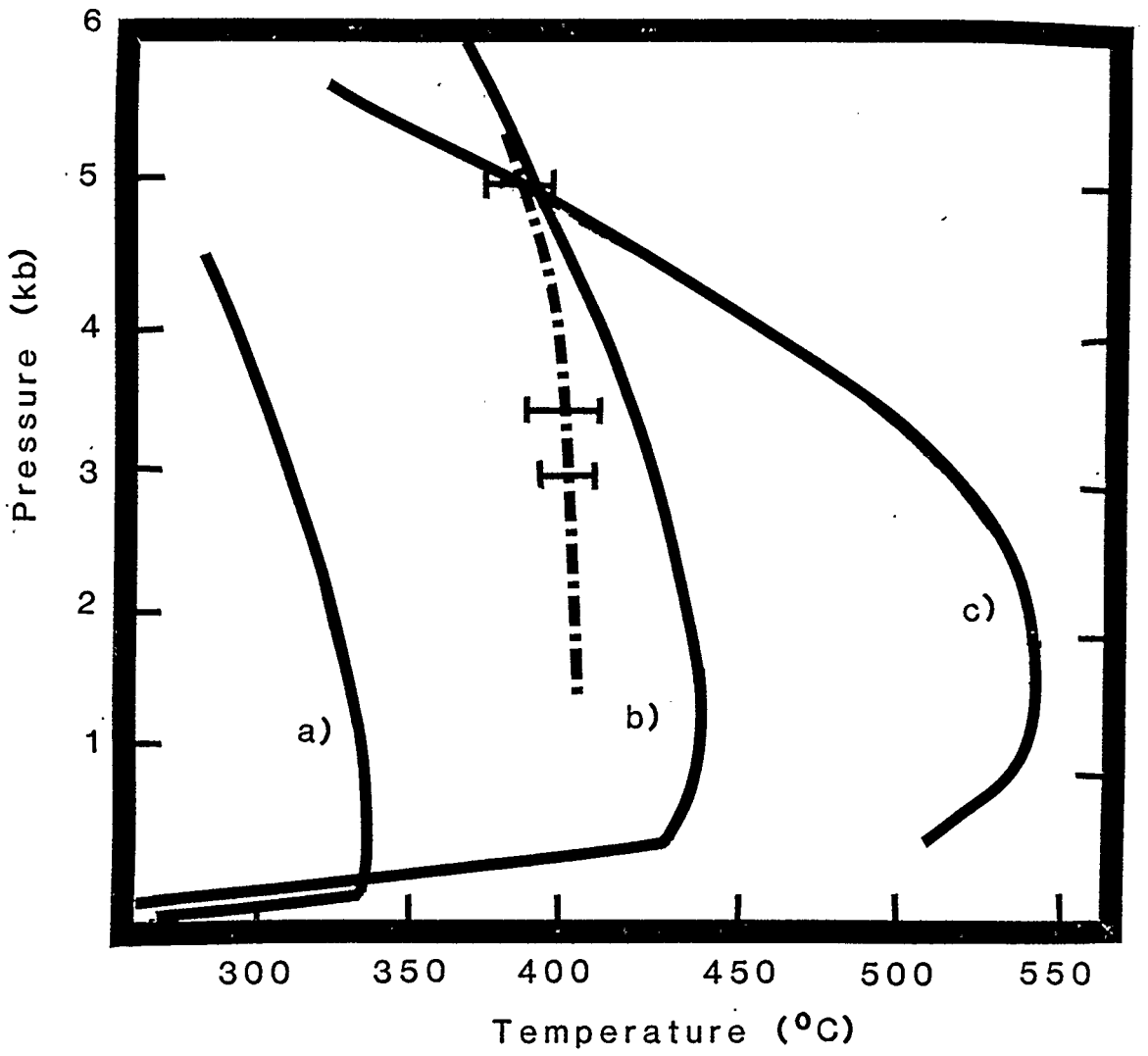

Figure 4.1. P-T curves for the reaction pr=zo+gr+q+H_2O which defines the upper stability limit of prehnite.
(a) Chatterjee et al. (1984) - derived from experimental results and calorimetric measurements using linear parametric programming.
(b) Hammerstrom (1981) - derived using linear parametric programming with curve constrained by Liou (1971b) 5kb bracket.
(c) Kerrick and Ghent (1979) - extrapolated from Liou (1971b) 5kb experimental bracket.
Entropies of prehnite used in the derivation of each curve are given in Table 4.1.

Table 4.1 Entropy Values for Prehnite used in Figure 4.1

Source	ΔS^{o} (cal $mol^{-1}K^{-1}$)	Curve in Figure 4.1
Chatterjee *et al.* (1984)	69.83	(a)
Hammerstrom (1981)	66.68	(b)
Kerrick and Ghent (1979)	62.83	(c)

The uncertainties inherent in the thermodynamic properties of prehnite are further complicated by the presence of Al^{3+}- Fe^{3+} substitution which produces a solid solution series similar to that of clinozoisite - epidote. Bird and Helgeson (1980) developed quantitative models to calculate the activity of end-members in epidote, prehnite, and grossular garnet solid solutions. The model for epidote entails the calculation of the distribution of Fe^{3+} and Al^{3+} on the three M-sites. The calculations are based on the assumption that the degree of ordering in epidote is dependent on temperature and independent of composition. Sample low temperature values for the ordering parameter (σ), and Fe^{3+}, M(1) - M(3) site occupancies are given in Table 4.2. Bird and Helgeson (1980) demonstrated that ordering in the epidote structure decreases with increasing temperature, and that at low temperatures essentially all of the Fe^{3+} is in the M(3) site.

As discussed in the epidote crystallography section, composition does appear to exert some control over the distribution of Fe^{3+}, in that substitution for Al^{3+} in M(1) sites occurs only at high $X_{Fe}3+$ values (Dollase, 1973). However, the model of Bird and Helgeson (1980) provides a fairly good fit for the data presently available. Further Moessbauer work on synthetic epidotes, of known composition and temperature of formation, is needed to rigourously test this model.

Table 4.2 Ordering parameter for epidote as a function of temperature. Calculated from the equations of Bird and Helgeson (1980).

T(^{o}C)	T(K)	$T-T_r$ (1)	lnK	$\tanh^{-1}(\sigma)$	σ	X_{Fe}^{M1}	X_{Fe}^{M3}
190	463	165	-7.322	1.830	0.95	0.025	0.975
200	473	175	-7.158	1.789	~0.95	0.025	0.975
220	493	195	-6.857	1.714	~0.94	0.03	0.97
250	523	225	-6.449	1.612	~0.92	0.04	0.96
300	573	275	-5.867	1.467	0.90	0.05	0.95

(1) T_r=298.15K

Since analyzed samples of prehnite from the Kleanza Creek - Kipulta Creek area are relatively pure ($X_{Fe} \leq 0.07$), it was treated as a pure solid, $a_{pr}=1$. Epidote solid solutions were discussed in relation to experimental results involving epidotes of known composition (e.g. Liou et al., 1985), and field observations of epidote assemblages in active geothermal fields (e.g. Bird et al., 1984; Bird and Helgeson, 1981).

Estimate of Metamorphic Pressure

The pressure of metamorphism can be estimated using an average density of overlying strata and the estimated thickness of the pile (6km). Strata overlying the Telkwa Formation consist primarily of pyroclastics, shales, sandstones and several volcanic flows. A package similar to this comprises the Murihiku rocks of the Hokonui Hills of New Zealand. Geophysical work in that area indicated a density of $\rho=2.6x10^3 kg/m^3$ for these rocks (Boles and Coombs, 1977). By adopting these density and thickness estimates, the load pressure during metamorphism would have been $P_{load} \sim 1.5kb$, assuming alteration occurred after deposition of all strata.

Maximum load pressure can also be estimated using the experimentally derived curve for (4.2) laumontite = lawsonite + 2quartz + H_2O (Liou, 1971c) which has a relatively flat slope in P-T space (Figure 4.2), and the lack of lawsonite in the Kleanza rocks. Since lawsonite and laumontite show very

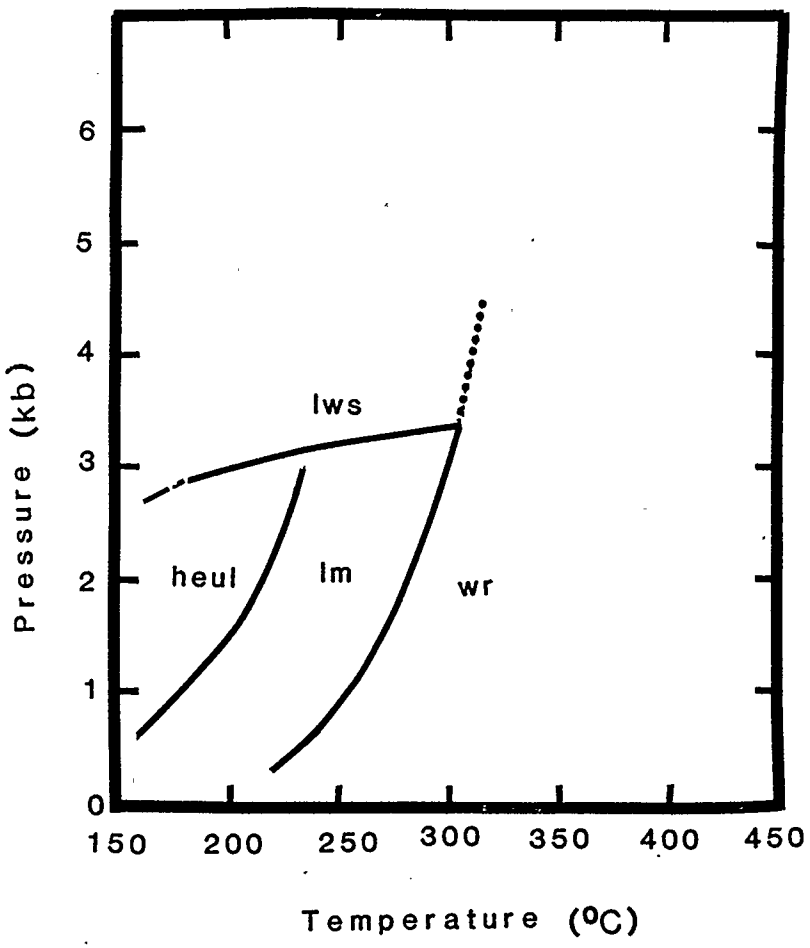

Figure 4.2. Experimental P-T stability curves for lawsonite, laumontite, wairakite (from Liou, 1971c) and heulandite (Liou et al., 1985). Note the relatively flat slope of the curve for the reaction $lm=lws+H_2O$.

little solid solution, these experimental results can be applied directly to nature. Therefore, from this curve, the maximum P_{load} is approximately 3kb, which does not contradict the estimate given above.

As in other fossil and active geothermal systems, the calcsilicate phases are present as groundmass and phenocryst alteration and as amygdaloidal and vein phases. To estimate fluid pressure in the rocks the treatment of Thompson (1955) was adopted. In this case, fluid causing matrix alteration is assumed to be under conditions of $P_{H2O} = P_{load}$, while the fluid in veins and amygdales is at $P_{H2O} = (1/\rho_{rock})P_{load}$. For the Kleanza Creek - Kipulta Creek area, this would correspond to $P_{H2O} = (1/2.6)P_{load} \tilde{-} 0.4P_{load}$. The pressure difference is maintained under osmotic conditions by the behaviour of the wall-rock as a semi-permeable membrane.

The effects of this pressure differential on dehydration equilibria have been discussed by Thompson (1955), Greenwood (1961) and more recently by Bruton and Helgeson (1983). Under conditions of osmotic equilibrium, the free energy equation for a dehydration reaction in fissures or interconnected open spaces is:

(4.3) $\Delta G=0=\Delta H_r - T\Delta S_r + \Delta V_s(P_f - 1) + nRT\ln \Gamma_{H2O}P_f$.

The free energy equation for the rock column is:

(4.4) $\Delta G=0=\Delta H_r - T\Delta S_r + \Delta V_s(P_s - 1) + nRT\ln \Gamma_{H2O}P_s$.

The treatment of equilibria between the fluid and the rocks in the fissure wall, which are in a non-hydrostatic

stress state, varies. Thompson (1955) substituted the mean stress on the minerals for P, and predicted that wall rock alteration would occur at higher temperatures than the alteration of the main body of rock. Bruton and Helgeson (1983) concluded, from a rigorous mathematical treatment of the effects of non-hydrostatic stress, that dehydration temperatures would decrease outwards from the rock column to the fluid-rock interface.

Greenwood (1961) suggested that for porous rocks filled with fluid sustaining a lower pressure than the surrounding mineral grains, these "wall-rock" grains tend to dissolve and recrystallize to fill the pores and distribute the load stress hydrostatically. The net tendency would be to eliminate pore space and the non-hydrostatic stress state simultaneously. The highly altered condition of grains surrounding amygdales in the Kipulta basalts may indicate that such a process has occurred. However this high degree of alteration may also be due to the greater access of these grains to the hydrothermal fluid.

Estimate of Metamorphic Temperature

Temperature can be estimated using experimental and computed phase equilibria and from assumed geothermal gradients. A normal geothermal gradient of $30^{o}C/km$ would give T_{max} ~$180^{o}C$ for an assumed depth of 6km. However, geothermal fields frequently have non-linear thermal

gradients. For example, two wells from the Salton Sea geothermal field show an initial gradient of approximately 150°C/km for 1.5km, which decreases with depth to approximately 25°C/km (Bruton and Helgeson, 1983). At 6km depth in these wells, the temperature is approximately 400°C.

Downhole observations of laumontite, pumpellyite, prehnite and epidote suggest a temperature range of ~150 - 300°C for calc-silicate mineralization (Bird et al., 1984; Coombs et al., 1959; Kristmannsdottir, 1978). Clay alteration (e.g. sericitization and/or chlorite alteration) can occur at temperatures ranging from 100°C to 260°C (Steiner, 1968).

As noted in Chapter 2, epidote, pumpellyite, chlorite, and to some extent, prehnite, are present both as replacement phases and as vein and amygdale phases. In contrast, laumontite and analcime are generally restricted to amygdales and veins. Maximum temperature conditions during the hydrothermal activity can be inferred from groundmass alteration, while vein and amygdale assemblages may represent transient temperature states which did not affect the bulk of the rock mass.

The only occurrence of laumontite as groundmass alteration is in the basalt dike at locality 83-5F. The absence of stilbite and presence of laumontite, related by the reaction (4.5) $st = lm + H_2O$ indicates that T_{min} at $P_f = P_{load} = 1kb$ was approximately 155°C and ~170°C at

$P_f=P_{load}$=2kb (Figure 4.2; Ghent and Miller 1974; Hammerstrom 1981). The absence of heulandite (4.6 heul = lm + q + H_2O) at $P_f=P_{load}$=1kb indicates $T_{min} \tilde{-}$ 190°C and 205°C at $P_f=P_{load}$=2kb (Figure 4.2; Liou et al. 1985).

The reaction (4.7)lm = wr + H_2O (Figure 4.2) can be used to estimate maximum temperature. At $P_f=P_{load}$=1kb and 2kb, the absence of wairakite and the presence of laumontite in these rocks indicates maximum temperatures less than 255°C and 280°C respectively (Liou, 1971c).

Liou et al. (1983, 1985) studied sliding equilibria involving epidote and prehnite solid soluiton and located an invariant point in the CASH system at ~1.4kb, 230°C for the continuous reactions:

(4.8) pu + q = pr + ep + chl + H_2O;

(4.9) pr + lm = ep + q+ H_2O;

(4.10) pu + lm + q + H_2O = chl + ep;

and the discontinuous reaction

(4.11) lm + pr + chl = pu + q + H_2O

(Figure 4.3). At temperatures or pressures above the invariant point, laumontite is no longer stable in the calc-silicate assemblage. By introducing Fe_2O_3 to the system, the invariant point is displaced along the discontinuous reaction

(4.12) lm + pu + q = pr + ep + chl + H_2O.

The intersection of the X^{ep}_{Fe}=0.2 isopleth (the average composition of epidote in all samples analyzed is ~0.25) with

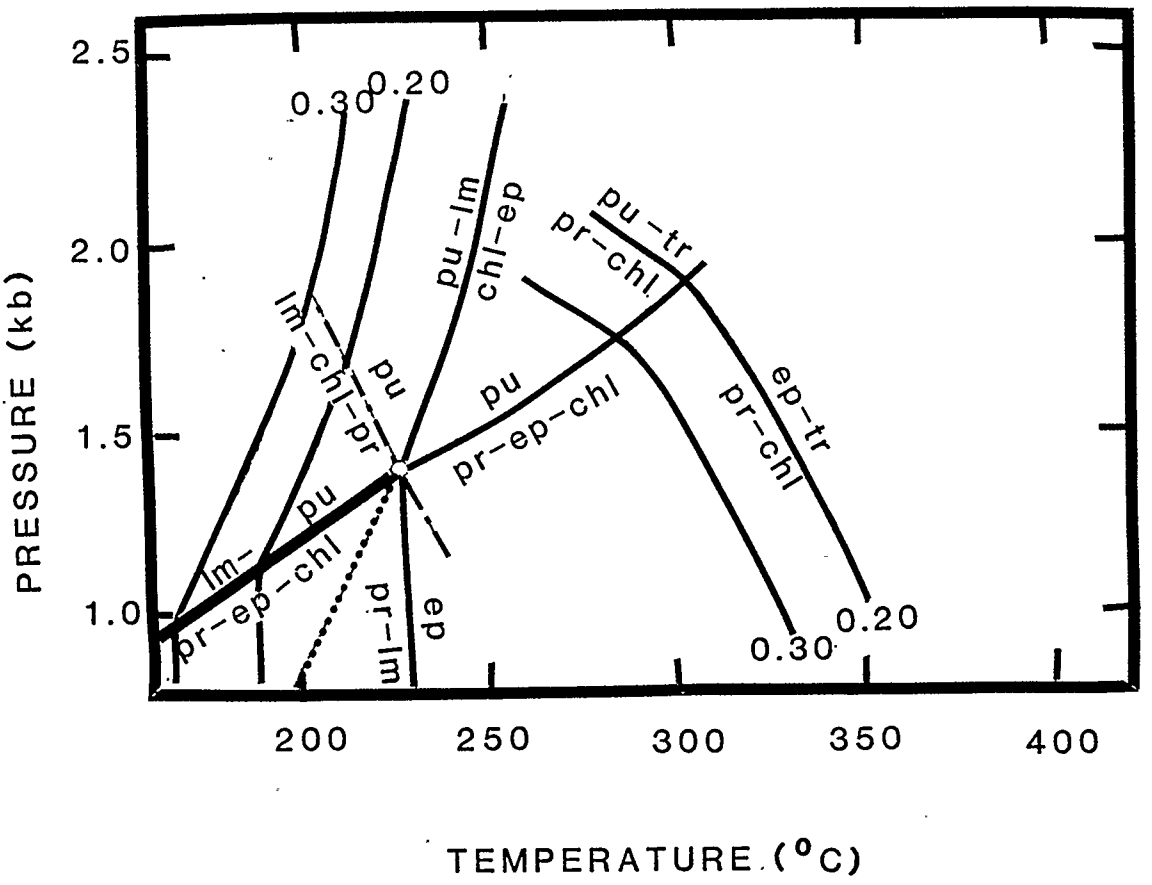

Figure 4.3. P_f-T diagram adapted from Liou et al. (1985) showing the distribution of phases in the system CaO-MgO-Al_2O_3-SiO_2-H_2O at low pressures and temperatures. The effect of the introduction of Fe_2O_3 to the system is shown by the X_{Fe}^{ep} isopleths. The average composition of epidote in the Kleanza Creek meta-basalts is approximately $X_{Fe}^{ep} = 0.25$.

the discontinuous reaction can be used to estimate T at $P_f=P_{load}=1.1kb$ as $\leq 190^oC$. Thus the rarity of laumontite alteration and predominance of ep + chl $\pm$ pr $\pm$ pu can be effected by temperatures in excess of 190^oC, which would also preclude the formation of heulandite and stilbite. Epidote compositions of ps25 and the lack of hydrothermal Ca-amphibole also indicates that T_{max} did not exceed 350^oC at the pressures of interest (Figure 4.3). This estimate is higher than that predicted by the absence of wairakite and therefore the latter estimate of $\sim 255^oC$ (P=1kb) more closely constrains the estimate of maximum temperature.

Temperature in the vein systems can be estimated from the reactions 4.3 to 4.5 and from:

(4.13) anal + q = ab + H_2O.

Albite, analcime and quartz stably coexist in veins in sample 16FL1. At $P=P_f=0.4kb$, temperature from the univariant curve is $\sim 200^oC$. Similarly, at $P_f=0.8kb$, $T\sim 190^oC$ (Thompson,1971; Liou, 1971a; Johnson, 1982). Helgeson et al. (1978) noted that slight amounts of solid solution in analcime would account for discrepancies of up to 50^oC in the experimentally determined dehydration temperatures at $P_f=P_{load}=5kb$. However, at $P\leq 1kb$, solid solution has little effect on temperature, and the analcime in the study area is almost stoichiometric ($NaAl_{0.95}Si_{2.05}O_6 \cdot H_2O$), indicating that vein temperatures were close to 200^oC. The absence of wairakite, heulandite and stilbite in veins containing laumontite

indicate a temperature range of T=140-250°C at P_f=400bars and T=180-270°C at P_f=800bars (Liou,1971c; Ghent and Miller 1974). Note that the less hydrous phases become more stable at lower temperatures in the veins than in the groundmass, as predicted above.

Effect of Bulk Composition on the Mineral Assemblages

As described in Chapter 2, the alteration of the basalts is quite different from that in the andesites, volcaniclastics, and quartz monzonite rocks. In these latter units, the dominant alteration is epidote + chlorite + muscovite + quartz ± calcite. Prehnite, laumontite and analcime are restricted to veins in the andesites and volcaniclastics and do not occur in the plutonic rocks. Pumpellyite was observed only in basaltic rocks.

The two alteration types occur in adjacent units which were not likely to have been under significantly different physical conditions of metamorphism. However, Coombs et al. (1970), and Dudley (1983) among others, noted the strong control of bulk rock composition on the authigenic assemblage. Ellis (1967) reviewed experimental results and published studies of natural hydrothermal areas, and concluded that the chemical characteristics of the waters were functions of temperature and the host rock composition. Ellis (1967) noted that for waters of relatively high potassium activity, the deep hydrothermal alteration

occurring in areas such as Wairakei, which has felsic volcanic and rhyolite-derived sedimentary host rocks, is quite different from that occurring in the andesitic and basaltic areas of Kamchatka and Iceland. At in-situ temperatures of 150° - 250°C (note that estimated temperature range for the Kleanza Creek area is 190° - 255°C) the alteration in the Wairakei-type environment consists of adularia, K-mica, epidote and wairakite. Assemblages of laumontite, calcite, chlorite and epidote are typical of basaltic areas in this temperature range.

Though there is some overlap of these alteration types in the basalt and andesite units of the Kleanza Creek area, the andesites and especially the quartz monzonite rocks do display a more limited suite of calc-silicate minerals and a tendency towards stronger clay alteration.

From this, several inferences may be made about the chemistry of the hydrothermal fluid that caused the alteration in the Kleanza Creek area:
(1) "leaching" of Ca^{2+} from Ca-pyroxenes and An-rich plagioclase in the basalts produced a fluid with comparatively higher $a_{Ca}2+$ than that which resulted from interaction with the more felsic, Ca-poor units;
(2) $a_{Na}+$ and $a_{K}+$ would be correspondingly higher in the fluid fluids interacting with the intermediate and felsic units than that with the basalts. Fluid composition is discussed in greater detail in the following section.

Fluid Composition - Activity of Ionic Species

Hemley (1959) and Hemley and Jones (1964) produced experimentally determined curves for m_{KCl}/m_{HCl} and m_{NaCl}/m_{HCl} versus T, and for m_{KCl}/m_{HCl} for the system Na-K-Al-Si-H_2O, using the equilibria listed in Table 4.3. These diagrams are reproduced in Figures 4.4a, b and c. Thermodynamic data published by Hemingway et al. (1982) and Helgeson et al. (1978) (Table 4.4) were used to recalculate the stability relations of these minerals using the reactions listed in Table 4.3 and assuming that $mKCl/mHCl=aK^+/aH^+$ and $mNaCl/mHCl=aNa^+/aH^+$ at $P_f=P_{load}=1kb$, $T=220^oC$, and $P_f=400b$, $T=200^oC$. These P-T pairs correspond to estimated geostatic and hydrostatic conditions, respectively (Figure 4.5). The thermodynamic properties of paragonite were used to estimate the equilibrium constant for reactions involving Na-montmorillonite because no data are presently available for this mineral.

Hemley and Jones (1964) found that these reaction curves tend toward higher ratios of mKCl/mHCl and mNaCl/mHCl at lower temperatures (Figure 4.4a). These observations support the results calculated at 1kb and 220^oC, shown in Figure 4.5, which have a topology similar to their experimental results at ~1kb and 550^oC, but at higher values of log a_{K^+}/a_{H^+} and log a_{Na^+}/a_{H^+}.

Table 4.3 List of reactions in the system Na_2O-K_2O-Al_2O_3-SiO_2-H_2O used to produce curves in Figure 4.4 and 4.5.

4.14 $musc + Na^+ = parag + K^+$

4.15 $3ab + 2H^+ + K^+ = musc + 6q + 3Na^+$

4.16 $3Kspar + 2H^+ = musc + 6q + 2K^+$

4.17 $musc + H^+ + 1.5H_2O = 1.5kaol + K^+$

4.18 $musc + H^+ + 3q = 1.5pyroph + K^+$

4.19 $Kspar + Na^+ = ab + K^+$

4.20 $3ab + 2H^+ = 2parag + 6q + 2Na^+$

4.21 $1.5pyroph + Na^+ = parag + 3q + H^+$

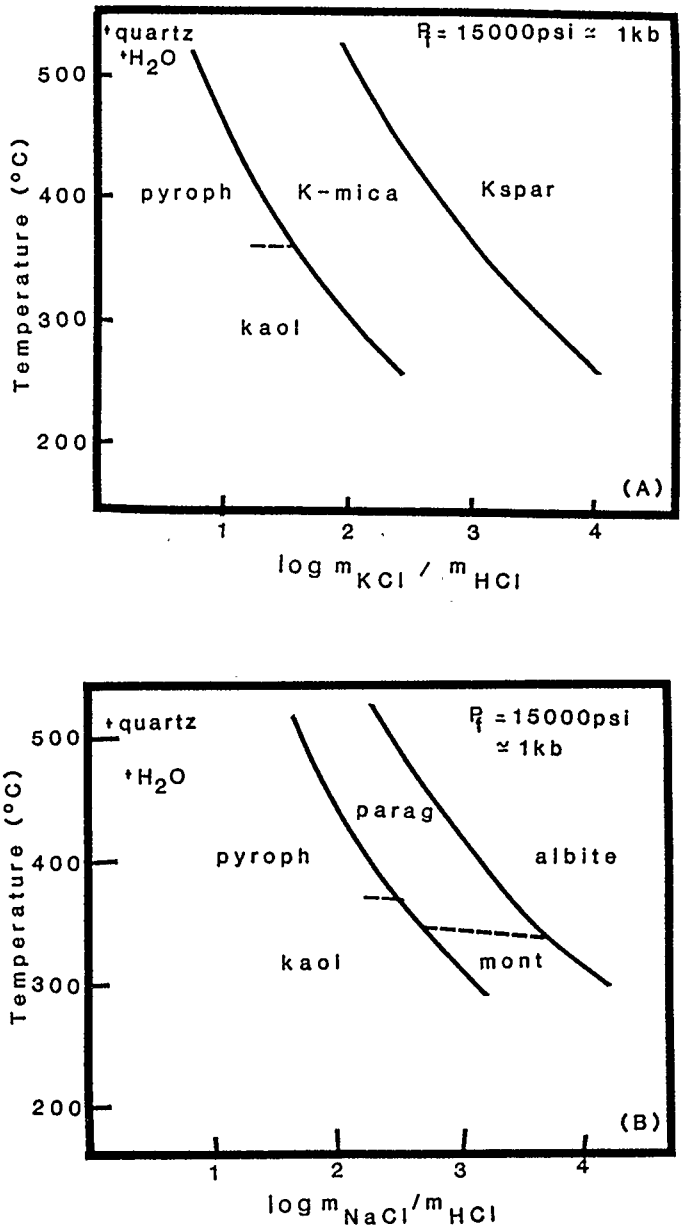

Figure 4.4. Reaction curves for the systems K_2O-Al_2O_3-SiO_2-H_2O (A) and Na_2O-Al_2O_3-SiO_2-H_2O (B), adapted from Hemley and Jones (1964). Relevant reactions are given in Table 4.3. Note the trend to higher ionic concentrations at lower temperatures.

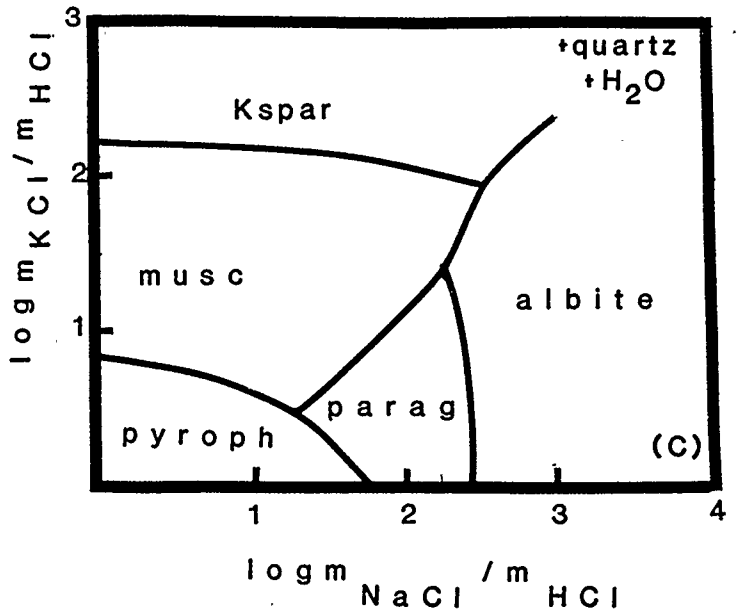

Figure 4.4c. Experimental log m_{KCl}/m_{HCl} versus log m_{NaCl}/m_{HCl} relations for the system Na_2O-K_2O-Al_2O_3-SiO_2-H_2O, at P_f=1kb, T=500°C. After Hemley and Jones, 1964. Relevant reactions are listed in Table 4.3. Compare Figure 4.5.

Table 4.4 Thermodynamic data used in calcuations. Data from Hemingway et al.(1982) unless otherwise indicated.

Name	Formula	$\Delta H^\circ_{f,298}$ (4)	$S^\circ_{,298}$ (5)	$\bar{V}$(6)
(1)quartz	SiO_2	-217,650	9.88	22.688
(1)steam	H_2O	-57,796	45.104	
(2)Ca^{2+}		-129,804	-13.5	
(2)K^+		-60,270	24.2	
(2)Na^+		-57,433	14.0	
(2)H^+		0.0	0.0	
kaolinite	$Al_2Si_2O_5(OH)_4$	-984651.05	48.989	99.520
prehnite	$Ca_2Al(AlSi_3)O_{10}(OH)_2$	-1480313.3	69.967	140.330
margarite	$CaAl_2(Al_2Si_2)O_{10}(OH)_2$	-1491302.5	63.011	133.800
pyrophyllite	$Al_2Si_4O_{10}(OH)_2$	-134875.8	57.223	125.900
(1)muscovite	$KAl_2(AlSi_3)O_{10}(OH)_2$	-1432068.6(3)	68.8	104.71
(1)paragonite	$NaAl_2(AlSi_3)O_{10}(OH)_2$	-1421623.6(3)	66.4	132.53
(1)clinozoisite	$Ca_2Al_3Si_3O_{12}(OH)$	-1648881.6(3)	70.64	136.2

(1)Helgeson et al. (1978)

(2)Helgeson et al. (1981)

(3)Tabulated values of ΔH°_f from Helgeson et al. (1978) adjusted to correct for Al standard state as per Hemingway et al.(1982).

$$\Delta H^\circ_{f,calc} = \Delta H^\circ_{f,table} + (-1.55 \text{ kcal/mol Al})(\text{number moles of Al})$$

(4)$cal\,mol^{-1}$

(5)$cal\,mol^{-1}K^{-1}$

(6)$cm^3\,mol^{-1}$

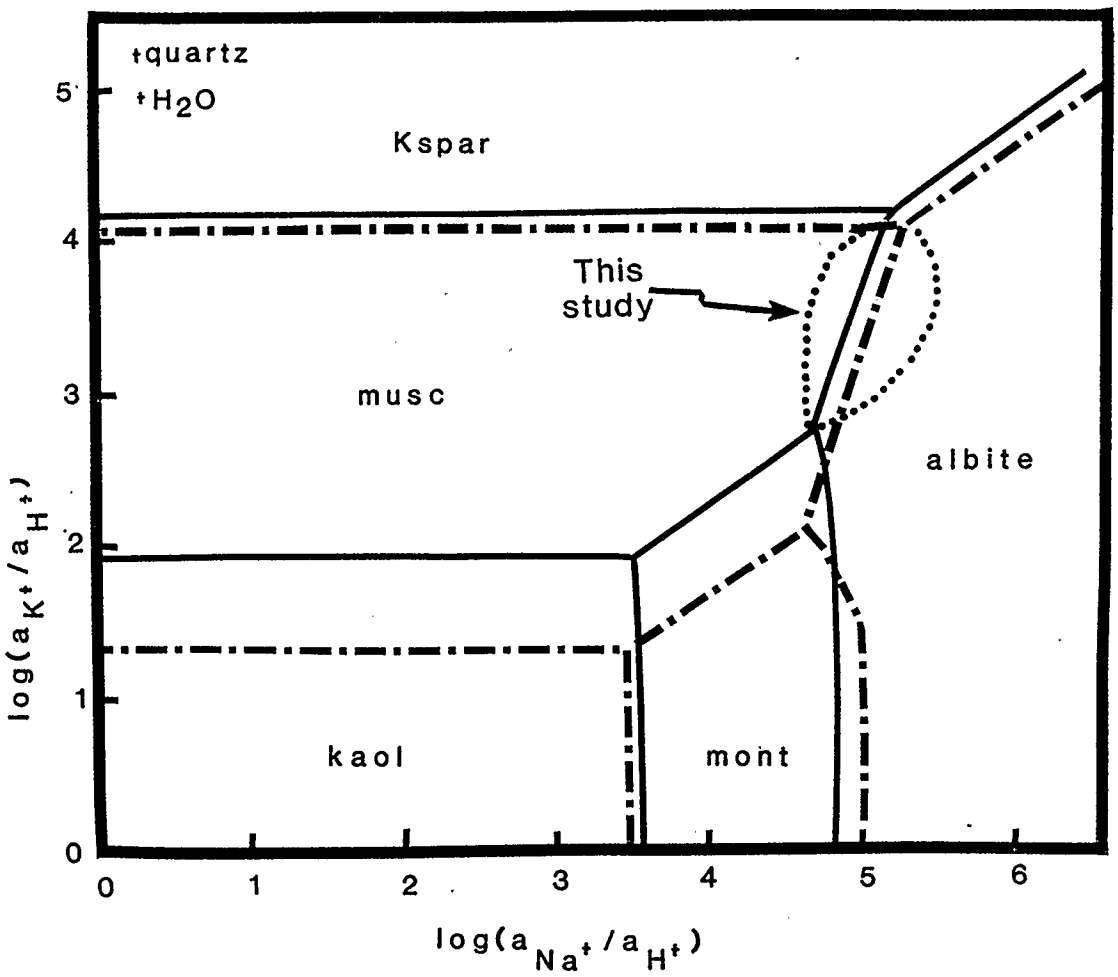

Figure 4.5. Calculated $\log(a_{K^+}/a_{H^+})$ versus $\log(a_{Na^+}/a_{H^+})$ relations for the system Na_2O-K_2O-Al_2O_3-SiO_2-H_2O.
Solid lines - $P_f=P_{load}$=1kb, T=220°C.
Dot-dashed lines - $P_f=P_{hydrostatic}$=400 bars, T=200°C.
Dotted curves represent range of possible fluid compositions for the Kleanza Creek - Kipulta Creek geothermal fluid based on observed assemblages.

Interpretation of authigenic clay and feldspar assemblages can be made using these diagrams. The ubiquitous presence of muscovite rather than kaolinite in all lithologies indicates that the a_{K^+}/a_{H^+} ratio of the fluid was high. K-feldspar alteration of groundmass feldspar is relatively rare, possibly indicating that $\log(a_{K^+}/a_{H^+}) < 4.2$. Similarly, the tendency for feldspars to be albitized, and the lack of Na-montmorillonite in these samples indicates a high value (~5) of $\log(a_{Na^+}/a_{H^+})$. The occurrence of the muscovite-albite assemblage in feldspars in most rocks may indicate that the fluid composition was in the narrow range indicated in Figure 4.5. This would correspond to a relatively low $\log(a_{Na^+}/a_{K^+})$ value (~1.5).

Authigenic albite and K-feldspar are relatively uncommon in fissures which are instead generally dominated by calc-silicates and chlorite in the basalts, and calcite and quartz in the other host rocks. This may indicate that $a_{Na^+}{}^2/a_{Ca^{+2}}$ and $a_{K^+}{}^2/a_{Ca^{+2}}$ were quite low.

Bird and Helgeson (1981) related the K-feldspar - albite authigenic groundmass assemblage to the epidote - muscovite - quartz assemblage by the reaction:

(4.22) $6KAlSi_3O_8 + 3NaAlSi_3O_8 + 4Ca^{+2} + 2H_2O =$

K-feldspar albite

$2Ca_2Al_3Si_3O_{12}(OH) + KAl_2(AlSi_3O_{10}(OH)_2 + 18SiO_2 + 3Na^+ + 5K^+$

clinozoisite muscovite quartz

Assuming the activities of the feldspars and muscovite are

unity (i.e. they are pure minerals), the equilibrium constant expression can be written as: (4.23) $K=a^3_{Na}+a^5_{K}+/a^4_{Ca}+2(a^2_{cz})$ or (4.24) $\log K-2\log(a_{cz})=\log(a^3_{Na}+a^5_{K}+/a^4_{Ca}+2)$. Figure 4.6 relates $\log(a^3_{Na}+a^5_{K}+a^{-4}_{Ca}+2)$ to temperature along compositional isopleths of epidote solid-solution for three active geothermal fields. The estimated temperature conditions and measured epidote compositions from the Kleanza Creek-Kipulta Creek area are also plotted on the diagram. There is coincidence with one set of analyses from the Otake field. Therefore, the ep - musc - q assemblage would be favoured over the Kspar - ab assemblage at $\log(a^3_{Na}+a^5_{K}+/a^4_{Ca}+2)<-1$ at $T\sim200^{o}C$ and $X_{Fe}^{ep}\sim0.25$. Also note that at temperatures in the range of interest (i.e. 190°C to 255°C) increasing X_{Fe}^{ep} from 0.00 to 0.20, essentially increasing the activity of Fe^{+3} in solution, has very little effect on the value of $\log(a^3_{Na}+a^5_{K}+/a^4_{Ca}+2)$.

The direct relationship between $\log(a_{Ca}+2/a^2_{H}+)$ and temperature is shown in Figure 4.7. Figure 4.8 shows the relationship between $\log(a_{Ca}+2/a^2_{H}+)$ and $\log(a_{Fe}+3/a^3_{H}+)$ at constant pressure and temperature. From these diagrams the crystallization order of the calc-silicates in veins and amygdales can be interpreted. The basic order is: pumpellyite + epidote - laumontite - prehnite.

In ep - pr - pu assemblages, Fe^{+3} tends to concentrate in the epidote structure (Schiffman and Liou, 1983). Mg^{+2}, Fe^{+2} and Fe^{+3} ions are then taken up by pumpellyite. Any

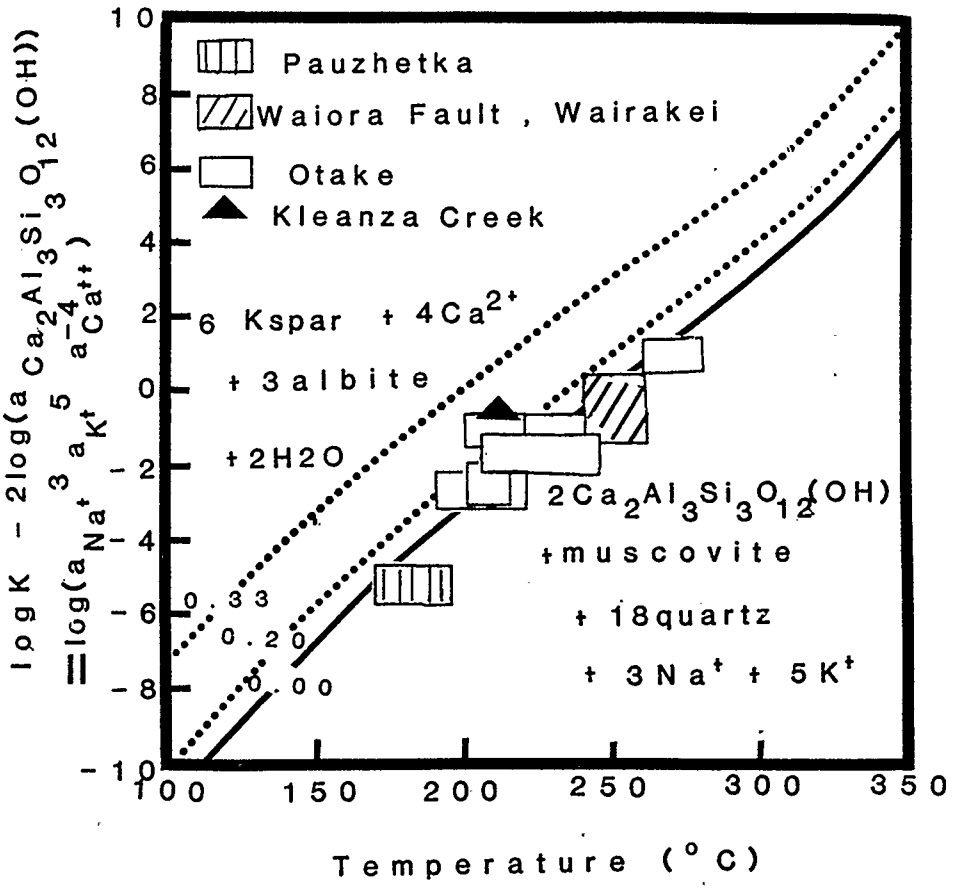

Figure 4.6. Activity-temperature diagram for an aqueous phase coexisting with albite, K-feldspar, muscovite, quartz and epidote solid solutions. After Bird and Helgeson, 1981. The solid and dotted curves represent compositional isopleths for epidote solid solutions in X_{Fe}^{ep}. The open symbols represent values of log (a_{Na+}^{3} + a_{K+}^{5} a_{Ca2+}^{-4}) computed from analyses of geothermal reservoir fluids coexisting with this assemblage. The triangle represents estimated log (a_{Na+}^{3}+a_{K+}^{5}+ a_{Ca2+}^{-4}) values for the Kleanza Creek-Kipulta Creek geothermal fluid based on estimated temperatures and measured epidote compositions.

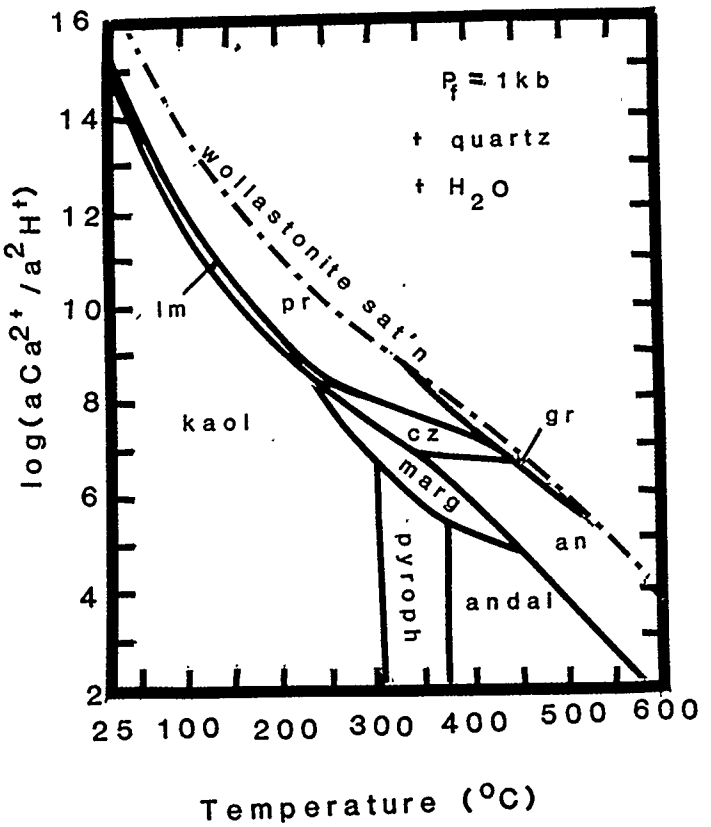

Figure 4.7. Phase relations of the system $CaO-Al_2O_3-SiO_2-H_2O$ at $P_f=P_s=1kb$ in the presence of quartz and an aqueous solution.

From Bird and Helgeson, (1981). Note the narrow range of laumontite stability in comparison to prehnite.

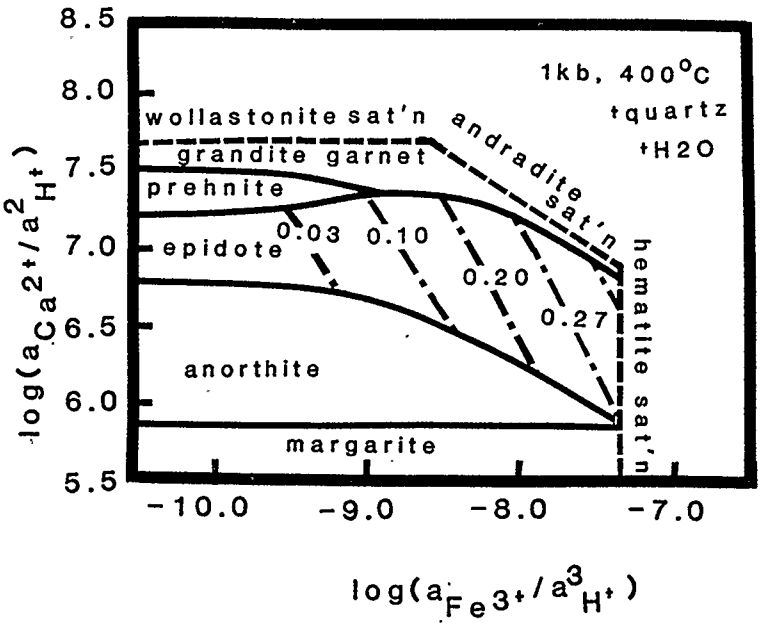

Figure 4.8. Phase relations in the system $CaO-Fe_2O_3-Al_2O_3-SiO_2-HCl-H_2O$ in the presence of quartz and an aqueous solution at P_f^2=1kb, T=400°C (Bird and Helgeson, 1981). The dashed curves represent compositional isopleths of epidote solid solutions. Since as temperature decreases to the lower limit of epidote stability, the prehnite stability field widens and, X_{Fe}^{ep} in solid solutions coexisting with Ca-Al silicates increases (Bird and Helgeson, 1981), epidote solid solutions coexisting with prehnite at temperatures around 200°C would have higher X_{Fe}^{ep} than 0.03.

remaining Fe^{+3} is incorporated into prehnite. Relatively high $\log(a_{Fe}{}^{+3}/a^3{}_{H}{}^{+})$ values are required for the crystallization of $X_{Fe}{}^{ep}\sim 0.25$, lower Fe^{+3} activity would be required for the formation of pumpellyite ($X_{Fe}{}^{pu}\sim 0.18$) and even lower for the low Fe^{+3} prehnites ($X_{Fe}{}^{pr}\sim 0.07$) observed in the Kleanza Creek rocks.

At the margins of veins or amgdales near fluid interaction with the host, the $a_{Fe}{}^{+3}/a^3{}_{H}{}^{+}$ ratio would be relatively high and would promote crystallization of pumpellyite and epidote, as well as chlorite. As these minerals precipitate from solution, $\log(a_{Ca}{}^{+2}a_{H}{}^{+}/a_{Fe}{}^{+3})$ would tend to increase to where laumontite (Fe-free) and prehnite would be stable. Since at constant temperature laumontite requires lower $a_{Ca}{}^{+2}/a^2{}_{H}{}^{+}$ values than prehnite (Figure 4.7), it would tend to be the more commonly crystallized of the two - as is observed in veins and amygdales. However, the presence of Fe^{+3} and Mg^{+2} ions in solutions reacting with groundmass minerals would tend to inhibit the formation of laumontite in favour of prehnite which can incorporate Fe^{+3} into its structure. This trend was also observed in the Kleanza Creek area basalts.

As shown in Figure 4.3, increasing $a_{Fe}{}^{+3}$ in solution widens the stability field of epidote at the expense of prehnite, pumpellyite and laumontite. From the $\log(a_{Ca}{}^{+2}/a^2{}_{H}{}^{+})$ versus temperature, and $T\text{-}X_{Fe}$ diagrams, the prevalence of epidote - chlorite - muscovite alteration in

the andesites and volcaniclastics can be attributed to relatively low $a_{Ca}+2/a_{H}+$ values. The K-feldspar - albite - quartz - muscovite assemblage in the quartz monzonite rocks can similarly be attributed to low $a_{Ca}+2/a^{2}_{Na}+$ and $a_{Fe}+3/a^{3}_{H}+$ ratios which would be expected of a fluid interacting with such a felsic bulk rock composition.

The activity of silica in metamorphic fluids also influences the equilibrium assemblage. Experimental results have shown that increasing $a_{SiO2(aqueous)}$, from saturation with respect to quartz to saturation with amorphous silica, increases the dehydration temperatures of silica-rich zeolites such as analcime and wairakite (Coombs et al., 1959). Bird and Helgeson (1981) and Bird et al. (1984) calculated the effects of changes in log $a_{SiO2(aq)}$ on the stability relations of other calc-silicates along the H_2O liquid vapour curve. They noted that clinozoisite can coexist only with an aqueous fluid which has $a_{SiO2(aq)}$ less than amorphous silica saturation. Prehnite can coexist with a wide range of $a_{SiO2(aq)}$ values, and laumontite is restricted to fluids with silica activity greater than or equal to saturation with quartz (Figure 4.9). From this, the assemblages q - ep - pr and pr - ep - lm in veins and amygdales indicate that $a_{SiO2(aq)}$ in the hydrothermal fluid was very close to silica saturation ($-2.5<\log a_{SiO2(aq)}<-2.0$ at P_f=0.4kb, Bruton and Helgeson, 1983).

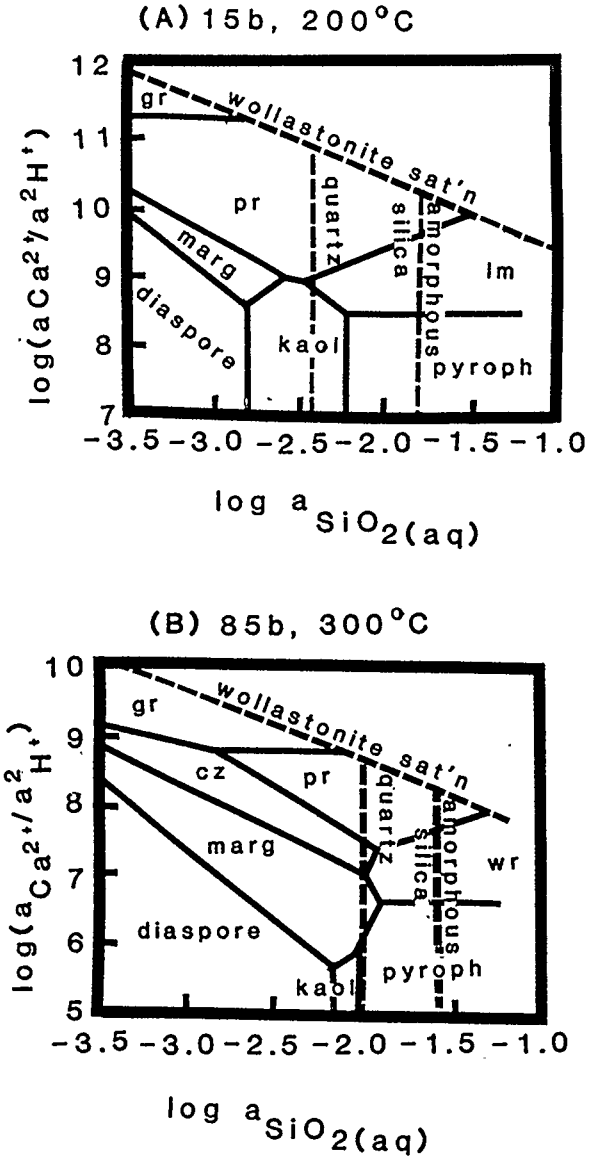

Figure 4.9. Phase relations in the system $CaO-Al_2O_3-SiO_2-H_2O$ as a function of $\log(a_{Ca^{2+}}/a_{H^+})$ and $\log a_{SiO_{2(aq)}}$ for temperatures of 200°C (A) and 300°C (B) and pressures corresponding to P_{H_2O} along the liquid-vapour boundary of H_2O as calculated by Bird et al. (1984). Dashed lines indicate saturation in the fluid phase with the indicated component. Open symbols show possible range of aqueous silica activity for the Kleanza Creek-Kipulta Creek geothermal fluid at these P-T conditions.

The concentration of aqueous silica in many hydrothermal systems is related to the devitrification of volcanic glass (Ellis, 1967). Since glass is not preserved in the Kleanza Creek - Kipulta Creek volcanics, it is a likely source of silica. Bruton and Helgeson (1983) demonstrated that the solubility of quartz increases with increasing P_{load} and temperature, and decreases as P_{fluid} approaches $P_{hydrostatic}$ (Figure 4.10). Groundwater in equilibrium with quartz at depth d_1 would become undersaturated with silica as it passed from d_1 to d_2 (P_f and T increase). The fluid would then dissolve silica until it was saturated at these P-T conditions. As the fluid heated, it would tend to rise through thin fissures ($P_f \sim P_{load}$ at great depth), the solubility of silica would decrease, and for a time the fluid would be in equilibrium with quartz. In shallower, more open fractures, P_f approaches $P_{hydrostatic}$ and the fluid would be supersaturated with silica. Depending on the $a_{SiO2(aq)}$, quartz or amorphous silica would precipitate out of solution. Similarly, silica removed from the groundmass (at $P_f=P_{load}$) would precipitate as the fluid moved laterally through the rock column to the fissure (P_f approaches $P_{hydrostatic}$), producing quartz lining fissures and amygdales.

In the study area, numerous large- and small-scale quartz veins and the presence of quartz lining calc-silicate veins and amygdales indicates that the hydrothermal fluid was saturated or slightly supersaturated with silica with respect

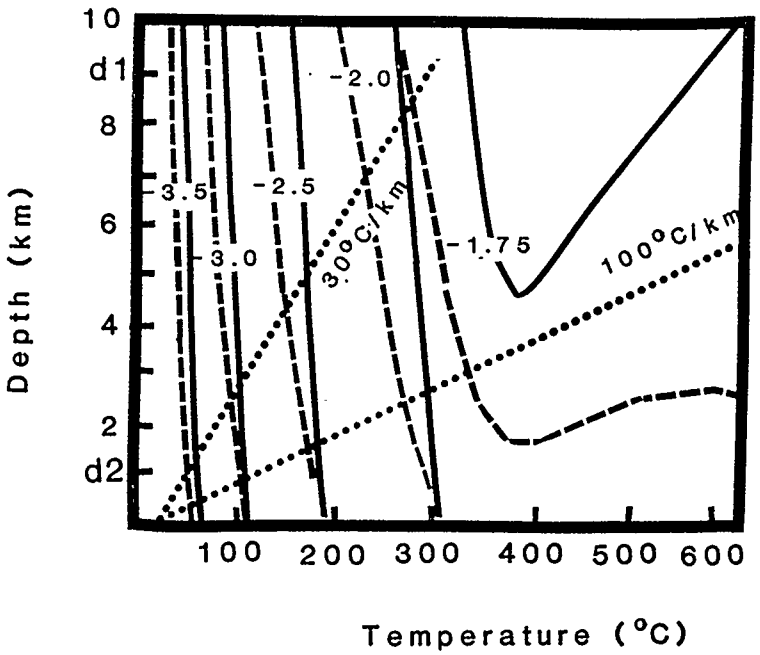

Figure 4.10. Isopleths of quartz solubility expressed as $\log m_{SiO_{2(aq)}}$ as a function of depth and temperature. Adapted from Bruton and Helgeson (1983). Solid lines are isopleths for $P_f = P_{hydrostatic}$. Dashed lines represent isopleths for $P_f = P_{load}$. Note that at constant depth and temperature, changing pressure conditions from hydrostatic to lithostatic increases the solubility of quartz. Linear geothermal gradients of 30°C/km and 100°C/km are shown as dotted lines. d_1 and d_2 are discussed in the text.

to quartz, as inferred from the calc-silicate assemblages.

Fluid Composition - Fugacities of Gaseous Components

Experiments involving synthesis and stability relations of prehnite, Fe-pumpellyite and epidote (Liou et al., 1983; Schiffman and Liou, 1983; Liou, 1973) are generally conducted over a range of oxygen fugacities and can therefore be used to interpret pumpellyite - epidote - hematite and prehnite - epidote - hematite assemblages with respect to temperature and f_{O2}. Because of solid solution in these minerals, the high fluid pressures and temperatures used in these experiments, and the possibility that hematite in the Kleanza Creek rocks is the result of weathering of magnetite, these experimental results can only be used for a qualitative estimate of f_{O2}.

The assemblage prehnite - epidote - hematite without garnet (refer to Table 2.3, GT19B) indicates a range of low values of log f_{O2} (-30 to -22) at P_f=2kb, T=300°C, Figure 4.11 (Liou et al., 1983) assuming that hematite resulted form the oxidation of primary magnetite during the hydrothermal alteration. The small range in prehnite and epidote compositions observed throughout the study area ($0.03 \leq X_{Fe}^{pr} \leq 0.07$; $0.22 \leq X_{Fe}^{ep} \leq 0.33$) seems to indicate widespread uniform relatively high f_{O2} conditions during metamorphism. These conditions could be produced by a circulating hot fluid having no contact with reducing organic material.

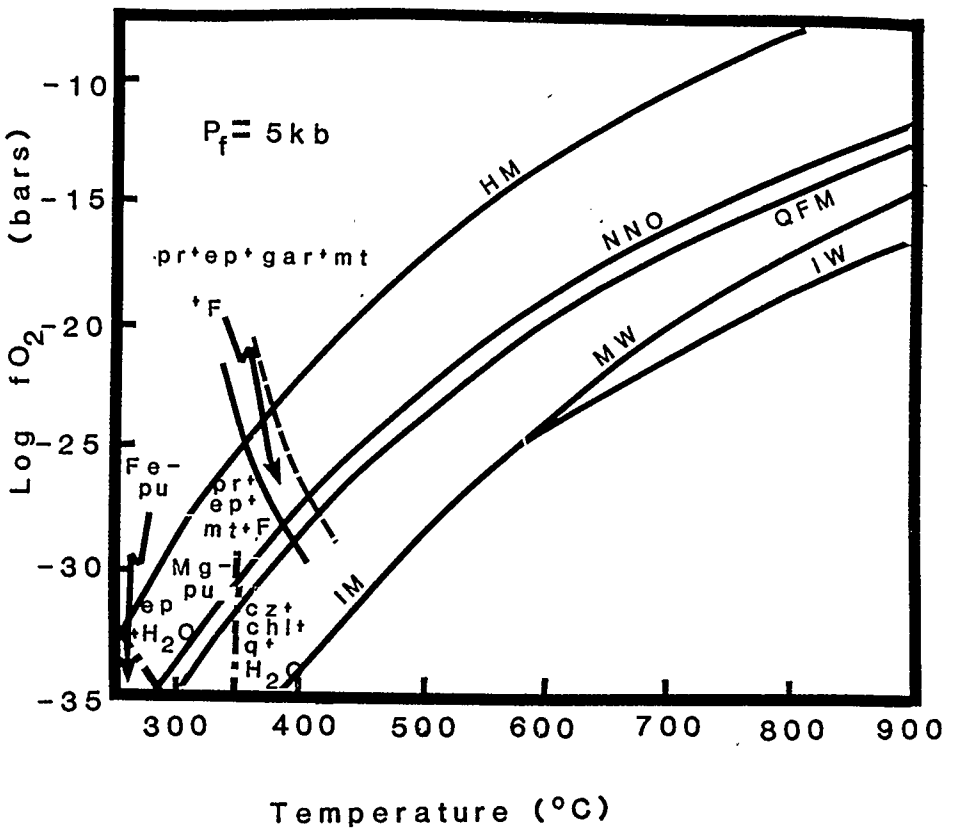

Figure 4.11. Log f_{O_2} - T diagram for the garnet-in and prehnite-out reactions of Liou et al. (1983). Maximum stability limits of pumpellyite-Fe and pumpellyite-Mg (Liou, 1979) as a function of f_{O_2} and T are also indicated.

The pumpellyite - epidote - hematite assemblage is more difficult to interpret because of the scarcity of experimental work at the P-T conditions of interest and the high magnesium content of the pumpellyites in the Kipulta basalts (average $X_{Mg}^{pu}=Mg/Mg+Al+Fe^{\sim}0.13$). Liou (1979) inferred the f_{O2}-T stability of Fe-pumpellyite from the reaction: (4.25)

$$2Ca_4Fe^{+2}Fe^{+3}Al_4Si_6O_{21}(OH)_7 + 1/2O_2 = 4Ca_2Fe^{+3}Al_2Si_3O_{12}(OH)$$

Fe-pumpellyite epidote

$$+ 5H_2O.$$

His estimated curve is given in Figure 4.11.

Increasing f_{O2} at constant T would reduce the stability of Fe-pumpellyite in favour of epidote. The presence of Mg^{+2} in pumpellyite would tend to stabilize it to slightly higher temperatures and f_{O2}. The relative abundance of epidote and rarity of pumpellyite in non-basaltic rocks of the Kleanza Creek area may result from high f_{O2} conditions ($f_{O2}\geq$HM buffer) and the influence of more aluminous bulk rock compositions.

The ubiquitous presence of calcite as a fracture-filling phase in the rocks of the study area, and its occurrence as patchy replacement of plagioclase with muscovite, chlorite or epidote in the volcanic map units indicates that the hydrothermal fluid also contained CO_2. The importance of the fugacity of CO_2 in metamorphic fluids in the development of zeolites and prehnite-pumpellyite facies minerals has been

discussed by numerous authors (Zen, 1961; Coombs et al., 1970; Thompson, 1971; Ghent and Miller, 1974; Kerrick, 1974; and others). Carbon dioxide greatly restricts the stability fields of low grade calc-silicates with respect to clay-carbonate assemblages.

The assemblage laumontite - calcite ± quartz was observed in several amygdales and veins. This assemblage is characteristic of fluids with low f_{CO2}. At P_f=2kb, laumontite stability is restricted to $X_{CO2} \leq 0.0075$ by the reaction (4.26) lm + CO_2 = cc + kaol + 2q + $2H_2O$ (Thompson, 1971). In his analysis of these results, Thompson (1971) concluded that at lower pressures both T and X_{CO2} of equilibrium would be lower. Therefore, the occurrence of lm+cc and absence of kaolinite in veins indicates that $X_{CO2} << 0.0075$.

Another common vein assemblage, epidote - prehnite - calcite, related by the reaction

(4.27) pr + CO_2 = cc + cz + q + H_2O

was shown by Kerrick (1974) to be stable at P_f=2kb and T=200°C at $X_{CO2} \sim 0.03$. The difference in these estimates could represent gradients in f_{CO2} in the study area. Veins of pure calcite generally cut calc-silicate and quartz veins and are interpreted to be late-stage injection of a more CO_2 rich fluid.

The presence of calcite in albitized plagioclase does not require high f_{CO2} values. Ghent and Miller (1974)

demonstrated that calcite can form from fluids with low f_{CO2} and high $\log(a_{Ca}{}^{+2}/a^2_{H}{}^{+})$ values. In the previous section, the hydrothermal fluid was shown to have had high $a_{Ca}{}^{+2}/a^2_{H}{}^{+}$ ratios. Also, the Ca^{+2} ions released to the solution during albitization (see below) would create local domains of very high $a_{Ca}{}^{+2}$, which could react with the available CO_2 to form calcite along with the calc-silicates and clays. Boles and Coombs (1977) and Dickinson et al. (1969) observed that plagioclase grains in calcareous sandstones were fresh, while those in interbedded non-calcareous sandstones were albitized. These observations and the low f_{CO2}/f_{H2O} ratios inferred above for the hydrothermal fluid of the Kleanza Creek area, and the prevalence of partly albitized and albitized plagioclase grains, indicates that high f_{CO2} actually impedes albitization.

Figure 4.12 is a schematic $\mu_{H2O} - \mu_{CO2}$ diagram, adapted from Coombs et al. (1970), which displays the stability relations of the calc-silicates and clays with respect to the chemical potentials of H_2O and CO_2. The relevant reactions are given in the legend of the diagram. Qualitative isobaric, isothermal $\mu_{H2O} - \mu_{CO2}$ diagrams allow trends in mineral occurrences with changing μ_{H2O}/μ_{CO2} to be predicted without considering problems in non-ideal mixing of the fluids at these low pressure and temperature conditions. The lack of reliable thermodynamic data can also be ignored in the construction of these diagrams. These diagrams are

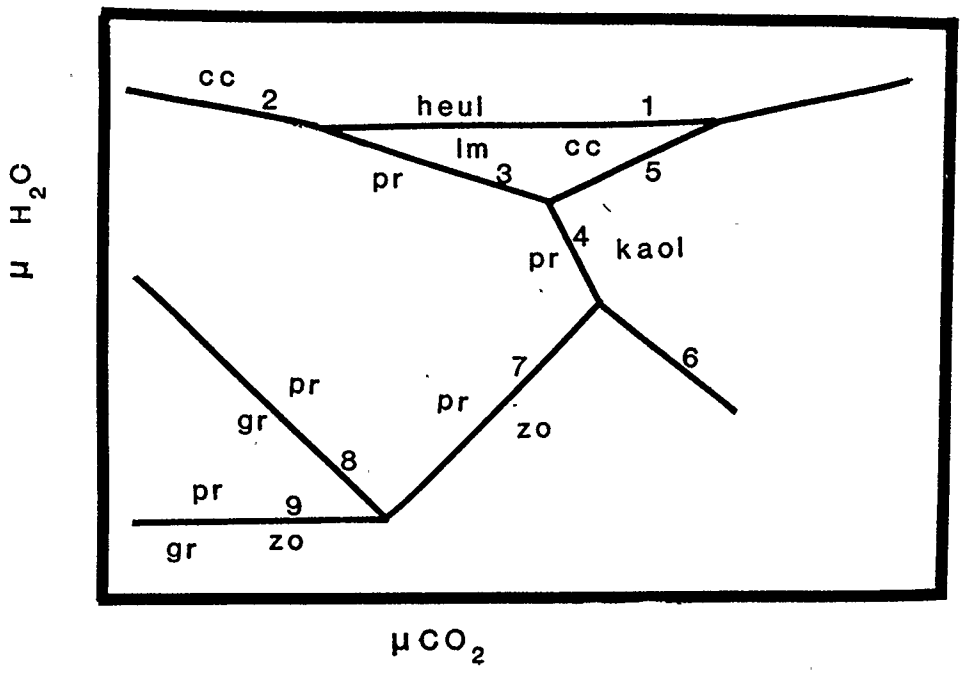

Figure 4.12. Schematic isobaric isothermal $\mu_{CO_2}-\mu_{H_2O}$ diagram, after Coombs et al. (1970). The relevant reactions are:

(1) heulandite = laumontite + 3quartz + $2H_2O$
(2) heulandite + calcite = prehnite + 4quartz + CO_2 + $5H_2O$
(3) laumontite + calcite = prehnite + quartz + CO_2 + $5H_2O$
(4) kaolinite + quartz + 2calcite = prehnite + CO_2 + H_2O
(5) laumontite + CO_2 = kaolinite + calcite + 2quartz + $2H_2O$
(6) 3kaolinite + 4calcite = 2zoisite + $4CO_2$ + $5H_2O$
(7) 3prehnite + $2CO_2$ = 2zoisite + 2calcite + 3quartz + $2H_2O$
(8) prehnite + calcite = grossular + CO_2 + H_2O
(9) 5prehnite = 2grossular + 2zoisite + 3quartz + $4H_2O$

calculated using the stoichiometric coefficients of the fluids in the reactions, i.e. $d\mu_{H2O}/d\mu_{CO2}=-n_{CO2}/n_{H2O}$, where n_i is the number of moles of the fluid.

It is interesting to note that the amygdale crystallization order (chl - ep - lm - pr), discussed above in relation to the activities of ionic species in the fluid, can also be loosely related to a decreasing trend in μ_{CO2}/μ_{H2O}.

Albitization and Permeability

Microprobe analyses of feldspars in the andesites and volcaniclastics indicate that the grains are partially albitized; albite-rich domains coexist with "fresh" calcic plagioclase in a single grain. This contrasts sharply with the complete albitization of the basaltic plagioclase.

Albitization of feldspars has been studied by Boles (1982) in the Frio sandstones of the Gulf Coast Tertiary basin and by Boles and Coombs (1977) in sandstones from the Southland syncline of New Zealand. The general form of the reaction according to Boles (1982) is:

(4.28) $Na^+ + H_4SiO_4 + NaAlSi_3O_8 \cdot CaAl_2Si_2O_8 =$

aqueous silica andesine

$2NaAlSi_3O_8 + Al^{3+} + Ca^{2+} + 4OH^-$.

albite

Boles and Coombs (1977) saw evidence in the Hokunui Hills that Na^+ ions for albitization were released by the

alteration of volcanic glass to chlorite and calcic heulandite. In the Kleanza Creek area, volcanic glass has generally been altered to chlorite and iron oxides, indicating that it could have been the source of Na^+ ions in the hydrothermal fluid. Boles (1982) found that the Frio pore fluids are somewhat modified dilute seawater, indicating that abnormally high salinities are not a prerequisite for albitization. This is important since the hydrothermal fluid involved in the alteration of the rocks in the Kleanza Creek - Kipulta Creek area was probably modified meteoric water. The common presence of quartz in veins and amygdales indicates that the hydrothermal fluid was saturated with respect to quartz. Calcium and aluminum released by the albitization reaction would have been consumed in the formation of clays, epidote, prehnite and minor amounts of calcite and laumontite: the commonly observed alteration products of plagioclase throughout the study area.

Feldspars in geothermal areas generally show a marked transition from An-rich to albitic compositions over a narrow range of depth and temperature. For example, in the Frio sandstones, the "albite zone" extends from 2500-2800m at temperatures corresponding to 110° to $120^{\circ}C$ (Boles 1982). Partially albitized grains are also observed in the albite zone of several areas (Boles, 1982; Boles and Coombs, 1977; Dickinson et al., 1969) and in the Kleanza Creek - Kipulta Creek area. Typical compositions of Ab-rich and An-poor

domains in plagioclase grains from this study area, the Gulf Coast Tertiary basin, and the Southland Syncline are given in Table 4.5.

SEM studies of partially albitized plagioclase in the Frio sandstones showed that these grains generally have dissolution porosity, which is lacking in completely albitized grains (Boles, 1982). This may be indicative of a dissolution - precipitation mechanism for albitization rather than solid-state diffusion. Such a mechanism would allow albitization to go to completion rather quickly within a specific portion of the grain, while other areas of the grain are unaltered. Boles (1982) also observed that albitization progresses preferentially along grain fractures and cleavage surfaces. This preferential alteration is particularly noticeable in the feldspars of the quartz monzonite rocks from the study area (Plate 2C,F).

Dickinson (1962), Boles and Coombs (1977) and Boles (1982) and others have noted that in sandstones, plagioclase is more commonly albitized in coarse grained rocks with little matrix or calcite cement. The implications of f_{CO2} will be discussed later. These observations on the effect of permeability, complement the observation of the presence of fresh and partially albitized plagioclase in the volcaniclastic, andesite and quartz monzonite units in the Kleanza Creek area. The permeability in these units is due to secondary fracturing, indicating that low permeability

Table 4.5 Electron microprobe analyses of partially albitized plagioclase grains. Each set of fresh and albitic analyses are domains within a single grain. Frio analyses taken from Boles(1982). Analyses of Southland Syncline taken from Boles and Coombs(1977).

Sample	Fresh	Mole% composition		Albitic		
	Ab	An	Or	Ab	An	Or
Frio Well 2 2519m	50.0	48.1	1.8	96.7	2.5	0.8
Frio Well 2 2521m	61.6	31.2	4.3	97.0	1.9	0.9
	63.8	32.1	4.1	81.7	16.1	2.4
Southland OU30147	79	13	8	91	7	2
16FL1	42.8	57.2	-	81.9	18.1	-
	43.1	56.9	-	80.4	19.6	-
GT19E3	73.3	17.0	9.7	94.9	3.6	1.5

restricted albitization, and other alteration, by limiting the access of grains to the hydrothermal fluid. A similar restriction was inferred to have occurred by Dudley (1983) in the zeolitization of the Howson facies, and by M. Mihalynuk (pers. comm.) in the alteration of adjacent volcanic and ignimbrite units in the Zymoetz River area.

The importance of permeability to albitization is also well illustrated by the selective albitization of the Karmutsen volcanics of northeastern Vancouver Island, British Columbia (Kuniyoshi and Liou, 1976). These volcanics consist of close-packed pillows, pillow breccias, and massive flows of oceanic tholeiite. The flows and pillow cores are amygdaloidal and plagioclase in these units has been extensively altered to albite + pumpellyite. The pillow breccias (aquagene tuffs) are composed of glassy fragments, unaltered primary augite, and calcic plagioclase that has been partially replaced by white mica. Pillow rims are chilled margins 1 to 2cm thick and are also unalbitized.

Kuniyoshi and Liou (1976) proposed that fluid composition (particularly $a_{Fe}+3$) was critical to the formation of albite + pumpellyite from plagioclase. Their metamorphic model provides for unmixing of primary Fe-Ti oxides of the flows and pillow cores into ilmenite and magnetite during cooling, and alteration of ilmenite to sphene during "burial metamorphism". The production of sphene would release Fe^{+2} ions to solution and remove Ca^{+2}

and SiO_2 from solution. The anorthite component of the plagioclase could then be altered to pumpellyite or chlorite. Since the Fe^{+2} ions in the tuff and pillow rims was quenched in the sideromelane glass, burial metamorphism resulted in the alteration of the glass to clays and chlorite and the Fe^{+2} ions were not available to the solution. This Fe-poor interstitial pore fluid was unable to alter calcic plagioclase to pumpellyite and albite.

The alteration of plagioclase to albite + pumpellyite was likely controlled by a mechanism similar to that suggested by Kuniyoshi and Liou (1976), but Fe-poor solutions should not impede the albitization reaction. If a model of hydrothermal alteration is applied to the Karmutsen volcanics, the lower permeability of the tuff and pillow rims would account for the lack of albitization in these units.

CHAPTER 5 CONCLUSIONS

Conclusions

1. The dominant authigenic minerals in the volcanics of the Kleanza Creek - Kipulta Creek study area are: epidote, prehnite, chlorite, K-mica, pumpellyite, albite, laumontite, K-feldspar and quartz. These minerals are the result of a late stage hydrothermal metamorphic event.
2. Fibrous actinolite present in volcanics adjacent to the contact with the pluton may be a relic of an earlier greenschist facies metamorphic event, possibly related to the intrusion of apophyses of the Coast Plutonic Complex.
3. Epidote, prehnite and pumpellyite do not show systematic variation in unit cell parameters with increasing iron content. Unit cell volume does tend to increase with increasing Fe^{3+}-content in the three minerals.
4. Laumontite from the study area is relatively pure and show little evidence of dehydration.
5. Epidote compositions are typical of very low-grade metamorphic and hydrothermal environments. $K_D^{pr-ep}{}_{Al-Fe}$ values are also typical of these environments.
6. The pressure of hydrothermal metamorphism ranged from hydrostatic pressure ($P_f \tilde{} 0.5$kb) in the vein and amygdale

systems to load pressure of approximately 1.5kb.

7. Peak temperatures of hydrothermal metamorphism were in the range of T_{min}~190°C to a maximum of approximately 255°C.

8. Bulk composition and permeability of the host rocks controlled the degree of albitization and the nature of the authigenic assemblage.

9. The hydrothermal fluid was characterized by high ratios of $a_{Ca^{2+}}/a^2_{H^+}$, a_{Na^+}/a_{H^+}, a_{Na^+}/a_{K^+}, and $a_{Fe^{3+}}/a^3_{H^+}$. These cations were derived from leaching of primary pyroxene, olivine and volcanic glass and from the albitization of plagioclase.

10. The fluid was saturated with respect to quartz.

11. The hydrothermal fluid was H_2O-rich, with X_{CO2} less than 0.0075.

PLATES

PLATE 1

A Glomeroporphyritic plagioclase and hematitic pseudomorph of pyroxene in basalt (sample 1FL2).

B Pumpellyite alteration of plagioclase in basalt (sample GT19A). Note the presence of unaltered rims and strongly altered cores in some plagioclase grains.

C Olivine phenocrysts pseudomorphed by epidote and hematite in basalt (sample 1FL1).

D Margin surrounding amygdale composed of Fe-oxides and minor feldspar laths. Amygdale consists of pumpellyite, prehnite and laumontite (sample GT19E). Laumontite is easily identified due to its broad cleavage traces.

E Typical appearance of sample GT19B in plane-polarized light. The feldspars initially appear relatively unaltered.

F Same view as in E, crossed polars. Note the mottled appearance of the feldspars which have been completely pseudomorphed by tiny (50 - 300um) prehnite grains.

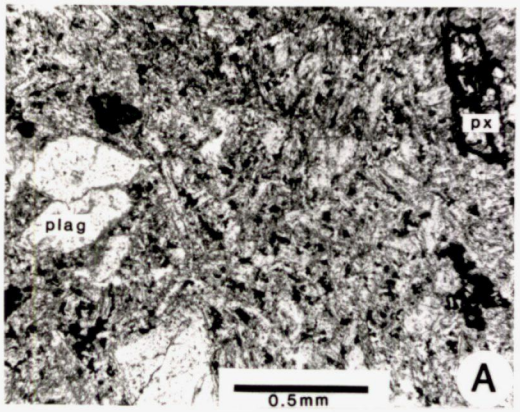

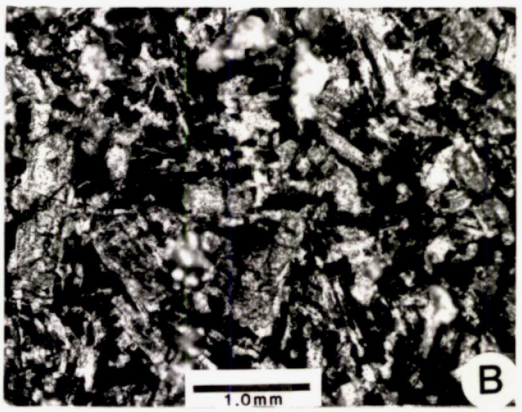

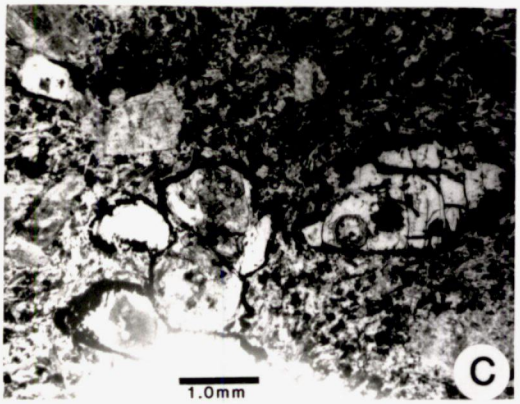

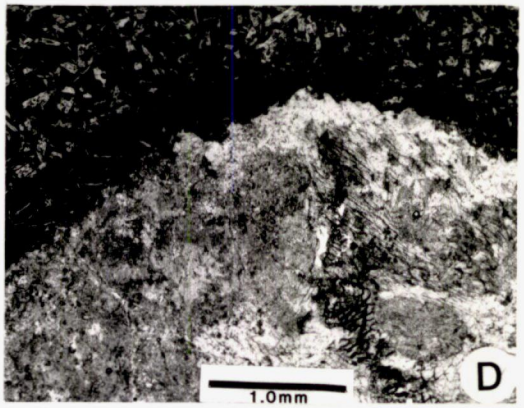

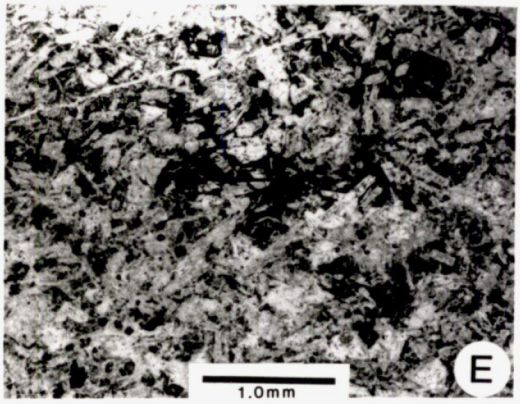

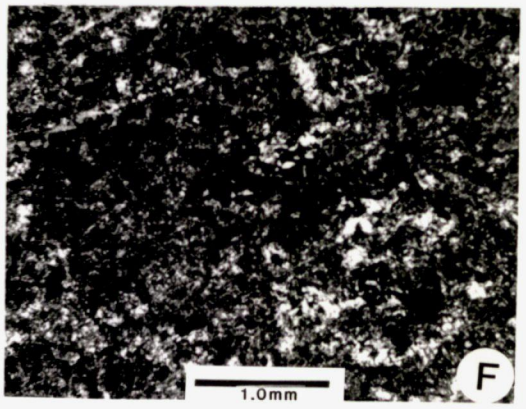

Plate 1

PLATE 2

A Fiamme texture in sample 13FL1. The original material has been replaced by hematite and quartz.

B Fibrous actinolite and hematite in andesite (sample 16FL1). Note the diffuse nature of the actinolite and its contact with hematite. The actinolite is believed to have formed prior to hydrothermal alteration.

C Allotriomorphic granular texture in the Kleanza Creek pluton (sample 18FL2; crossed polars).

D Graphic granite texture and sericitized plagioclase in the quartz monzonite (sample 10FL2; crossed polars).

E Chloritized biotite with sphene and epidote inclusions adjacent to relatively fresh primary igneous hornblende (sample 18FL2). Note the heavily altered condition of the surrounding feldspar and the concentration of the alteration along cleavage planes of the "fresher" grains.

F Uralitized igneous hornblende with hematite inclusions (sample 18FL2). Note the highly altered state of the surrounding feldspar.

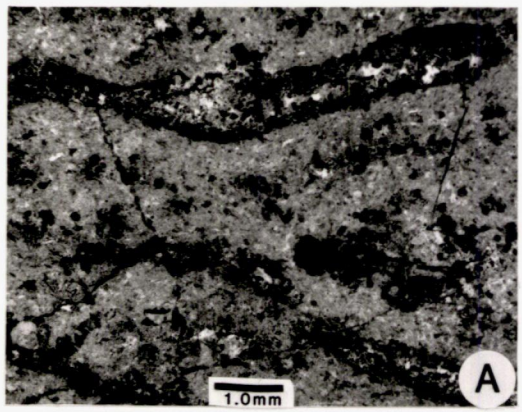

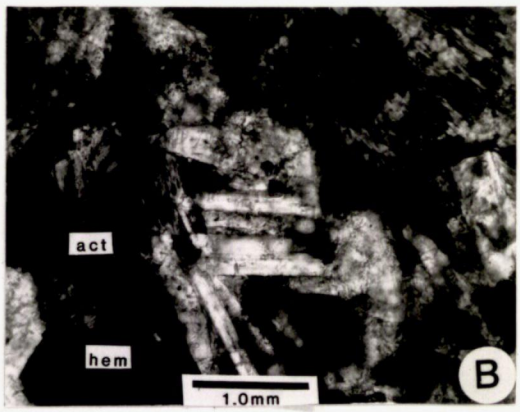

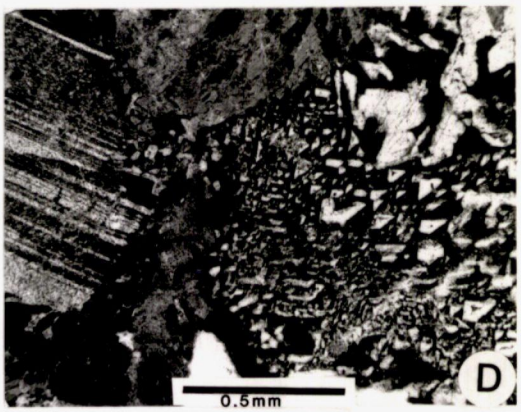

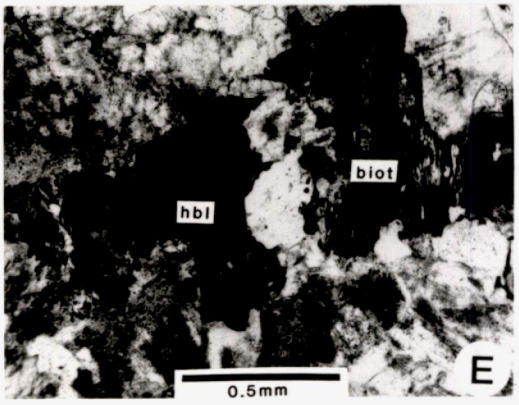

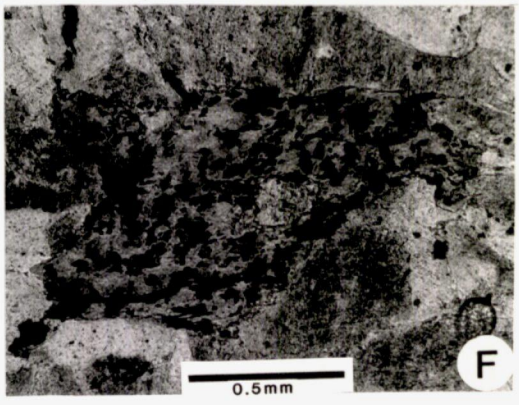

Plate 2

PLATE 3

A Vein containing analcime and calcite in andesite host (sample 16FL1; crossed polars). Note the weak anisotropy of analcime.

B Amygdale of epidote, diopside and calcite in sample 5FL4, (crossed polars). Diopside has well-developed {001} twinning.

C Phenocryst of plagioclase in lapilli tuff (sample 3FL2) partially replaced by epidote and muscovite.

D Amygdaloidal epidote displaying its three main habits (sample GT19F). The brown epidote tends to be slightly Fe-poor in comparison to the surrounding epidotes.

E Amygdaloidal laumontite and prehnite in contact (sample 2FL1; crossed polars). Note the broad cleavage traces which allow laumontite to be readily distinguished from prehnite, and which may indicate that the laumontite is metastable in this assemblage.

F "Sunflower texture" of amygdaloidal prehnite (sample GT19B; crossed polars). Microprobe analyses showed no significant compositional differences between the blades and cores.

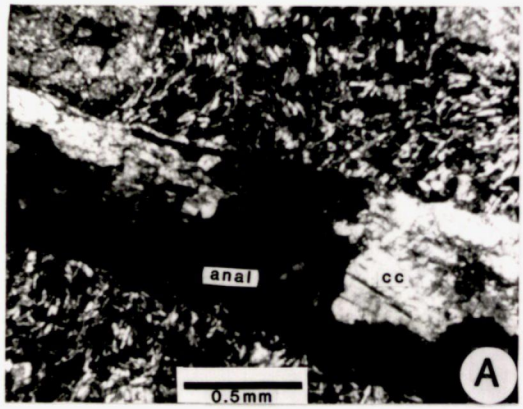
anal
cc
0.5mm
A

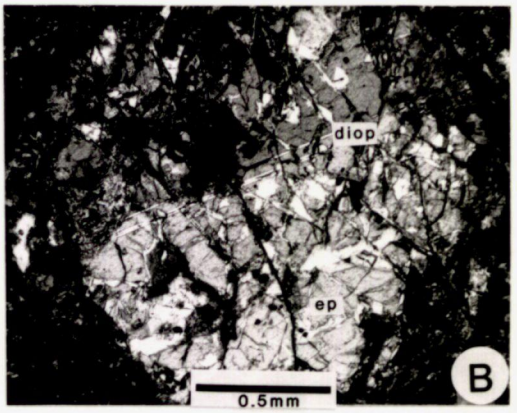
diop
ep
0.5mm
B

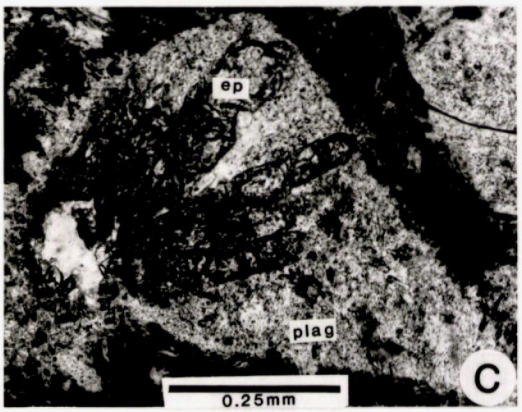
ep
plag
0.25mm
C

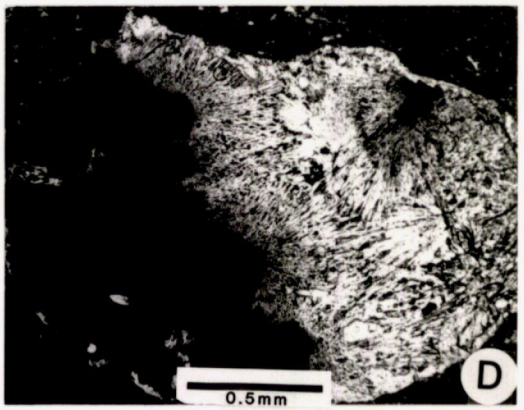
0.5mm
D

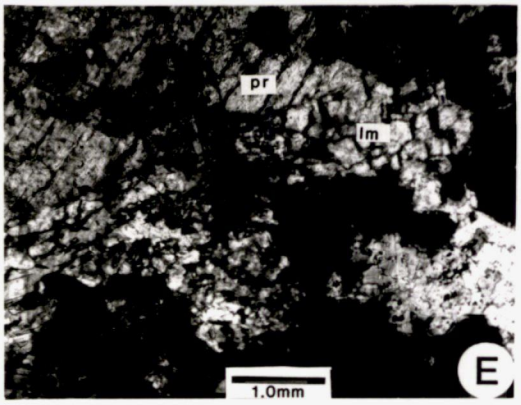
pr
lm
1.0mm
E

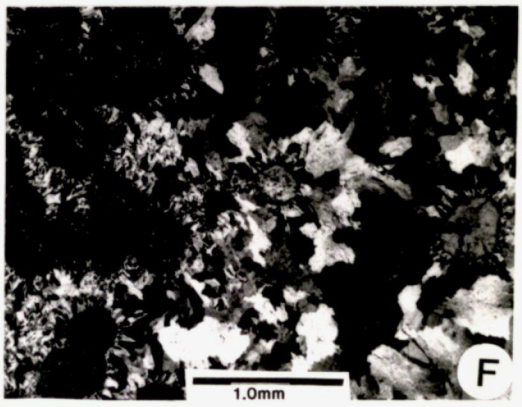
1.0mm
F

Plate 3

PLATE 4

A Amygdaloidal epidote mantled by pumpellyite needles (sample GT19F). Note the sharp contact between the phases.

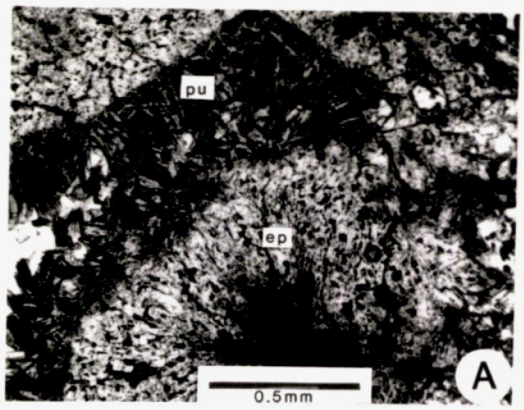

Plate 4

LIST OF REFERENCES

Allman, R. and Donnay, G. (1971). Structural relations between pumpellyite and ardennite. Acta Crystallographica, B27, pp. 1871-1875.

Amirov, S.T., Ilyukhin, V.V., and Belov, N.V. (1967). Crystal structure of Ca-zeolite laumontite (leonhardite) $CaAl_2Si_4O_{12}.nH_2O$ ($2<n<4$). Doklady Nauk SSSR, 174, pp. 121-124.

Appleman, D.E., Evans Jr., H.T., and Handwerker, D.S. (1972). JOB9214: Indexing and least-squares refinement of powder diffraction data. United States Geological Survey Computer Contribution No. 20.

Aumento, F. (1968). The space group of prehnite. Canadian Mineralogist, 9, pp. 484-492.

Bartl, H. and Fischer, K.F. (1967). Untersuchung der Kristallstruktur des Zeolithes Laumontit. Neues Jarbuch fuer Mineralogie, Monatshefte 1967, pp. 33-42.

Bence, A.E. and Albee, A.L. (1968). Empirical correction factors for the electron microanalysis of silicates and oxides. Journal of Geology, 76, pp. 382-403.

Bird, D.K. and Helgeson, H.C. (1981). Chemical interaction of aqueous solutions with epidote-feldspar mineral assemblages in geologic systems.II. Equilibrium constraints in metamorphic/geothermal processes. American Journal of Science, 281, pp. 576-614.

Bird, D.K. and Helgeson, H.C. (1980). Chemical interaction of aqueous solutions with epidote-feldspar mineral assemblages in geologic systems.I. Thermodynamic analysis of phase relations in the system $CaO-FeO-Fe_2O_3-Al_2O_3-SiO_2-H_2O-CO_2$. American Journal of Science, 280, pp. 907-941.

Bird, D.K., Schiffman, P., Elders, W.A., Williams, A.E., and McDowell, S.D. (1984). Calc-silicate mineralization in active geothermal systems. Economic Geology, 79, pp. 676-695.

Boles, J.R. (1982). Active albitization of plagioclase, Gulf Coast Tertiary. American Journal of Science, 282, pp. 165-180.

Boles, J.R. and Coombs, D.S. (1977). Zeolite facies alteration of sandstones in the Southland Syncline, New Zealand. American Journal of Science, 277, pp. 982-1012.

Brown, E.H. and Ghent, E.D. (1983). Mineralogy and phase relations in the blueschist facies of the Black Butte and Ball Rock areas, northern California Coast Ranges. American Mineralogist, 68, pp.365-372.

Bruton, C.J. and Helgeson, H.C. (1983). Calculation of the chemical and thermodynamic consequences of pressure in hydrothermal systems. American Journal of Science, 283A, pp. 540-588.

Burnham, C.W., Holloway, J.R., and Davis, N.F. (1969). Thermodynamic properties of water to 1000°C and 10,000bars. Geological Society of America, Special Paper 132, 96p.

Campbell, A.S. and Fyfe, W.S. (1965). Analcime-albite equilibria. American Journal of Science, 263, pp. 807-816.

Carter, N.C. (1982). Porphyry copper and molybdenum deposits west-central British Columbia. Province of British Columbia, Ministry of Energy, Mines and Petroleum Resources Bulletin, 64. 150p.

Chatterjee, N.D., Johannes, W., and Leistner, H. (1984). The system $CaO-Al_2O_3-SiO_2-H_2O$: new phase equilibria data, some calculated phase relations, and their petrological applications. Contributions to Mineralogy and Petrology, 88, pp. 1-13.

Coombs, D.S. (1953). The pumpellyite mineral series. Mineralogical Magazine, 30, pp. 113-135.

Coombs, D.S., Ellis, A.J., Fyfe, W.S., and Taylor, A.M. (1959). The zeolite facies with comments on the interpretation of hydrothermal synthesis. Geochimica and Cosmochimica Acta, 17, pp. 53-107.

Coombs, D.S., Horodyski, R.J., and Naylor, R.S. (1970). Occurrence of prehnite-pumpellyite facies metamorphism in northern Maine. American Journal of Science, 268, pp. 142-156.

Coombs, D.S., Nakamura, Y., and Vuagnat, M. (1976). Pumpellyite-actinolite facies schists of the Taveyanne Formation near Lo`eche, Valais, Switzerland. Journal of Petrology, 17, pp.440-471.

Deer, W.A., Howie, R.A., and Zussman, J. An introduction to the rock-forming minerals. John Wiley and Sons Inc., New York: 1978. 528p.

Dickinson, W.R. (1962). Petrology and diageneisis of Jurassic andesitic strata in central Oregon. American Journal of Science, 260, pp. 481-500.

Dickinson, W.R., Ojakangas, R.W. and Stewart, R.J. (1969). Burial metamorphism of the Late Mesozoic Great Valley Sequence, Cache Creek, California. Geological Society of America Bulletin, 80, pp. 519-526.

Dollase, W.A. (1971). Refinement of the crystal structures of epidote, allanite, and hanockite. American Mineralogist, 56, pp.447-464.

Dollase, W.A. (1973). Moessbauer spectra and iron distribution in the epidote-group minerals. Zeitschrift fuer Kristallographie, 138, pp.41-63.

Dudley, J.W. (1983). Zeolitization of the Howson Facies, Telkwa Formation, British Columbia. Unpublished doctoral thesis, University of Calgary.

Duffell, S. and Souther, J.G. (1964). Geology of Terrace Map-Area British Columbia (103E 1/2). GSC Memoir 329, 117p.

Ellis, A.J. (1967). The chemistry of some explored geothermal systems. In: Geochemistry of hydrothermal ore deposits. ed. H.L. Barnes. Holt, Rinehart and Winston, Inc., New York: 1967. 670p.

Evarts, R.C. and Schiffman, P. (1983). Submarine hydrothermal metamorphism of the Del Puerto Ophiolite, California. American Journal of Science, 283, pp. 289-340.

Fisher, R.V. and Schmincke, H.-U. (1984). Pyroclastic Rocks. Springer-Verlag: Berlin. 472p.

Galli, E. (1972). Nuovi dati sulla pumpellyite di Hicks Ranch (California). Societa Toscana di Science Naturali di Pisa. Atti. Memorie, Processi Verbali. Series A. 79, pp. 29-35.

Galli, E. and Alberti, A. (1969). On the cyrstal structure of pumpellyite. Acta Crystallographica, B25, pp. 2276-2281.

Ghent, E.D. and Miller, B.E. (1974). Zeolite and clay-carbonate assemblages in the Blairmore Group (Cretaceous) southern Alberta Foothills, Canada. Contributions to Mineralogy and Petrology, 44, pp.313-329.

Greenwood, H.J. (1961). The system $NaAlSi_2O_6$ - H_2O - Argon: total pressure and water pressure in metamorphism. Journal of Geophysical Research, 66, pp.3923-3946.

Halbach, H. and Chatterjee, N.D. (1984). An internally consistent set of thermodynamic data for twenty-one $CaO-Al_2O_3-SiO_2-H_2O$ phases by linear parametric programming. Contributions to Mineralogy and Petrology, 88, pp. 14-23.

Hammerstrom, L.T. (1981). Internally consistent thermodynamic data and phase relations in the $CaO-Al_2O_3-SiO_2-H_2O$ system. Unpublished M.Sc. thesis, University of British Columbia.

Helgeson, H.C. (1967). Solution chemistry and metamorphism. In: Researches in Geochemistry, vol. 2. ed. P.H. Abelson. Wiley and Sons, New York: 1967. 663p.

Helgeson, H.C., Delany, J.M., Nesbitt, H.W., and Bird, D.K. (1978). Summary and critique of the thermodynamic properties of rock-forming minerals. American Journal of Science, 278A, 229p.

Helgeson, H.C., Kirkham, D.H., and Flowers, G.C. (1981). Theoretical prediction of the thermodynamic behaviour of aqueous electrolytes at high pressures and temperatures, IV. Calculation of activity coefficients, osmotic coefficients, and apparently molal and standard and relative partial molal properties to 5kb and 600°C. American Journal of Science, 281, pp. 1249-1516.

Hemingway, B.S., Haas Jr., J.L., and Robinson Jr., G.R. (1982). Thermodynamic properties of selected minerals in the system Al_2O_3-CaO-SiO_2-H_2O at 298.15K and 1 bar (10^5 Pascals) pressure and at higher temperatures. United States Geological Survey, Bulletin 1544, 70p.

Hemley, J.J. (1959). Some mineralogical equilibria in the system K_2O-Al_2O_3-SiO_2-H_2O. American Journal of Science 257, pp. 241-270.

Hemley, J.J. and Jones, W.R. (1964). Chemical aspects of hydrothermal alteration with emphasis on hydrogen metasomatism. Economic Geology, 59, pp. 538-569.

Irving, J., Vonsen, M., and Gonyer, F.A. (1932). Pumpellyite from California. American Mineralogist, 17, pp. 338-342.

Ito, T., Morimoto, N., and Sadanaga, R. (1954). On the structure of epidote. Acta Crystallographica 7, pp. 53-59.

Johnson, G.K., Flowtow, H.E., O'Hare, P.A.G., and Wise, W.S. (1985). Thermodynamic studies of zeolites: heulandite. American Mineralogist, 70, pp. 1065-1071.

Johnson, G.K., Flowtow, H.E., O'Hare, P.A.G., and Wise, W.S. (1982). Thermodynamic studies of zeolites: analcime and dehydrated analcime. American Mineralogist, 67, pp. 736-748.

Kerrick, D.M. and Ghent, E.D. (1979). P-T-X_{CO2} relations of equilibria in the system: $CaO-Al_2O_3-SiO_2-CO_2-H_2O$. pre-print: D.Z. Korzhinskii Memorial Volume, "Problems of physicochemical petrology", Zharikov, V.A., Fonarev, V.I., and Korikovshii, V.A. (editors). Academy of Sciences of the USSR.

Kretz, R. (1983). Symbols for rock-forming minerals. American Mineralogist, 68, pp.277-279.

Kristmannsdottir, H. (1979). Alteration of basaltic rocks by hydrothermal activity at 100-300°C. In: Developments in Sedimentology, v. 27. ed. M.M. Mortland and V.C. Farmer. Proceedings of the VI International Clay Conference (1978). Elsevier, Amsterdam: 1979. 662p.

Kuniyoshi, S. and Liou, J.G. (1976). Burial metamorphism of the Karmutsen volcanic rocks, northeastern Vancouver Island, British Columbia. American Journal of Science, 276, pp. 1096-1119.

Liou, J.G. (1971a). Analcime equilibria. Lithos, 4, pp. 389-402.

Liou, J.G. (1971b). Synthesis and stability relations of prehnite $Ca_2Al_2Si_3O_{10}(OH)_2$. American Mineralogist 56, pp. 507-531.

Liou, J.G. (1971c). P-T stabilities of laumontite, wairakite, lawsonite and related minerals in the system $CaAl_2Si_2O_6-SiO_2-H_2O$. Journal of Petrology 12, pp. 379-411.

Liou, J.G. (1973). Synthesis and stability relations of epidote, $Ca_2Al_2FeSi_3O_{12}(OH)$. Journal of Petrology 14, pp. 381-413.

Liou, J.G. (1979). Zeolite facies metamorphism of the East Taiwan ophiolite. American Mineralogist 64, pp. 1-14.

Liou, J.G., Kim, H.S., and Maruyama, S. (1983). Prehnite - Epidote equilibria and their petrologic applications. Journal of Petrology, 24, pp. 321-342.

Liou, J.G., Maruyama, S., and Cho, M. (1985). Phase equilibria and mineral parageneses of metabasites in low-grade metamorphism. Mineralogical Magazine, 49, pp.321-333.

Myer, G.H. (1965). X-ray determinative curve for epidote. American Journal of Science, 263, pp. 78-86.

Nicholls, J., Fiesenger, D.W., and Ethier, V.G. (1977). Fortran IV programs for processign routine electron microprobe data. Computers and Geosciences, 3, pp. 49-83.

Nuffield, E.W. (1943). Prehnite from Ashcroft, British Columbia. University of Toronto Studies, Geological Series, 48: Contributions to Canadian Mineralogy, pp. 49-64.

Palache, C. and Vassar, H.E. (1925). Some minerals of the Keweenaw copper deposits: pumpellyite a new mineral; sericite; saponite. American Mineralogist, 10, pp. 412-418.

Passaglia, E. and Gottardi, G. (1973). Crystal chemistry and nomenclature of pumpellyites and juglodites. Canadian Mineralogist, 12, pp. 219-223.

Powder Diffraction File (1984). JCPDS - International Centre for Diffraction Data: Swathmore, Pennsylvania.

Rudashevskiy, N.S., Kasatov, B.K., and Tsekhovol´skaya, D.J. (1974). X-ray thermal and infrared spectroscopy analyses of the isomorphic series, prehnite - Fe-prehnite. Kristallokhimiya i Structura Mineralov, pp. 118-124.

Schiffman, P. and Liou, J.G. (1980). Synthesis and stability relations of Mg-Al pumpellyite, $Ca_4Al_5MgSi_6O_{21}(OH)_7$. Journal of Petrology, 21, pp. 441-474.

Schiffman, P. and Liou, J.G. (1983). Synthesis of Fe-pumpellyite and its stability relations with epidote. Journal of Metamorphic Geology, 1, pp. 91-101.

Schmid, R. (1981). Descriptive nomenclature and classification of pyroclastic deposits and fragments. Neues Jahrbuch fuer Mineralogie, Monatshefte, 4, pp. 190-196.

Seki, Y. (1959). Relation between chemical composition and lattice constants of epidote. American Mineralogist, 44, pp. 720-730.

Steiner, A. (1968). Clay minerals in hydrothermally altered rocks at Wairakei, New Zealand. Clays and Clay Minerals, 16, pp. 193-213.

Streckeisen, A. (1974). Classification and nomenclature of plutonic rocks: Recommendations of the IUGS Subcommission on the systematics of igneous rocks. Geologische Rundschau, 63, pp. 773-786.

Surdam, R.C. (1969). Electron microprobe study of prehnite and pumpellyite form the Karmutsen Group, Vancouver Island, British Columbia. American Mineralogist, 54, pp. 256-266.

Thompson, A.B. (1971a). PCO_2 in low grade metamorphism; zeolite, carbonate, clay mineral, prehnite relations in the system $CaO-Al_2O_3-SiO_2-CO_2-H_2O$. Contributions to Mineralogy and Petrology, 33, pp. 145-161.

Thompson, A.B. (1971b). Analcime equilibria at low temperatures. American Journal of Science, 271, pp. 79-92.

Thompson, J.B. (1955). The thermodynamic basis for the mineral facies concept. American Journal of Science, 253, pp. 65-103.

Tipper, H.W. and Richards, T.A. (1976). Jurassic stratigraphy and history of north-central British Columbia. GSC Bulletin, 270, 73p.

Traube, H. (1894). Ueber die pyroelecktrischen Eigenschaften und die Kristallformen des Prehnits. Neues Jahrbuch fuer Mineralogie, Beilage, 9, pp. 134-146.

Viereck, L.G., Brendon, J.G., Schmincke, H., and Pritchard, R.G. (1982). Volcaniclastic rocks of the Reydarfjordur drill hole, eastern Iceland. 2. Alteration. Journal of Geophysical Research , 87, pp. 6459-6476.

Woodsworth, G.J., Crawford, M.L., and Hollister, L.S. (1983) Metamorphism and structure of the Coast Plutonic Complex and adjacent belts, Prince Rupert and Terrace areas, British Columbia. In: GAC, MAC and Canadian Geophysical Union, Joint Annual Meeting - Victoria, British Columbia. Field Trip Guidebook volume II, Trips 9-16.

Woodsworth, G.J., Hill, M.L., and van der Heyden, P. (1985). Geology, Terrace map area, British Columbia (103IE1/2). 1:125,000. Geological Survey of Canada. Open File Map 1136.

Yoshiasa, A. and Matsumoto, T. (1985). Crystal structure refinement and crystal chemistry of pumpellyite. American Mineralogist, 70, pp.1011-1019.

Zen, E-an (1961). The zeolite facies: an interpretation. American Journal Science, 259, pp.401-409.